Understanding and Modifying the Properties of Permanently Microporous Liquids: Towards Selective and Scalable Systems

Thesis submitted in accordance with the requirements of the

University of Liverpool for the degree of Doctor of Philosophy by

Benjamin David Egleston

November, 2021

This thesis is dedicated to my Grandma, Audrey Egleston.

Acknowledgements

Submitting this thesis marks the end of my link to Liverpool after nearly 10 years. I can look back now on my time in the city with fondness and gratitude. This place has been a bubble I've been lucky to exist in, it has been filled with people and opportunities that have helped form who I am.

Special thanks need to be directed towards my primary supervisor, Andy Cooper, I greatly appreciate him for giving me the opportunity to study for this PhD. Becky Greenaway has been especially important to me through my time completing this work, she has been amazingly, unwaveringly supportive as an advisor, colleague and friend. I'd also like to extend my gratitude to Michael Briggs, Konstantin Luzyanin, Rob Clowes and Tom Hasell for their very useful advice. Many thanks to Team Porous Liquids too: Rachel, Andy, Mike and Aiting, as well as Annabel and Steven for putting up with me at the end of this, and the rest of the Cooper and Greenaway groups.

I'm grateful for my Mum and Dad who have always believed in me and provided me with support, without which I wouldn't have made it. Thanks definitely need to go to Will and Tolly for their great friendship, for discussing everything important (and not) for all this time and for being great fun. I also want to thank the Brothers Mad for providing a safe place for me in a time of need, particularly Alex who has been an amazing friend.

Abstract

Porous liquids are a new class of material defined by their permanent microporosity and fluidity. In this thesis, an investigation of control over the properties of these materials is described, transferring knowledge of microporous solids into the liquid state. The progress made to date in this relatively young field is outlined, as well as an overview of the properties of microporous solids. New type 2 and 3 porous liquids with modified gas uptake and selectivity were generated using synthetic pore control in porous organic cages, based on previous understanding of these organic cage molecules. In a type 2 porous liquid cage solution, introduction of methyl groups to occlude the pore window effect was used to invert selectivity for Xe. New type 3 porous liquid dispersions were prepared from organic cage microcrystals, pore modification among the materials was also shown to enhance or reduce gas uptake. Hydrophobicity is also explored as a driving force for introducing porosity in a liquid, microporous polymer dispersions were investigated for gas and liquid absorption.

Contents

List of Abbreviations

BET Brunauer–Emmett–Teller

CD cyclodextrin

CTF covalent triazine framework

CMP conjugated microporous polymer

COF covalent organic framework

CWA chemical warfare agents

DCM dichloromethane

DOSY diffusion ordered spectroscopy

DLS dynamic light scattering

DSC differential scanning calorimetry

FDA formaldehyde dimethyl acetal

HCP hypercrosslinked polymer

HOF hydrogen-bonded organic framework

HPLC high-performance liquid chromatography

IL ionic liquid

IUPAC The International Union of Pure and Applied Chemistry

CONTENTS

MD molecular dynamics

MOC metal organic cage

MOF metal organic framework

ND neutron diffraction

NMR nuclear magnetic resonance

OMIM organic molecule of intrinsic microporosity

P4MP1 poly(4-methyl-1-pentene)

PALS positron annihilation lifetime spectroscopy

PEG poly(ethylene glycol)

PEGS poly(ethylene glycol) sufonate

PFG pulsed field gradient

PIM polymer of intrinic microporosity

PL porous liquid

POC porous organic cage

PCP perchloropropene

PXRD powder X-ray diffraction

SEM scanning electron microscopy

SLS static light scattering

TFB 1,3,5-triformylbenzene

TGA thermogravimetric analysis

THF tetrahydrofuran

TMS tetramethylsilane

TPB 1,3,5-triphenylbenzene

VOC volatile organic compound

XRD X-ray diffraction

ZIF zeolitic imidazolate framework

List of Publications

Parts of the work in this thesis have appeared in the following publications:

- Benjamin D. Egleston, Konstantin V. Luzyanin, Michael C. Brand, Rob Clowes, Michael E. Briggs, Rebecca L. Greenaway and Andrew I. Cooper, *Angew. Chem. Int. Ed.*, 2020, **59**, 7362-7366.

- Aiting Kai, Benjamin D. Egleston, Andrew Tarzia, Rob Clowes, Michael E. Briggs, Kim E. Jelfs, Andrew I. Cooper and Rebecca L. Greenaway, *Adv. Funct. Mater.*, 2021, Early View DOI: 10.1002/adfm.202106116

Work for the following publications was also carried out during the PhD studentship:

- Benjamin D. Egleston, Michael C. Brand, Francesca Greenwell, Michael E. Briggs, Stuart L. James, Andrew I. Cooper, Deborah E. Crawford and Rebecca L. Greenaway, *Chem. Sci.*, 2020, **11**, 6582-6589

- Michael C. Brand, Francesca Greenwell, Rob Clowes, Benjamin D. Egleston, Aiting Kai, Andrew I. Cooper, Thomas D. Bennett and Rebecca L. Greenaway, *J. Mater. Chem. A*, 2021, **9**, 19807-19816

1 Microporous solids and liquids

Porous materials are found widely on earth and they are used to perform a huge number of functions due to their wide variety of properties. Some important examples of their use are in filtration and absorption and in sound, heat, and vibration suppression.[1] Porous materials, such as natural sponges[2] and porous carbons[3] have been used by humans since prehistory in water purification. In particular, *microporous* solids and liquids have received much attention in chemical research laboratories over the past several decades. Microporous solids are effective in filtrations due to having high specific surface area and large free volume, and as thermal and mechanical insulators due to their low density and rigidity.

While microporous solids are found in nature and thousands of examples have been prepared synthetically, microporous liquids are relatively rare and must be prepared with careful design considerations.[4] Since porous liquids are reasonably unknown due to their youth as a category of material, it is important to outline the progress that has been made so far within the field, and how they can be related to the many different categories of microporous solids.

1.1 Porous materials

The International Union of Pure and Applied Chemistry (IUPAC) defines a porous solid as 'a solid with pores, *i.e.* cavities, channels or interstices, which are deeper than they are wide'.[5] These appear often as channels and cavities in pore networks within materials, or often as isolated pores within a bulk material than

are inaccessible to external fluids (1.1). The definition encompasses a broad variety of different substances, materials and objects. One historic example is ocean sponges' skeletons, that when prepared, have a very high porosity due to their heavily interconnected network of cavities and channels. This high porosity and small pore size made them a very early example of a porous material used in liquid filtrations, water decontamination in this instance.[2]
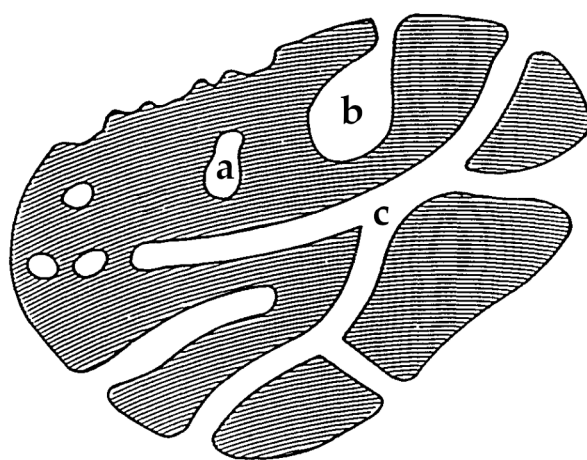
Figure 1.1:   Some different pore topologies: **a** isolated pores, **b** pore cavity and **c** pore channels are shown here, adapted from Rouquerol *et al.*[5]

Porous materials are often categorised based on the size of their pores, as this has a large impact on their design and applications. According to IUPAC, these are broadly defined as macroporous, mesoporous or microporous materials (Table 1.1). This property determines the kind of filtrations and separations a material is capable of being used in. Porous materials are selected based on the size of the components of a mixture which may need separating. For example, macroporous materials are useful for filtering macroscopic particles from finer fluid mixtures, or

if separation is not needed they can provide very high surface areas, for example as heterogeneous catalysts.[6]

Table 1.1: Categorisation of porous materials based on the size of their constituent pores

Category	Pore Diameter
Macroporous	> 50 nm
Mesoporous	< 50 nm, > 2 nm
Microporous	$d < 2$ nm

1.2 Microporous materials

In order for a material to exhibit microporosity it must satisfy some requirements: 1) the width of pores in a microporous materials must lie in the range of sizes <2 nm;[5,7] 2) the pores must be interconnected such that they are accessible to some fluid phase.[1] This second point is important when the material is intended for using for separations or controlling reactions so that liquids and gases can access or pass through the material's bulk.

Microporous materials are of particular interest to chemists since the pore sizes are on the same scale as individual molecules and various functional groups. By their nature, small changes to the chemical structure of a microporous material will have a large impact on its porosity, allowing design of new microporous materials to be carried out through modifying the synthesis of these materials.[8] Generally, these types of materials gain functionality from the size and shape of its pore network, which allows for molecular selectivity. For example, introduction
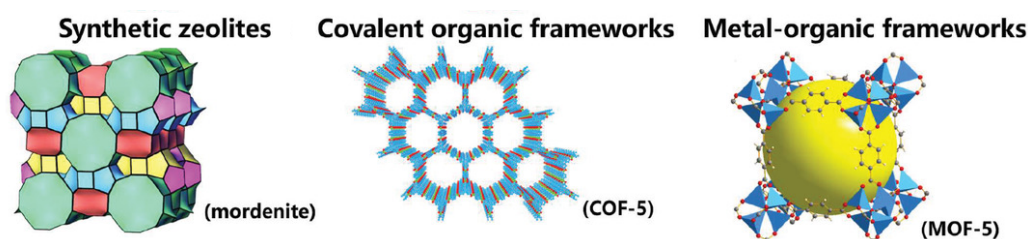
Figure 1.2:   Microporous materials from the three compositions: Mordenite (left) is a synthetic zeolite prepared from inorganic components, **COF-5** (centre) is an organic covalent organic framework (COF), and **MOF-5** is a metal organic framework (MOF) composed of both inorganic metal centres and organic linkers, *i.e.* hybrid.[10]

of bulky groups into the pore channels in a microporous material will lead to hindrance of molecular diffusion, maximally to the extent that H_2 and D_2 can be separated from microporous materials with very small pores.[9] Many other interactions beyond steric effects are important in these materials, such as intermolecular or covalent interactions between functional groups within the structure and small molecules occupying the pores.

1.2.1   Inorganic, organic and hybrid microporous materials

Often microporous materials are categorised based on the origin of their precursors, thus their composition: inorganic, organic, or hybrid; a combination of both (Figure 1.2, Table 1.2). While this may seem largely arbitrary with respect to porosity, there are large divergences among these classes.

Zeolites are the archetypal inorganic microporous material, they were the first microporous material to be discovered and are found as minerals in nature.[11] Zeolites are aluminosilicate minerals, they are produced either by mining

natural sources or synthetically from siloxane monomers.[12] Alternatively, many microporous materials are composed entirely of organic components. There are a multitude of different types of rigid, microporous polymer materials prepared from organic monomers,[13] as well as organic molecular porous materials such as porous organic cages (POCs) and organic molecules of intrinsic microporosity (OMIMs).[14]

The third possible composition category is that of hybrid materials, or those that contain both inorganic and organic building blocks. The most important examples of these are metal organic frameworks (MOFs) and metal organic cages (MOCs), which have been investigated in great depth in the literature.[20,21] These materials are versatile and easily predictable due to the strong directionality of the metal-ligand coordination bonds of which they are mostly constructed.

1.2.2 Molecular and polymer/framework porous solids

Microporous materials can be further categorised by the bonding that makes up the overall structure of the material. Many microporous materials are polymer (*e.g.* conjugated microporous polymers (CMPs), hypercrosslinked polymers (HCPs) or polymers of intrinsic microporosity (PIMs)) or framework (*e.g.* zeolites, MOFs and covalent organic frameworks (COFs)) type materials. These materials are composed of extended networks of strong covalent, ionic or coordination bonds, resulting in rigid and inefficiently packed solid materials. The rigidity is imparted on the structure by the fact that the extended network is interconnected with strong covalent or coordination bonds, extending in all dimensions to provide support to avoid collapsing of pores.

Table 1.2: Different families of microporous materials categorised by their composition.

Inorganic	Organic	Hybrid
Zeolites, Aluminophosphates, Porous Silicas[15]	Porous Carbons, conjugated microporous polymers (CMPs),[16] covalent organic frameworks (COFs), covalent triazine frameworks (CTFs),[17] hypercrosslinked polymers (HCPs),[13] polymers of intrinsic microporosity (PIMs),[18] porous organic cages (POCs),[4] organic molecules of intrinsic microporosity (OMIMs)[19]	metal organic frameworks (MOFs),[20] metal organic cages (MOCs),[21] zeolitic imidazolate frameworks (ZIFs)[22]

In contrast materials like POCs[4], MOCs[23] and OMIMs[19] are molecular microporous materials, in that they are comprised of discrete molecular species that pack together to form an extended porous network in the solid state. Since the individual molecules are only weakly bound by intermolecular forces, rather than by covalent bonds as found in in other porous solids, the materials can be dissolved in organic solvents, allowing for easy processing.[24] To be classed as a porous material, the pore networks must remain intact even when they are unoccupied. This means porous molecular materials must be sufficiently rigid to avoid collapse of pores on removal of solvent, as they cannot rely on the strength of an extended framework as found in MOFs, for example. As the individual molecules are only weakly bound together compared to the strong bonds in framework materials, careful design has to be taken in order to produce individual molecules that are sufficiently rigid separate from the bulk material to not collapse.

1.2.3 Amorphosity and crystallinity in porous materials

Some microporous materials favour formation of amorphous, or disordered, phases rather than crystalline phases, such as polymer network materials like CMPs, HCPs and PIMs,[13] as they are synthesised from small organic building blocks that pack poorly in the solid state and do not form a regular network due to the fast kinetics of the polymer formation. These materials can have exceptionally high surface areas, **PAF-1** is a prolific material with a Brunauer–Emmett–Teller (BET) surface area of 5600 m^2/g,[25] derivatives of which can exhibit surface areas as high as 6461 m^2/g.[26] Despite having low densities and very high surface areas, these amorphous materials lack in particularly well defined pore sizes due to the

statistical nature of their structure and micropore formation. In contrast, well ordered microporous materials are prepared using slower and more reversible processes that allow formation of well defined repeating structures over much longer ranges in the bulk material. For example, framework materials such as MOFs and COFs are formed using more dynamic chemical reactions where the reversibility allows for 'error-correction' during the crystal structure formation.[27,28] Generally, POCs, hydrogen-bonded organic frameworks (HOFs) and OMIMs are also known for forming highly crystalline solids. Rather than relying on reversible covalent or coordination bonds as in crystalline framework materials, these form highly ordered solids by crystallization where the lattice structure is determined by weaker intermolecular forces.[14] Different crystal packing structures are important in the formation of porous networks in the solid, **CC1** an imine POC forms a non porous polymorph when crystallised from ethyl acetate (Figure 1.3 a), but can be interconverted to several different porous polymorphs in the solid state by exposure to organic vapour triggers.[29] In **CC2**, another imine POC, the 'static' crystal structure indicates that the cage cavity is not included in the pore network, which consists of extrinsic pore channels hypothesised to solely determine the gas uptake in the material (Figure 1.3 b).[30] However, Holden and coworkers found that in this POC the pores are accesible to small gas molecules such as H_2 *via* openings created by the structural disorder of the vertex methyl groups, *in situ* powder X-ray diffraction (PXRD) data also shows that CO_2 and Xe gas molecules can access the internal pore sites.[31] This shows how the dynamic and cooperative nature of gas adsorption in these materials needs to be considered when determining the pore accessibility as the static crystal structure cannot provide complete information

about porosity of the system.

Although MOFs and POCs are known for their crystallinity, there is much interest in methods to produce amorphous analogues of these materials. 'Scrambled' POCs can be synthesised by combining different precursors in the reaction mixture to produce POC mixtures with statistical structural vertex disorder.[32] The solid state packing of these cage mixtures is amorphous, the structural disorder of each cage removes the preference of the molecules to crystallize into a well ordered unit cell. Another example of a usually crystalline material that can be converted to an amorphous state is shown in the recent work developing melt-quenched MOF glasses from the Bennett group.[34] These glasses are amorphous, and while most examples do not exhibit permanent porosity in the resulting glasses, some recent examples have successfully shown microporosity and gas uptake.[35]

1.2.4 Intrisic and extrinsic porosity

Porous materials are classified as either intrinsically or extrinsically porous. Intrinsic porosity arises when the structures of discrete, individual molecules possess internal free volume, resulting in voids in the bulk solid material.[19] This includes both molecular capsule/cage molecules as well as OMIMs, the former contain free volume as molecular cavities that are completely included within the structure, surrounded by 'struts' that maintain the void shape and size. The latter also have free volume within the molecular structure, but the voids result from a combination of molecular rigidity and frustrated packing that stops adjacent molecules in the solid occupying the free volume of the molecules. Extrinsically
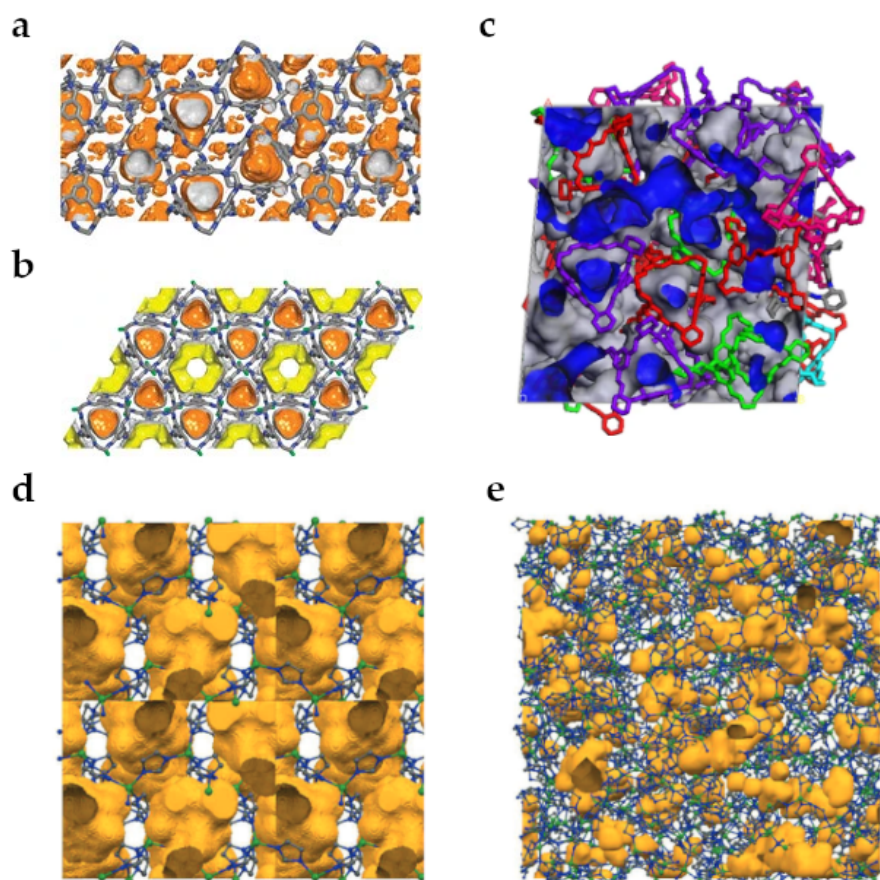
Figure 1.3: Amorphous and crystalline POCs and MOFs. Crystal structures of (**a**) **CC1** and (**b**) **CC2** containing significant void volume, the externally accessible pore surfaces are coloured in yellow while inaccessible pore surfaces are coloured in orange, calculated with a 1.82 Å probe size.[30] (**c**) The amorphous packing structure in solid scrambled imine cage mixture **CC1³:3³**, the internal pore surface calculated with a 1.82 Å probe is shown here in blue.[32] Solid state structures of (**d**) crystalline and (**e**) amorphous **ZIF-4** with pore surfaces shown in orange and calculated with probe size of 1.2 Å.[33]

porous materials are composed from molecules that do not have this intrinsic void or free volume, instead forming a porous network in the solid state from spaces generated between molecules due to the packing in the bulk material.[24] As these materials do not rely on the steric exclusion of neighbouring molecules, strong, rigid bonding between the component building blocks is required to avoid collapse of the free volume. These two types of porosity are not completely exclusive, as intrinsically porous molecules can also pack inefficiently in the solid state due to strong interactions between adjacent molecules, giving rise to further extrinsic pores in addition to the internal pores, leading to interconnected microporous networks.

1.3 Porous liquids

Porous liquids are a recently conceptualized type of material.[36] By definition, a porous liquid must contain permanently unoccupied cavities, like those found in porous solids, but must exhibit fluid behaviour. Like in porous solids, in a permanently porous liquid the pores present must retain their structure and size over time and remain persistently associated to molecular structures in the liquid.

1.3.1 Porosity in conventional liquids

It is important to outline how porosity in porous liquids is distinct from that in conventional, or normal, liquids since pores, or cavities, do exist in all liquids. These cavities form between the molecules in a normal liquid due to the liquid's disordered and dynamic structure.[37] For example, using analysis of molecular

dynamics (MD) simulations, the cavity size probability distributions for H_2O and

n-hexane can be measured (Figure 1.4), here the most probable cavity size is very

small (*ca.* 0.2 Å).[38] The greater probability to form small pores (< 0.7 Å) in water

over n-hexane is attributed to the short range structuring in the liquid, in this case

due to hydrogen bonding, allowing for a larger overall free volume.
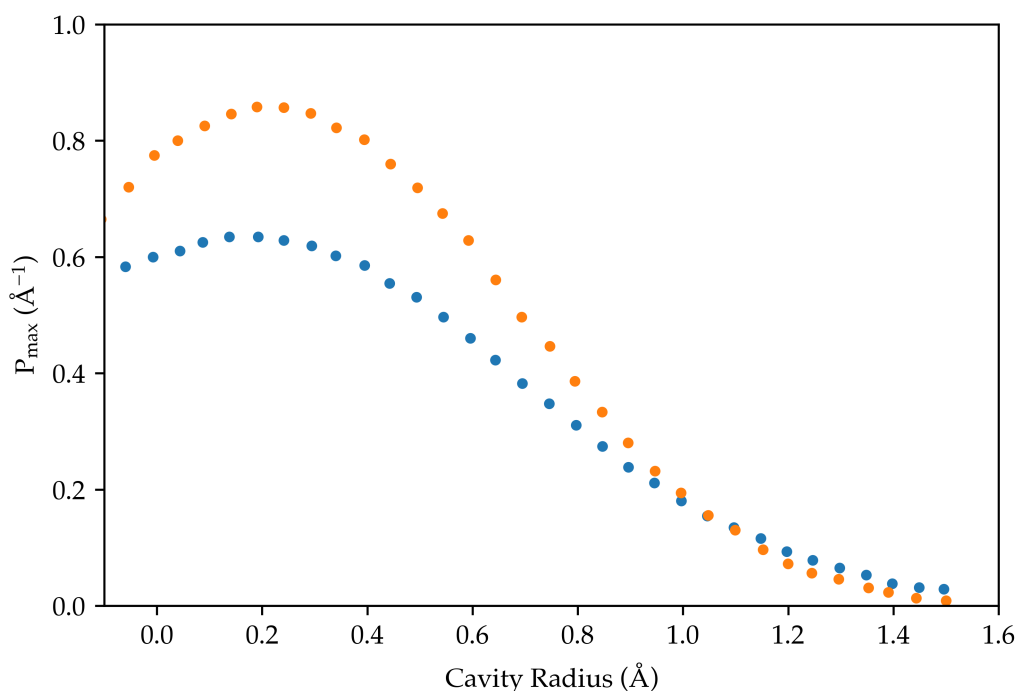
Figure 1.4: Cavity size distribution functions for H_2O at 300 K (orange) and n-hexane at 320 K (blue) determined by analysis of MD simulations.

In these normal liquids pore sizes over *ca.* 1.5 Å are very rare, although it has

also been postulated by Lindquist *et al.* that much larger pore radii could be formed

in normal liquids by further exploiting intermolecular forces to produce much

larger equilibrium structures.[39] The theoretical study found that by optimising

the interaction between adjacent molecules liquids could be produced that have a variety of complex and ordered pore networks, including isolated pores, columnar networks, lamellae and lattice networks. While these pores are found to exist, the voids are fleeting and temporary in nature, only existing on the picosecond timescale,[37] so do not contain the kind of persistent and well defined cavities that is found in a permanently porous liquid. In most liquids, gas uptake is usually only observed as a result of chemisorption rather than physical adsorption of molecules within the pores, since the pores are both too small and too short-lived to contribute to the uptake.

There are also some liquids with characteristics that may indicate a more robust porosity in the liquid state. One example of this is in the use of He gas to compress isotactic poly(4-methyl-1-pentene) (P4MP1) melt at 270 °C and pressures up to 20 kbar.[40] The gas compression of the melt at high pressures is compared to the solid compression using a pair of diamonds. As the polymer was compressed, the position of the first X-ray diffraction peak was measured (Figure 1.5), which corresponds to the density of the material.

The researchers found that when the P4MP1 melt was placed under He gas at 1.8 kbar, it only compressed half as much as when P4MP1 was compressed between diamonds.[41] The authors argue that this shows that the He is able to occupy the interstices between the polymer chains as this effect is also observed in the He compression of SiO_2 where the penetration of He into the crystal network results in reduced compression at similar pressures.[42] While it is apparent that He can occupy the cavities in P4MP1, this does not necessarily correspond to a porosity significantly different to that found in all normal liquids, as the structure
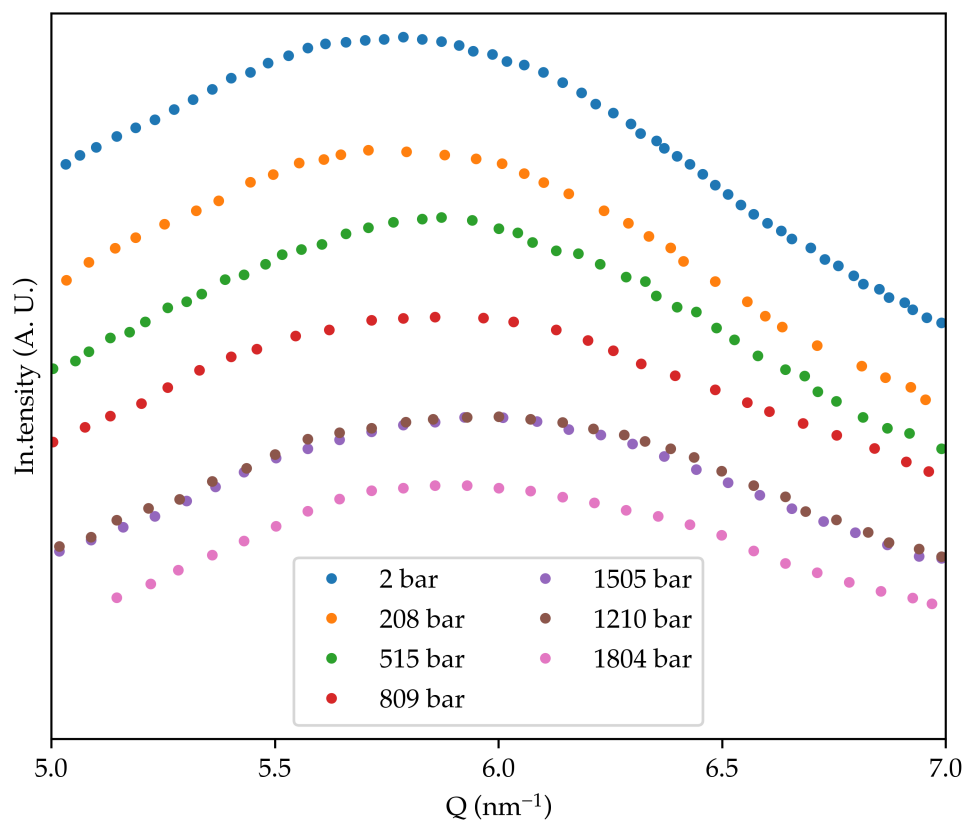
Figure 1.5: The first X-ray diffraction peak of P4MP1 at a variety of pressures up to 1.8 kbar using He.

of liquid polymers is dynamic and there is no evidence that pore structure would be retained permanently in this material. Despite this, the study represents an important example of how gas uptake properties usually only found in solid state materials can be transferred to liquids if specific design considerations are taken.

Another recent example of a liquid material with the question of porosity attached are those produced as a result of the drive to develop amorphous glasses from usually crystalline MOFs.[34] A series of ZIFs were found to all have melting points in excess of 700 K and on cooling were found to form glasses. More importantly, in a later study Gaillac *et al.* were able to characterise the melting process in ZIF-4 and determine the short range structure using neutron and X-ray total scattering and pair distribution function analysis combined with Monte Carlo modelling (Figure 1.6).[33] Not only were they able to confirm the material's structure in the melt, but also fully characterised the structural change over the entire phase transition.

The pore volume in the Monte Carlo experiments remains reasonably well defined above the melting point of the liquid, breaking down at temperatures above 1000 K (Figure 1.6 b). This indicates the local pore structure formed from the local structure of the network remains in the liquid phase, as is also observed in the atomic structures produced from these experiments (Figure 1.6 a).

1.3.2 Permanent microporosity in the liquid state

Permanent microporosity is a property usually observed only in the solid state. In IUPAC's recommendations for describing and characterising porous materials, reference is only made to solids and methods in which their porosity can be
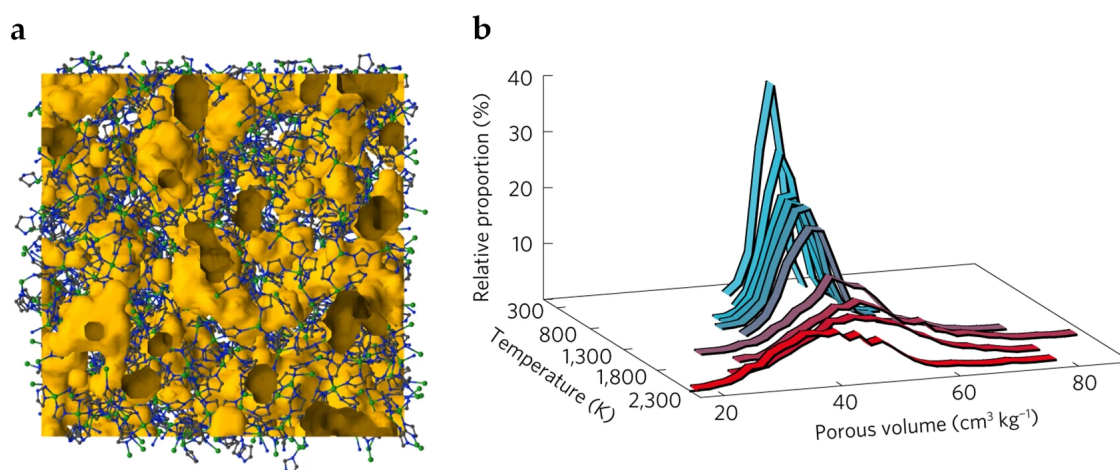
Figure 1.6: (**a**) Atomic structure of ZIF-4 melt generated from reverse Monte Carlo modelling based on experimental scattering data at 856 K. Pore surfaces in orange, Zn atoms in green. (**b**) The evolution of pore volume in structures generated from Monte Carlo across the range of temperatures measured.[33]

analysed.[5] Porosity in porous liquids differs from that in conventional liquids in that it is permanent and intrinsic, rather than the transient pores present in conventional liquids which rely on formation of extrinsic voids between the molecules of a liquid.

Microporous liquids were first hypothesised and theorised by O'Reilly *et al.* in 2007[36] where they outlined a series of definitions that can be used to categorise these materials and begin to develop some design principles for porous liquids. They defined 3 broad categories for porous liquids (Figure 1.7):

- Type 1 porous liquids: neat liquid molecules with permanent cavities that do not collapse and a structure that doesn't lead to interpenetration.

- Type 2 porous liquids: solution of molecules with cavities in a solvent too

sterically hindered to occupy the cavities.

- Type 3 porous liquids: dispersion of porous framework particles in a dispersant too sterically hindered to penetrate the pore network.

O'Reilly *et al.* repeatedly refer to the fact that these materials need to be designed in such a way that all the components present are excluded from the cavities in order for the liquid to be porous.[36] This has been emphasised recently in reviews covering the topic of porous liquids.[4,43–46] In each type of porous liquid, this has to be approached from a different perspective in order to make the material porous. Bavykina *et al.* outlined the importance of selection of the pore generator, or porogen, *i.e.* the component of the porous liquid that contributes the porous structure.[47] The pore generator must be sufficiently rigid such that they do not collapse when unoccupied and must have cavities or portals significantly restricted to the extent that other components of the liquid cannot enter and occupy the pore. This is then complemented by ensuring other parts of the material are selected based on whether they would be excluded from the pores, whether they be appended functional groups, or another molecular liquid in the case of type 2 or type 3 porous liquids.

1.4 Type 1 porous liquids: melting pores

According to O'Reilly *et al.*,[36] a type 1 porous liquid (PL) is composed of molecules with an internal cavity, or pore, with rigidity such that it does not collapse when its cavity is unoccupied, and has a structure that cannot lead to filling of cavities in other component molecules. While a multitude of supramolecular materials with

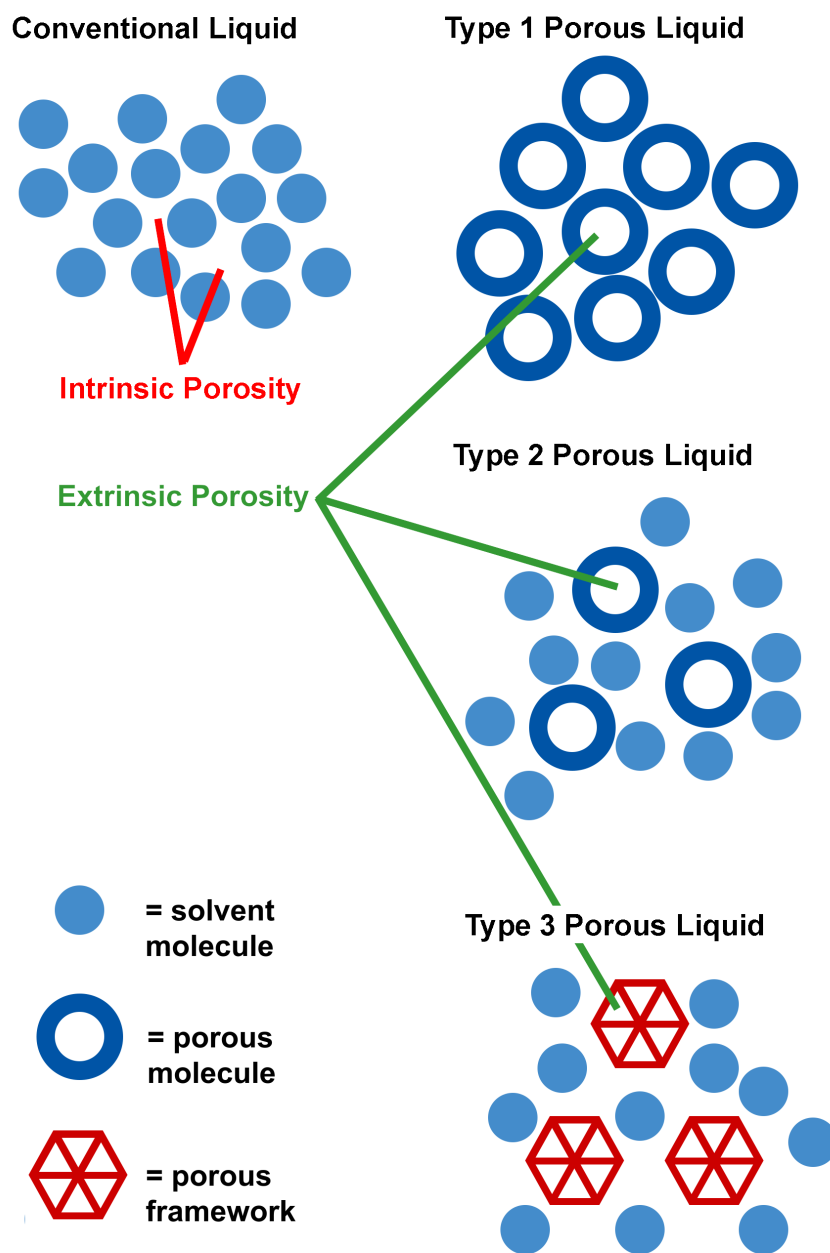**Figure 1.7:** The different types of porosity in liquids. Conventional liquids only consist of small molecules with no pore. Type 1 porous liquids consist of molecules with an internal cavity, or pore, type 2 porous liquids consist of porous molecules dissolved in a liquid with molecules too bulky to occupy the pore, while type 3 porous liquids consist of some solid porous framework dispersed in an excluded bulky molecular liquid.

these properties existed at the time of writing, the majority were highly crystalline solids with onset of decomposition occurring before melting. O'Reilly *et al.* also outlined some cyclic molecular materials, such as crown ethers and calixarenes, as possible candidates for porous liquids, but pointed out that generally the cavities were shallow and easily filled by neighbouring molecules. Upon the discovery of POCs in 2009, the researchers anticipated that these materials would be used to form porous liquids.[30]

Early attempts to generate permanent porosity in the liquid state utilised the modularity of the [4+6] iminospherand POCs, developed by Cooper *et al.*,[30] to produce low melting point POCs from alkylated diamines (Scheme 1.1).[48] The best performing material synthesised by Giri *et al.*, the *n*-octyl decorated cage (Scheme 1.1, **9**), had a melting point of 50 °C and rheological analysis showed it exhibited fully Newtonian fluid properties above 80 °C. While this was the first demonstration of meltable organic cages, with reasonable low melting points, these materials were shown to be non-porous in the solids produced upon cooling and presumed to be non-porous in the liquid state due to interpenetration of the long alkyl groups among neighbouring cage molecules. Despite the efforts to produce a type 1 porous liquid, the range of alkyl pendant cages synthesised in these studies were not porous in the liquid state.

The researchers proposed inclusion of bulkier terminating groups to avoid this, and followed up with a study of even longer alkyl groups, including two examples terminated with *t*-butyl groups in order to add steric bulk to avoid inclusion in neighbouring cavities.[50] Despite this, simulations indicated that none of these new examples would exhibit porosity, in fact the bulkier *t*-butyl groups are a better fit
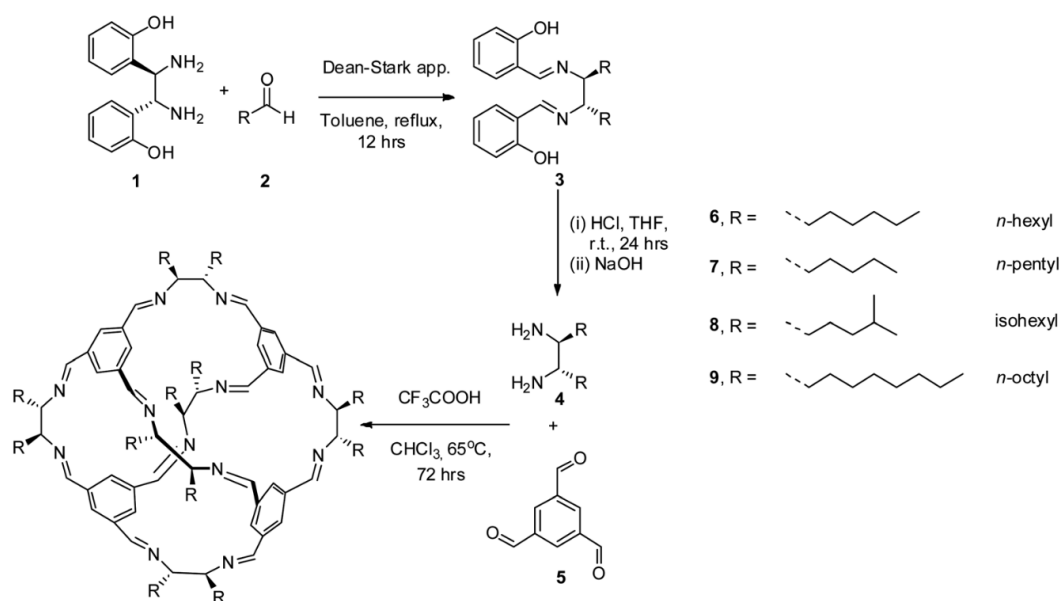
Scheme 1.1: Synthesis of low melting organic cages prepared by Giri *et al* by varying the vicinal diamines from which the cages were prepared. These chiral diamines are synthesised in two steps from *R,R*-1,2-bis(2-hydroxyphenyl)ethylene diamine and various aldehydes in a diaza-Cope rearrancgement[49] followed by hydrolysis of the formed diimine. The [4+6] iminospherand cages were formed by combining 6 equivalents of chiral diamine with 4 equivalents of 1,3,5-triformylbenzene (TFB), resulting in formation of cages with varying lengths of pendant alkyl chains.[48]

for the cavity of these [4+6] iminospherand cages, with increased binding energies compared to the *n*-alkyl chains. Recently, Brand *et al.* showed that melting cages can be quenched to for POC glasses, outlining another possible utility for porous liquids as a route for processing materials into new phases.[51]

The first successful example of a type 1 permanently microporous liquid was based on the family of MOCs developed in the Nitschke group.[52] These cages were functionalised with poly(ethylene glycol) (PEG) groups terminated with an

imidazolium triflimide structure found commonly in ionic liquids (ILs)[53] (Scheme 1.2), yielding a MOC that was liquid at room temperature. Differential scanning calorimetry (DSC) of the material showed a phase transition at -44 °C, confirming the compound was liquid above this temperature. Positron annihilation lifetime spectroscopy (PALS) was used to confirm the porosity in the porous liquid. PALS is a technique used to determine porosity based on the lifetime of positrons generated within a material, where the average size of pores determines the length of time the particle can travel before annihilating with atoms within the material. The measured value of the *ortho*-positronium lifetime in the sample (2.34±0.05 ns) corresponded to an average pore diameter of 6.29±0.08 Å which was in good agreement with the calculated value. Ma *et al.* demonstrated how the large pore in the MOC selectively binds branched alcohols over *n*-alkyl alcohols, and effectively absorbs the ozone depleting agents $CFCl_3$, CF_2Cl_2 and CF_3Cl. The permanence of porosity in this porous liquid is afforded by the termination of the PEG chains with the IL groups; the strong ionic bonding between the imidazolium ion and the triflimide anion stops the chain from penetrating the MOC core. This also qualifies the material as the first example of a truly ionic porous liquid, as it only consists of ionic molecular species in the liquid state.

Cyclodextrins (CDs) are a family of organic macrocycles with a pore-like interior synthesised from glucose units.[54] Recently, the development of CDs as 'supramolecular solvents' has led to the production of fluids with very high concentrations of CD.[55] Following a method reminiscent of Ma *et al.*, coupling an imidazolium phosphite to the CDs molecule (Scheme 1.3), resulting in pendant IL groups, giving a neat liquid with a melting point of -63.15 °C. The study
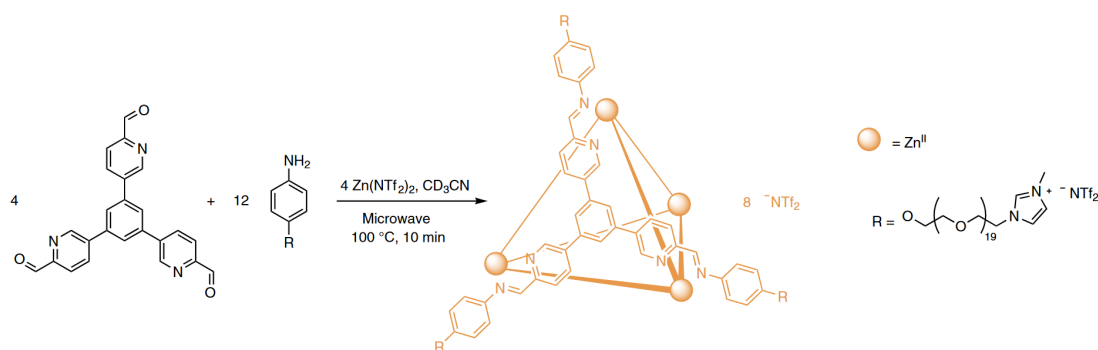
Scheme 1.2: Synthesis of the MOC for room temperature porous ionic liquids prepared by Ma *et al.*[52]

primarily focussed on enantiorecognition and separation of Nucleosides, some of the building blocks of DNA. This solution based on γ-CD was shown to be effective at the targeted task, achieving an 84.81% enantiomeric excess in the separation of D- and L-β-2'-deoxycytidine. However, while no attempts have been made to directly quantify or investigate the porosity in this material, the authors analyse the CD's structure using spectroscopy to show the pendant imidazolium is located in a position such that it is blocked from occupying the cavity.

So far, only 2 examples of type 1 permanently microporous liquids have been presented in the literature. As predicted by O'Reilly *et al.*, they have all been based on organic based molecules with internal cavities. The small number that have been prepared so far reflects the complex design considerations and trade-offs required in making these materials. Introduction of groups to aid a lower melting point often lead to reductions in porosity due to interpenetration. PALS was shown as a useful technique for determining whether a sample contains micropores.

α-CD:n=6,x=1-4,y=1-4;
β-CD:n=7,x=1-6,y=1-4;
γ-CD:n=8,x=1-6,y=1-4.

Cyclodextrin

Cyclodextrin esterification product

Cyclodextrin porous liquid
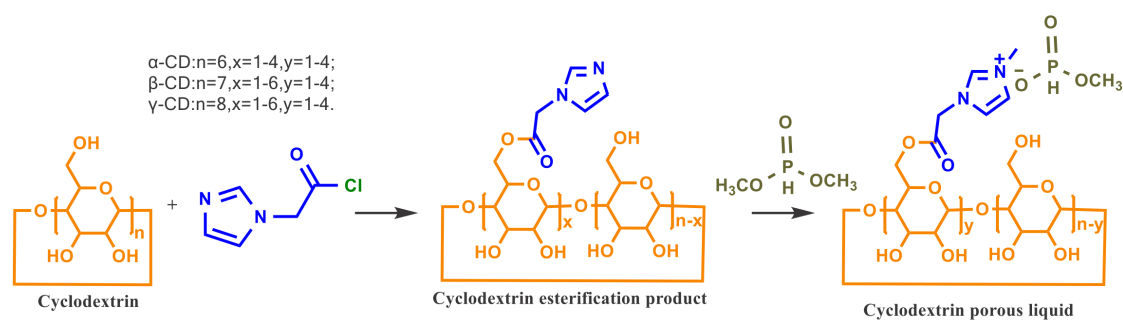
Scheme 1.3: Synthesis of CDs for CD based type 1 porous liquids.[56] First, the imidazolyl acyl chloride is coupled with the CD to form an ester which is then combined with dimethyl phosphonate to form an ionic CD liquid.

1.5 Type 2 porous liquids: pore solutions

Type 2 porous liquids consist of molecular pore generators dissolved in a solvent composed of molecules sufficiently bulky that they are excluded sterically from the cavity of the pore generator.[36] Arguably, molecular design in type 2 porous liquids includes more complexity that in a type 1 porous liquid as, not only do the porous molecules have to be excluded from adjacent pores, the selection of solvent has to be carefully considered as it has to allow for a sufficiently high solubility of the pore generator to allow for a significant porosity while also enabling that porosity through a structure that compliments the pore size in order to remain excluded. Thus, simply creating solutions of Giri's alkylated POCs[48] would not be sufficient to produce a porous liquid as the long alkyl chains would still act as interpenetrating groups, while finding a suitable solvent for Ma's cage IL would be difficult due to the very large cavity portals.[52] An earlier possible example of a type 2 porous liquid was presented by Cram's group in 1990, where a hemicarcerand

39
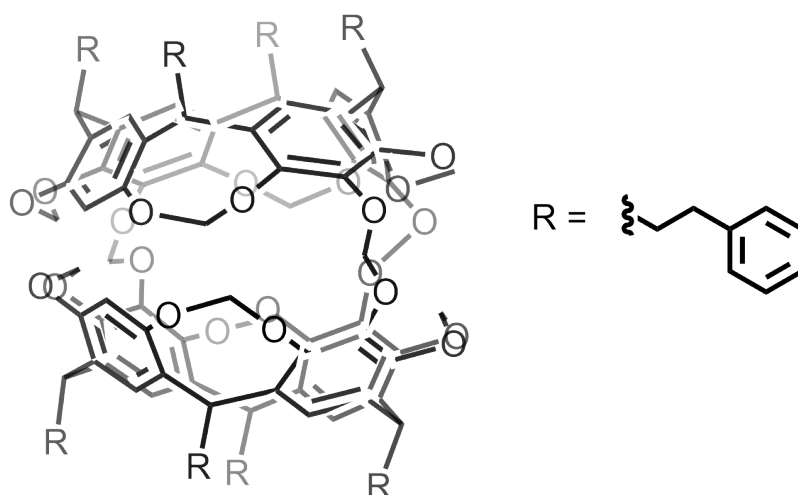
Figure 1.8: Window restricted hemicarcerand prepared by Tanner *et al.*[57]

with very small and restricted windows (Figure 1.8) readily formed a complex with Xe in CHCl$_3$, characterised by a significant shifting of the Xe peak in the ^{129}Xe NMR spectrum ($\Delta\delta$ = -101 ppm).[57] This observation indicated that the CHCl$_3$ was not competing with the absorption of Xe, a sign that permanent pores existed in the solution.

The first successful examples of permanently microporous liquids were type 2 porous liquids presented in 2015, two systems using modified [4+6] imine cages were demonstrated.[58] The first example was a crown-ether-modified POC that was found to be highly soluble (44% wt) in 15-crown-5 (Scheme 1.4). This system was selected as a target since the molecules of the 15-crown-5 solvent was expected to be excluded from these POCs as the windows are too narrow to allow the bulky solvent molecules to enter. In order to confirm the porosity of this cage solution, a combination of MD simulations and PALS were used to confirm both the solvent exclusion and pore permanence. The MD indicated that on a 100 ns

timescale, the 15-crown-5 molecules would not occupy the cage cavities, while the *ortho*-positronium lifetime was measured and fitted for contributions from both the crown ether solvent and POC to determine a lifetime for the cage cavity in the porous liquid as 1.91 ± 0.08 ns. This is in reasonable agreement with the value measured for the neat solid cage (2.05 ± 0.01 ns).
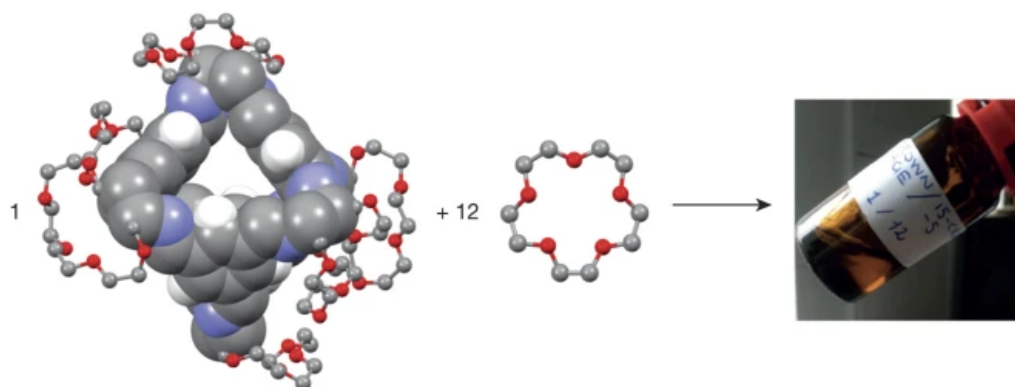
Scheme 1.4: Preparation of Giri's type 2 porous liquid by dissolving the crown-ether-POC in 15-crown-5 solvent to produce a single fluid phase.[58]

The next step in the study of this system was to determine if any gas uptake enhancement occurs in the porous liquid when compared to the neat 15-crown-5. Using an isochoric method, methane uptake was measured for the porous liquid and solvent at *ca.* 600 mbar and then adjusted based on the fugacity and compressibility of CH_4 gas to predict what the gas solubility would be at 1 bar. In these experiments, the gas uptake was indeed improved in the porous liquid, it was predicted that if these experiments were carried out at 1 bar, the gas uptake would be enhanced by 45.3 μmol/g (52 μmol/g for the porous liquid *vs.* 6.7 μmol/g for the solvent).

A second system based on [4+6] imine cages was also studied as a part of this
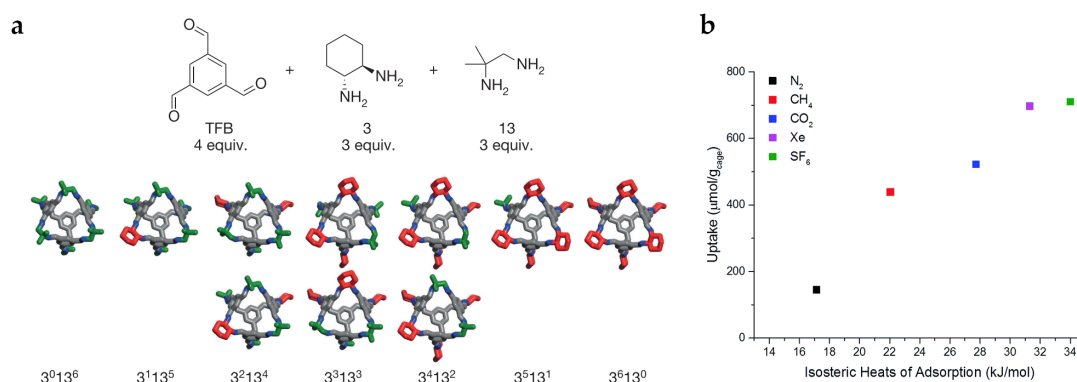
Figure 1.9: (**a**) Precursors used to prepare the scrambled cage mixture **CC3³:13³**-*R* (top) and the full series of different cages from which the scrambled cage mixture **CC3³:13³**-*R* is composed (bottom). (**b**) Plot showing the relationship between gas absorption in the porous liquid and the isoteric heat of adsorption of each gas in the structurally analogous cage **CC3**-*R*.

work. By exploiting the scrambling technique originally developed by Jiang *et al.*[32], a scrambled cage mixture (**CC3³:13³**-*R*) was prepared (Figure 1.9 a) that was found to be highly soluble in perchloropropene (PCP), up to 20% w/v. Though this porous liquid has nearly half the pore concentration compared to the crown ether based porous liquid (**CC3³:13³**-*R* porous liquid 120 μmol/g *vs.* crown porous liquid 209 μmol/g), the methane gas uptake enhancement in the two porous liquids is comparable (**CC3³:13³**-*R* porous liquid 44.3 μmol/g$_{PL}$ *vs.* crown porous liquid 45.3 μmol/g$_{PL}$).

Beyond the gas uptake being comparable despite a lower pore concentration, the **CC3³:13³**-*R* porous liquid also had a much lower viscosity (**CC3³:13³**-*R* porous liquid 11.7 cP at 295 K *vs.* crown porous liquid >140 cP at 298 K) and is considerably easier to synthesise at a larger scale (77% yield in one step) compared

to the crown ether based porous liquid (3.1%-6.7% yield, 6 steps). As such, a subsequent follow-up study of the **CC3³:13³**-*R* porous liquid was carried out, demonstrating that selectivity can be observed in a porous liquid.[59] In this work, Greenaway *et al.* demonstrated that the gas uptake in the porous liquid can be measured volumetrically by displacing gas molecules from the permanent pore volume, greatly broadening the range of gases it is possible to easily measure in the porous liquid. Greenaway *et al.* also found that gas uptake is closely related to the isoteric adsorption energy, indicating the uptake was influenced by the affinity of the gas for occupying the molecular pore in **CC3³:13³**-*R* (Figure 1.9 b). More recently, Kearsey *et al.* built on this work through the exploitation of high-throughput robotic platforms to synthesise more analogous imine scrambled cages and screen for new size excluded solvents in order to improve solubility and access higher pore concentrations.[60] While the porous liquids generated acheived solubilities as high as 35% w/v, the highest gas uptake of Xe (178 μmol/g_{PL}) was at a lower concentration due to viscosity limiting the absorption of gas. Furthermore, gas capacity did not improve linearly with improving concentration, and many of the solvents utilised led to decreased porosity in the liquids produced.

Following on from Giri's crown ether porous liquid, Jie *et al.* developed another type 2 porous liquid by synthesising a POC with an appended potassium carboxylate group which was highly soluble in both 15-crown-5 and dicyclohexano-18-crown-6 due to complexation of the potassium cation with the crown ethers.[61] In particular, the porous liquid in dicyclohexano-18-crown-6 produced a 44% wt solution of POC, with a pore concentration of 502 μmol/g, over 2 times greater than that in Giri's crown porous liquid. Permanent porosity

in the liquid was verified using PALS, giving o-positronium lifetimes of 0.436 ns and 0.468 ns, this was found to be in good agreement with the simulations the group carried out. Since this porous liquid was prepared in crown ether solvents, its lack of vapour pressure means that conventional manometric gas sorption can be carried out, the group carried out CO_2 sorption experiments at pressures up to 10 bar. Over this pressure range, dicyclohexano-18-crown-6 has a negative adsorption isotherm with CO_2, while the porous liquid in this solvent absorbed 54 μmol/g_{PL} at 1 bar (compared to 55 μmol/g_{PL} in Greenaway's **CC3^3:13^3**-R porous liquid) and gave a solubility of 425 μmol/g_{PL} at 10 bar. While the gas uptake is only comparable to Greenaway's porous liquid despite the very high pore concentration, the advantage of a much lower vapour pressure would make this material more applicable to gas sorption processes.

While the above three examples of type 2 porous liquids are all based on POCs, MOCs have also been reported for formation of porous liquids.[62] This example was prepared by dissolving MOP-18, a rhombicuboctahedron MOC with a cavity diameter of 13.8 Å and portal diameters of 3.8 Å and 6.6 Å, decorated with C_{12} alkyl chains in order to aid solubility[63], in 15-crown-5 at 5% w/w (Figure 1.10 a). While the researchers didn't verify the porosity explicitly, MD simulations were carried out on the porous liquid system to determine that the energy barrier of 238 kJ/mol for 15-crown-5 to occupy the cage, and the 15-crown-5 molecules in the experiment largely existed around the periphery of the the MOC. The porous liquid was formulated into a membrane on a graphene oxide support and compared to a 15-crown-5 membrane, finding that the presence of the MOC significantly increases the permeability of the membrane to H_2, CO_2 and N_2 (Figure 1.10 b).
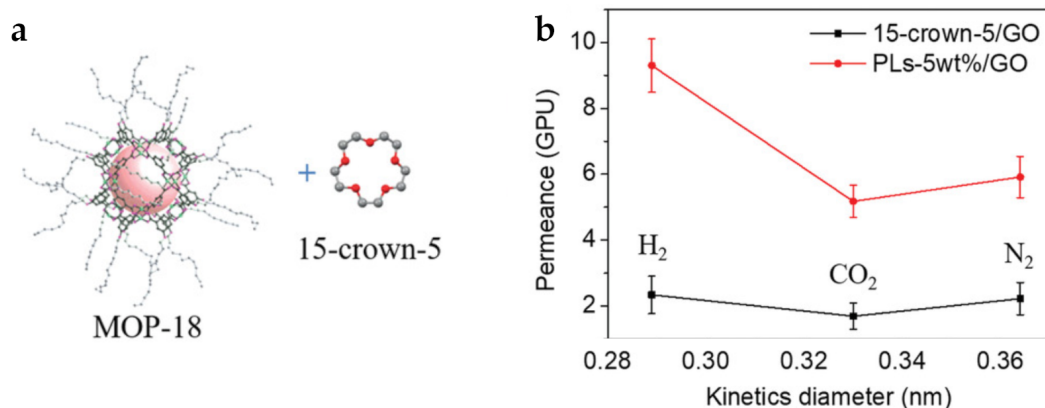
Figure 1.10: (**a**) MOP-18 and 15-crown-5 are combined to produce a porous liquid. (**b**) Plot showing the improvement in permeance across the porous liquid membrane over the 15-crown-5 membrane.

In type 2 porous liquids we see a broader range of design methods employed so far to impart solubility on the pore generating molecules compared to type 1 porous liquids. In type 1 porous liquids, addition of long alkyl or oligo(ethylene glycol) groups are added to produce liquids, employment of this has also been used in type 2 liquids, as well as using molecular complexation and vertex disorder in order to improve solubility. Furthermore, due to the different properties of these porous liquids, different techniques are used to measure gas absorption; the low vapour pressure in Greenaway's **CC3³:13³**-*R* porous liquid required development of NMR and displacement methods to determine gas solubility, and Deng *et al.* were mainly focussed on gas permeability and diffusion in their MOP-18 porous liquid membrane. Type 2 porous liquids have also been investigated computationally in a bid to better understand gas occupancy and selectivity in the systems.[64–66]

1.6   Type 3 porous liquids: heterogenous pore dispersions

Type 3 porous liquids have been described recently in the literature using a combination of solid porous framework materials, nanocrystalline zeolites and MOFs were proposed by O'Reilly *et al*, with some bulky excluded dispersant such as an ionic liquid or polymeric oil.[36] Design of the pore generator in type 3 porous liquids is less involved than in type 1 and 2 porous liquids, the main constraint for improving dispersibility is particle size, which, for example, has been well explored in MOFs recently due to their potential applications as chemical sensors, biological probes, and for preparation of membrane materials.[67] Selection of a dispersant requires more consideration, as it must be sufficiently bulky such that it won't infiltrate the pore network of the solid, although Cahir *et al.* recently showed that dispersants can be selected reasonably indiscriminately while still being effective for preparing porous liquids.[68]

Prior to the first report of type 3 porous liquids, an example composed of **ZIF-8** dispersed in an imidazole-modified poly(ethylene glycol) (PEG), which was shown to be effective as a hybrid absorbant-adsorpant for CO_2 in breakthrough experiments.[69]

The first report of a permanently microporous dispersion, or type 3 porous liquid, was a study investigating the use of a bulky IL ([DBU-PEG][NTf$_2$], Figure 1.11 a,b) as a dispersant for two zeolites, **ZSM-5** and Silicalite-1, as well as for a MOF, **ZIF-8**.[70] Significant gas uptake enhancement over the neat [DBU-PEG][NTf$_2$] was observed with all three solids, the most notable was that of the **ZIF-8** porous liquid due to the possibility of very high stable dispersion concentration (up to
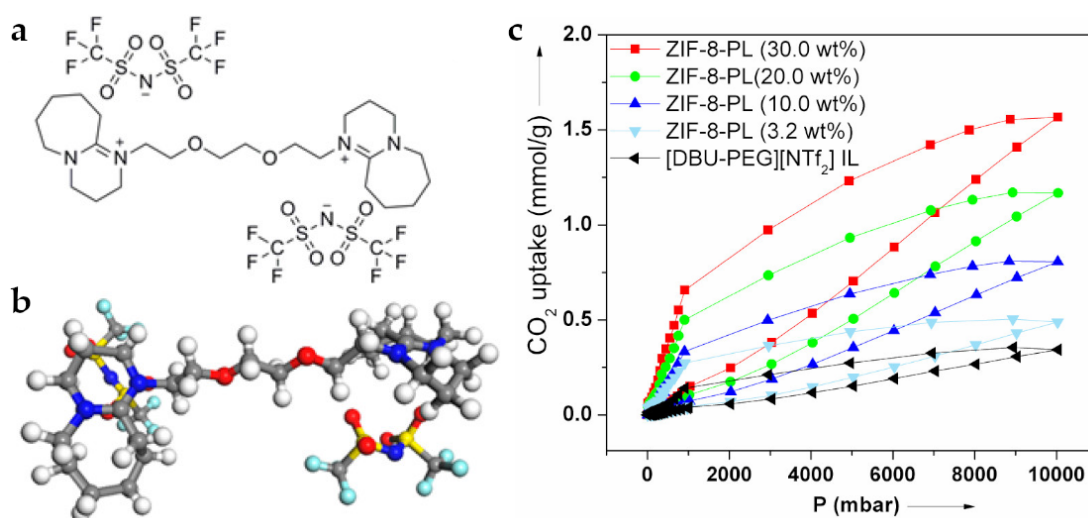
Figure 1.11: (**a**) Structure and (**b**) optimized molecular conformation of the IL used to prepare Shan's porous liquids, [DBU-PEG][NTf$_2$]. (**c**) Plot showing the gas uptake enhancement in the **ZIF-8**/[DBU-PEG][NTf$_2$] porous liquid at various dispersion concentrations compared to neat [DBU-PEG][NTf$_2$].[70]

30% wt) in [DBU-PEG][NTf$_2$]. At maximum loading, the **ZIF-8** dispersion has a CO$_2$ uptake of 1.54 mmol/g, *ca.* 5 times higher capacity than that of the neat [DBU-PEG][NTf$_2$]

Similar systems were reported by Liu *et al.*[71] and Costa Gomes *et al.*,[72] where microcrystalline **ZIF-8** was dispersed in other bulky ionic liquids expected to be excluded from the ZIF pore cavity. In these cases, the porosity was confirmed by PALS in the former, and by manometric gas sorption measurements in the latter, indicating this method is reasonably robust for finding fluid porous systems, largely owing to the small pore apertures in **ZIF-8** (3.4 Å) limiting access of molecules in the liquid phase. Costa Gomes *et al.* verified this by comparing the **ZIF-8** based porous liquid with the MOF **Mg-MOF-74** with has the single pore
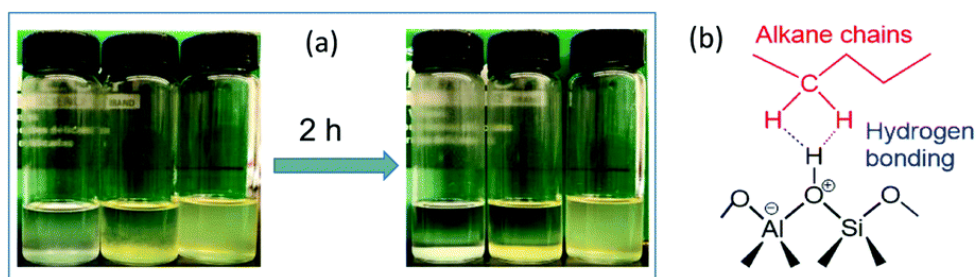
Figure 1.12: (**a**) **H-ZSM-5** nanoparticles (left), **Na-ZSM-5** porous liquid (center) and **H-ZSM-5** porous liquid dispersed in chloroform and after settling for 2 hours. (**b**) the hydrogen bonding interaction formed between the alkyl chains in the IL and the H atom at the surface of **H-ZSM-5** crystals.

channel diameter of 11 Å, which is comparable to the pore diameter in **ZIF-8** (11.6 Å). The **Mg-MOF-74** dispersion did not exhibit gas uptake enhancement, while the **ZIF-8** system did, showing the limited pore window was instrumental in enabling porosity.

Li *et al.* presented a system based on a zeolite, **H-ZSM-5**, which exploited the possibility of hydrogen bond formation with the molecules of an alkyl-functionalised ionic liquid at the surface of the zeolite crystals (Figure 1.12 b).[73] This resulted in the formation of a more stable dispersion when compared to the Na decorated equivalent zeolite (Figure 1.12 a). Similarly, Liu *et al.* synthesised another surface modified zeolite, based on silicalite-1, with ammonium containing organosilanes bonded to hydroxyl groups at the surface of the particles, enabling dispersion in a poly(ethylene glycol) sufonate (PEGS) to produce a porous liquid (Figure 1.13 a).[74] Porosity was confirmed by PALS. When dispersion was attempted in this liquid with the unmodified zeolite, no dispersion was formed.
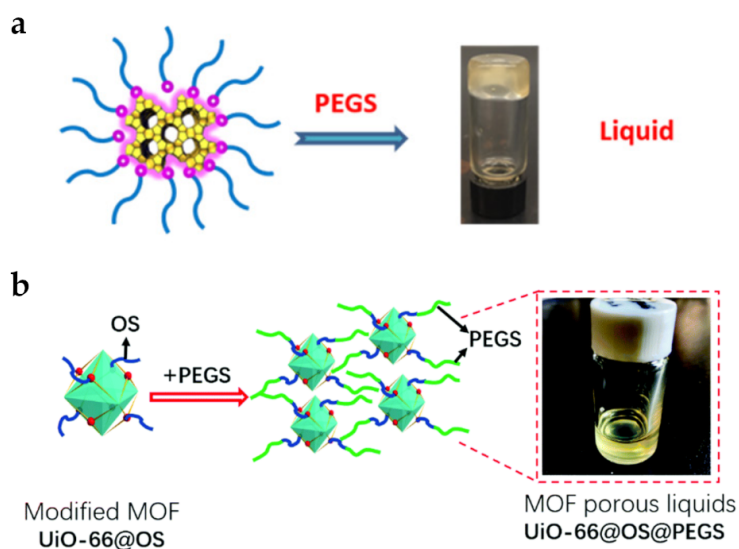
Figure 1.13: Porous liquids based on ammonium organosilane modification. (**a**) Silicalite-1 nanoparticles modified with ammonium organosilanes are dispersed in poly(ethylene glycol) sufonate (PEGS) to produce a porous liquid. (**b**) Ammonium organosilane modified UiO-66 nanocrystals are dispersed in PEGS to form a porous liquid.

Zhao *et al.* applied the same strategy to the MOF UiO-66, selecting a different positively charged organosilane to bind to the MOF surface to enable dispersion in PEGS. In all of these cases, CO_2 gas uptake enhancement was observed compared to the neat liquids, although control experiments were not carried out to account for any effect introducing the charged organosilane groups may have. These examples show that introducing favourable interactions at the interfaces in type 3 porous liquids can be used to improve dispersion stability and produce dispersions from microporous materials that may not be easily dispersed in their unmodified form.

Building upon these first works Cahir *et al.* demonstrated that a wide range of porous liquids can be produced by combining a variety of microporous materials with bulky non-ionic molecular and polymer liquids.[68] The researchers showed that its is possible to qualitatively screen for porosity in a large number of these systems, and that there are numerous examples that exhibit porosity as liquid dispersions. The group then chose specific examples and were able to demonstrate a proof of concept for gas adsorption separations with Al(fum)(OH) MOF dispersed in a silicone oil that could be used for significant CO_2 separation as part of a pressure-temperature swing process.

Mow *et al.* recently showed that permanent porosity can be developed in COF dispersions too, using controlled crystallisation to form colloidal COF-300 which could be stably dispersed in a bulky IL.[75] This material was confirmed as porous by gas soprtion experiments, as well as demonstration that the bulky IL used could not access the micropores when compared with less bulky derivatives. It was also demonstrated that cooling of porous liquids past their solid/liquid phase transition can be used to control release of gas when compared to the solid. Thermally programmed desorption experiments were carried out to show how the release of absorbed gas can be held to higher temperatures and lead to a more sustained release by trapping the gas by slowing the diffusion in the 'frozen' porous liquid (Figure 1.14).

Lai *et al.* have shown that type 3 porous liquids can be used for ethane/ethene separations by selecting specific solid phases with desired properties.[76] In this case, selection of a Ag containing zeolite was dispersed in an ionic liquid, much greater absorption capacity at low pressures was demonstrated, albeit with
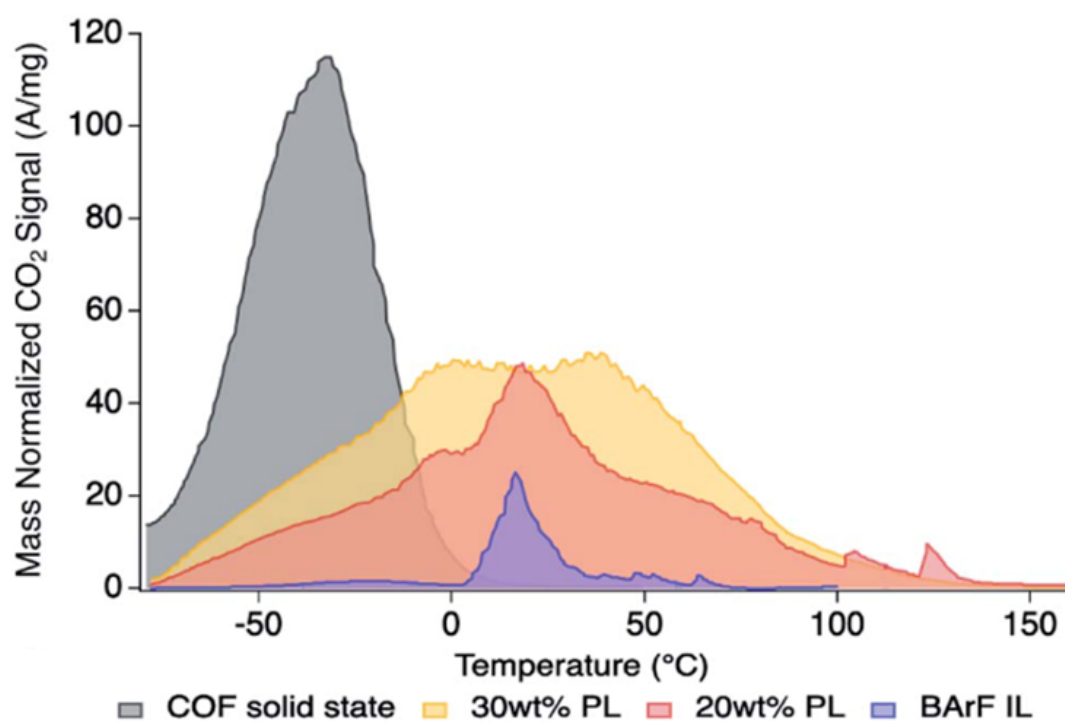
Figure 1.14: CO_2 thermally programmed desorption spectra of solid COF, neat BArF IL and the porous liquid at 20% w/v and 30% w/v.[75] The release of CO_2 in the solid occurs rapidly at a much lower temperature, whereas in the porous liquid, the release is skewed to much higher temperatures.

poorer selectivity than an IL control standard. Other porous liquids were also investigated, containing MOFs with open metal sites, which also demonstrated reasonable selectivies and promise for separation due to high capacity at lower working pressures.

1.7   Mesoporous liquids

Another example of porous liquids were the organosilane functionalised hollow silica spheres prepared by Zhang *et al.*[77] Similar concepts to those used in the preparation of type 1 porous liquids were applied here, but rather than basing their material around a microporous cage molecule, the researchers instead used larger hollow nanospheres with a much larger internal cavity, fitting into the category of mesopores, with a microporous surface that effectively excludes the organosilanes from the mesopore (Figure 1.15). These materials are colloidal rather than molecular, while still retaining a single pore; the particles in the liquids produced still contain a solid core and are fluidized by the coating of organosilane polymers. The porous liquid was shown to be effective as a membrane for separating CO_2 and N_2 in breakthrough experiments.

Another similar example from the same group was demonstrated, consisting of hollow carbon spheres with an imidazolium based polymer ionic liquid (IL) corona bound to the surface *via* π-π interaction between the cation and the carbon surface.[78] Other examples of these materials include surfactant modified silica nanorods[79] and encapsulation of Pt nanoparticles in silica nanosphere porous liquids as porous catalysts.[80]

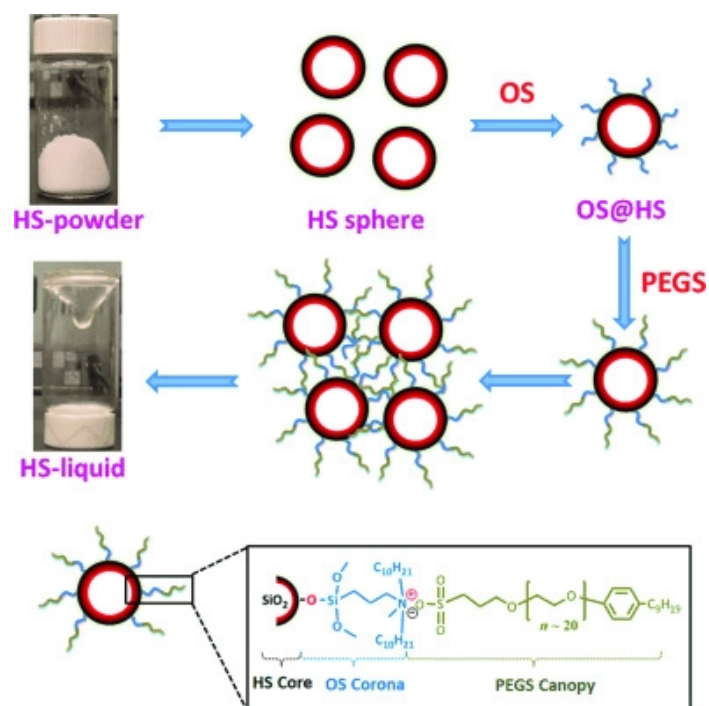**Figure 1.15:** Silica nanosphere based porous liquids developed by Zhang *et al.*[77] (Top) Synthetic route to producing the porous liquid, first coupling of the organosilane (OS) is carried out before addition of a cationic poly(ethylene) glycol. (Bottom) Molecular structure of the fluidising polymer corona as the surface of the silica nanospheres.

Ultimately these materials do not fit into the 3 categories of porous liquid outlined by O'Reilly *et al.* as they consist of solid particles with a single mesopore fluidized by some corona, *i.e.* not dispersed in a liquid phase.[36] This means that the system shares characteristics of both type 1 and type 3 porous liquids while fully fitting into neither.

1.8   Conclusions

While it has only been 6 years since the first publications of permanently porous liquids, there are now a multitude of techniques demonstrated for accessing these kinds of materials. Among the 3 types of porous liquids, we see similar fluidising methods applied crossing the different categories. Appending ionic or polymeric groups is effective in both fluidising molecular and colloidal porous materials, but also greatly improves cohesion between the fluid and porous components of type 2 and 3 porous liquids. So far, type 1 porous liquids are the least common, with only a single example of a permanently microporous type 1 porous liquid. This is due to the stringent set of requirements the material must meet, the material must be fluidized without the fluidising groups occupying adjacent cavities while also having a rigid enough core that remains porous in the liquid state. This combination of properties in a single molecule requires careful design and synthesis in order to successfully produce a type 1 porous liquid.

Type 3 porous liquids have been demonstrated as the most robust category of porous liquid, with several examples already being demonstrated as able to carry out gas separations. This is based on the vast library of already well

understood porous solid materials that can easily be transferred to a biphasic colloidal dispersion, transferring the properties of the microporous solid to a fluid system. We are already seeing targeted properties in porous liquids for specific separations in the case of Lai's porous liquid systems.[76]

Type 2 porous liquids have also received relatively little attention compared to the type 3 porous dispersions, with examples only existing based on the same series of imine [4+6] POCs and a single MOC. Challenges that remain include finding suitable solvents with little to no vapour pressure to carry out separations with reduced pressure without mass loss and contamination of gas mixtures. Since the properties of individual porous molecules in solution differ greatly from their porous solid counterparts, properties from the solid state cannot be selected and easily transferred to the porous liquid like with type 3 porous liquids. Thus, much more understanding of these systems is required to allow for design and targeting of specific properties to be feasible.

References

(1) P. Liu and G. Chen, in *Porous Materials*, 2014, pp. 1–20.

(2) R. Pronzato and R. Manconi, *Marine Ecology*, 2008, **29**, 146–166.

(3) V. K. Gupta and T. A. Saleh, *Environmental Science and Pollution Research*, 2013, **20**, 2828–2843.

(4) A. I. Cooper, *ACS Cent. Sci.*, 2017, **3**, 544–553.

(5) J. Rouquerol, D. Avnir, C. W. Fairbridge, D. H. Everett, J. M. Haynes, N. Pernicone, J. D. F. Ramsay, K. S. W. Sing and K. K. Unger, *Pure and Applied Chemistry*, 1994, **66**, 1739–1758.

(6) X.-Y. Yang, L.-H. Chen, Y. Li, J. C. Rooke, C. Sanchez and B.-L. Su, *Chem. Soc. Rev.*, 2017, **46**, 481–558.

(7) B.-L. Su, C. Sanchez and X.-Y. Yang, in *Hierarchically Structured Porous Materials*, Wiley-VCH Verlag GmbH & Co. KGaA, 2011, pp. 1–27.

(8) G. Férey, *Chem. Mater.*, 2001, **13**, 3084–3098.

(9) H. Oh and M. Hirscher, *European Journal of Inorganic Chemistry*, 2016, **2016**, 4278–4289.

(10) J. Yu, A. Corma and Y. Li, *Adv. Mater.*, 2020, **32**, 2006277.

(11) A. F. Cronstedt, *Kungl. Svenska vetenskapsakademiens handlingar.*, 1756, **17**, 120–123.

(12) S. Valencia and F. Rey, *New Developments in Adsorption/Separation of Small Molecules by Zeolites*, Springer, Cham, Switzerland, 2020.

(13) D. Wu, F. Xu, B. Sun, R. Fu, H. He and K. Matyjaszewski, *Chem. Rev.*, 2012, **112**, 3959–4015.

(14) M. A. Little and A. I. Cooper, *Adv. Funct. Mater.*, 2020, **30**, 1909842.

(15) Y. Ma, W. Tong, H. Zhou and S. L. Suib, *Microporous and Mesoporous Materials*, 2000, **37**, 243–252.

(16) A. I. Cooper, *Adv. Mater.*, 2009, **21**, 1291–1295.

(17) M. Liu, L. Guo, S. Jin and B. Tan, *J. Mater. Chem. A*, 2019, **7**, 5153–5172.

(18) P. M. Budd, B. S. Ghanem, S. Makhseed, N. B. McKeown, K. J. Msayib and C. E. Tattershall, *Chem. Commun.*, 2004, 230–231.

(19) N. B. McKeown, *Organic Materials*, 2020, **02**, 020–025.

(20) H. Furukawa, K. E. Cordova, M. O'Keeffe and O. M. Yaghi, *Science*, 2013, **341**, 1230444.

(21) R. Chakrabarty, P. S. Mukherjee and P. J. Stang, *Chem. Rev.*, 2011, **111**, 6810–6918.

(22) L. Chen, P. S. Reiss, S. Y. Chong, D. Holden, K. E. Jelfs, T. Hasell, M. A. Little, A. Kewley, M. E. Briggs, A. Stephenson, K. M. Thomas, J. A. Armstrong, J. Bell, J. Busto, R. Noel, J. Liu, D. M. Strachan, P. K. Thallapally and A. I. Cooper, *Nat Mater*, 2014, **13**, 954–960.

(23) A. J. Gosselin, C. A. Rowland and E. D. Bloch, *Chem. Rev.*, 2020, **120**, 8987–9014.

(24) J. R. Holst, A. Trewin and A. I. Cooper, *Nature Chemistry*, 2010, **2**, 915–920.

(25)   T. Ben, H. Ren, S. Ma, D. Cao, J. Lan, X. Jing, W. Wang, J. Xu, F. Deng, J. M. Simmons, S. Qiu and G. Zhu, *Angew. Chem. Int. Ed.*, 2009, **48**, 9457–9460.

(26)   D. Yuan, W. Lu, D. Zhao and H.-C. Zhou, *Adv. Mater.*, 2011, **23**, 3723–3725.

(27)   M. Safaei, M. M. Foroughi, N. Ebrahimpoor, S. Jahani, A. Omidi and M. Khatami, *TrAC, Trends Anal. Chem.*, 2019, **118**, 401–425.

(28)   K. Geng, T. He, R. Liu, S. Dalapati, K. T. Tan, Z. Li, S. Tao, Y. Gong, Q. Jiang and D. Jiang, *Chem. Rev.*, 2020, **120**, 8814–8933.

(29)   J. T. A. Jones, D. Holden, T. Mitra, T. Hasell, D. J. Adams, K. E. Jelfs, A. Trewin, D. J. Willock, G. M. Day, J. Bacsa, A. Steiner and A. I. Cooper, *Angewandte Chemie - International Edition*, 2011, **50**, 749–753.

(30)   T. Tozawa, J. T. a. Jones, S. I. Swamy, S. Jiang, D. J. Adams, S. Shakespeare, R. Clowes, D. Bradshaw, T. Hasell, S. Y. Chong, C. Tang, S. Thompson, J. Parker, A. Trewin, J. Bacsa, A. M. Z. Slawin, A. Steiner and A. I. Cooper, *Nature materials*, 2009, **8**, 973–978.

(31)   D. Holden, S. Y. Chong, L. Chen, K. E. Jelfs, T. Hasell and A. I. Cooper, *Chemical Science*, 2016, **7**, 4875–4879.

(32)   S. Jiang, J. T. a. Jones, T. Hasell, C. E. Blythe, D. J. Adams, A. Trewin and A. I. Cooper, *Nature communications*, 2011, **2**, 207.

(33)   R. Gaillac, P. Pullumbi, K. A. Beyer, K. W. Chapman, D. A. Keen, T. D. Bennett and F.-X. Coudert, *Nat. Mater.*, 2017, **16**, 1149–1154.

(34) T. D. Bennett, Y. Yue, P. Li, A. Qiao, H. Tao, N. G. Greaves, T. Richards, G. I. Lampronti, S. A. T. Redfern, F. Blanc, O. K. Farha, J. T. Hupp, A. K. Cheetham and D. A. Keen, *J. Am. Chem. Soc.*, 2016, **138**, 3484–3492.

(35) C. Zhou, L. Longley, A. Krajnc, G. J. Smales, A. Qiao, I. Erucar, C. M. Doherty, A. W. Thornton, A. J. Hill, C. W. Ashling, O. T. Qazvini, S. J. Lee, P. A. Chater, N. J. Terrill, A. J. Smith, Y. Yue, G. Mali, D. A. Keen, S. G. Telfer and T. D. Bennett, *Nat. Commun.*, 2018, **9**, 5042.

(36) N. O'Reilly, N. Giri and S. L. James, *Chemistry - A European Journal*, 2007, **13**, 3020–3025.

(37) A. Pohorille and L. R. Pratt, *Journal of the American Chemical Society*, 1990, **112**, 5066–74.

(38) G. Graziano, *Biophysical Chemistry*, 2003, **104**, 393–405.

(39) B. A. Lindquist, R. B. Jadrich and T. M. Truskett, *Soft Matter*, 2016, **12**, 2663–2667.

(40) A. Chiba, M. Inui, Y. Kajihara, K. Fuchizaki and R. Akiyama, *J. Chem. Phys.*, 2017, **146**, 194503.

(41) A. Chiba, N. Funamori, K. Nakayama, Y. Ohishi, S. M. Bennington, S. Rastogi, A. Shukla, K. Tsuji and M. Takenaka, *Physical Review E - Statistical, Nonlinear, and Soft Matter Physics*, 2012, **85**, 2–6.

(42) G. Shen, Q. Mei, V. B. Prakapenka, P. Lazor, S. Sinogeikin, Y. Meng and C. Park, *Proceedings of the National Academy of Sciences of the United States of America*, 2011, **108**, 6004–6007.

(43)   S. L. James, *Advanced Materials*, 2016, **28**, 5712–5716.

(44)   P. F. Fulvio and S. Dai, *Chem*, 2020, **6**, 3263–3287.

(45)   T. D. Bennett, F.-X. Coudert, S. L. James and A. I. Cooper, *Nat. Mater.*, 2021, DOI: `10.1038/s41563-021-00957-w`.

(46)   K. Jie, Y. Zhou, H. P. Ryan, S. Dai and J. R. Nitschke, *Adv. Mater.*, 2021, **33**, 2005745.

(47)   A. Bavykina, A. Cadiau and J. Gascon, *Coordination Chemistry Reviews*, 2019, **386**, 85–95.

(48)   N. Giri, C. E. Davidson, G. Melaugh, M. G. Del Pópolo, J. T. a. Jones, T. Hasell, A. I. Cooper, P. N. Horton, M. B. Hursthouse and S. L. James, *Chemical Science*, 2012, **3**, 2153.

(49)   H. Kim, Y. Nguyen, C. P.-H. Yen, L. Chagal, A. J. Lough, B. M. Kim and J. Chin, *J. Am. Chem. Soc.*, 2008, **130**, 12184–12191.

(50)   G. Melaugh, N. Giri, C. E. Davidson, S. L. James and M. G. Del Pópolo, *Physical chemistry chemical physics : PCCP*, 2014, **16**, 9422–31.

(51)   M. C. Brand, F. Greenwell, R. Clowes, B. D. Egleston, A. Kai, A. I. Cooper, T. D. Bennett and R. L. Greenaway, *J. Mater. Chem. A*, 2021, DOI: `10.1039/D1TA01906F`.

(52)   L. Ma, C. J. E. Haynes, A. B. Grommet, A. Walczak, C. C. Parkins, C. M. Doherty, L. Longley, A. Tron, A. R. Stefankiewicz, T. D. Bennett and J. R. Nitschke, *Nature Chemistry*, 2020, **12**, 270–275.

(53) D. Zheng, L. Dong, W. Huang, X. Wu and N. Nie, *Renewable Sustainable Energy Rev.*, 2014, **37**, 47–68.

(54) S. S. Braga, *Biomolecules*, 2019, **9**, 801.

(55) T. E. Achkar, T. Moufawad, S. Ruellan, D. Landy, H. Greige-Gerges and S. Fourmentin, *Chem. Commun.*, 2020, **56**, 3385–3388.

(56) Y. Wang, Y. Sun, H. Bian, L. Zhu, D. Xia and H. Wang, *ACS Appl. Mater. Interfaces*, 2020, **12**, 45928.

(57) M. E. Tanner, C. B. Knobler and D. J. Cram, *J. Am. Chem. Soc.*, 1990, **112**, 1659–1660.

(58) N. Giri, M. G. Del Pópolo, G. Melaugh, R. L. Greenaway, K. Rätzke, T. Koschine, L. Pison, M. F. C. Gomes, A. I. Cooper and S. L. James, *Nature*, 2015, **527**, 216–220.

(59) R. L. Greenaway, D. Holden, E. G. B. Eden, A. Stephenson, C. W. Yong, M. J. Bennison, T. Hasell, M. E. Briggs, S. L. James and A. I. Cooper, *Chem. Sci.*, 2017, **8**, 2640–2651.

(60) R. J. Kearsey, B. M. Alston, M. E. Briggs, R. L. Greenaway and A. I. Cooper, *Chem. Sci.*, 2019, **10**, 9454–9465.

(61) K. Jie, N. Onishi, J. A. Schott, I. Popovs, D.-e. Jiang, S. Mahurin and S. Dai, *Angewandte Chemie*, 2020, **132**, 2288–2292.

(62) Z. Deng, W. Ying, K. Gong, Y.-j. Zeng, Y. Yan and X. Peng, 2020, **1907016**, 1–6.

(63) H. Furukawa, J. Kim, K. E. Plass and O. M. Yaghi, *J. Am. Chem. Soc.*, 2006, **128**, 8398–8399.

(64) F. Zhang, F. Yang, J. Huang, B. G. Sumpter and R. Qiao, *The Journal of Physical Chemistry B*, 2016, **120**, 7195–7200.

(65) P. Zhang and S. Dai, *J. Mater. Chem. A*, 2017, **5**, 16118–16127.

(66) M. Atilhan, A. Cincotti and S. Aparicio, *J. Mol. Liq.*, 2021, **330**, 115660.

(67) S. Wang, C. M. McGuirk, A. D'Aquino, J. A. Mason and C. A. Mirkin, *Adv. Mater.*, 2018, **30**, 1800202.

(68) J. Cahir, M. Y. Tsang, B. Lai, D. Hughes, M. A. Alam, J. Jacquemin, D. Rooney and S. L. James, *Chem. Sci.*, 2020, **11**, 2077–2084.

(69) H. Liu, B. Liu, L.-C. Lin, G. Chen, Y. Wu, J. Wang, X. Gao, Y. Lv, Y. Pan, X. Zhang, X. Zhang, L. Yang, C. Sun, B. Smit and W. Wang, *Nature Communications*, 2014, **5**, 5147.

(70) W. Shan, P. F. Fulvio, L. Kong, J. A. Schott, C. L. Do-Thanh, T. Tian, X. Hu, S. M. Mahurin, H. Xing and S. Dai, *ACS Applied Materials and Interfaces*, 2018, **10**, 32–36.

(71) S. Liu, J. Liu, X. Hou, T. Xu, J. Tong, J. Zhang, B. Ye and B. Liu, *Langmuir*, 2018, **34**, 3654–3660.

(72) M. Costa Gomes, L. Pison, C. Červinka and A. Padua, *Angewandte Chemie - International Edition*, 2018, **57**, 11909–11912.

(73) P. Li, H. Chen, J. A. Schott, B. Li, Y. Zheng, S. M. Mahurin, D. E. Jiang, G. Cui, X. Hu, Y. Wang, L. Li and S. Dai, *Nanoscale*, 2019, **11**, 1515–1519.

(74) Y. Liu, Y. Bai and T. Tian, *Materials*, 2019, **12**, 3984.

(75) R. E. Mow, A. S. Lipton, S. Shulda, E. A. Gaulding, T. Gennett and W. A. Braunecker, *J. Mater. Chem. A*, 2020, **8**, 23455–23462.

(76) B. Lai, J. Cahir, M. Y. Tsang, J. Jacquemin, D. Rooney, B. Murrer and S. L. James, *ACS Appl. Mater. Interfaces*, 2021, **13**, 932–936.

(77) J. Zhang, S. H. Chai, Z. A. Qiao, S. M. Mahurin, J. Chen, Y. Fang, S. Wan, K. Nelson, P. Zhang and S. Dai, *Angewandte Chemie - International Edition*, 2015, **54**, 932–936.

(78) P. Li, J. A. Schott, J. Zhang, S. M. Mahurin, Y. Sheng, Z.-A. Qiao, X. Hu, G. Cui, D. Yao, S. Brown, Y. Zheng and S. Dai, *Angew. Chem. Int. Ed.*, 2017, **56**, 14958–14962.

(79) R. Kumar, P. Dhasaiyan, P. M. Naveenkumar and K. P. Sharma, *Nanoscale Advances*, 2019, **1**, 4067–4075.

(80) E. B. Hemming, A. F. Masters and T. Maschmeyer, *Chem. Eur. J.*, 2020, **26**, 7059–7064.
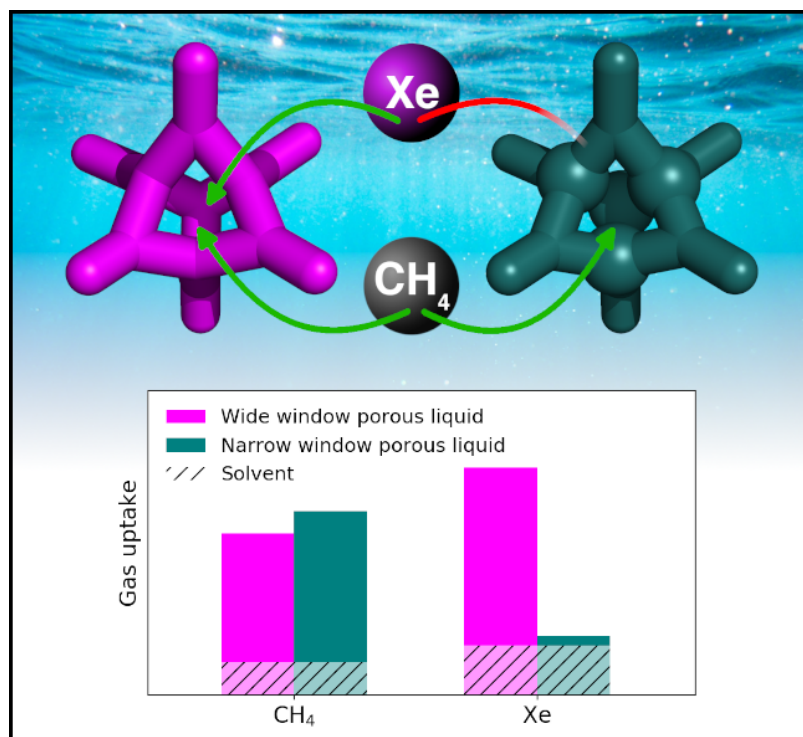
2 Controlling porosity in type 2 porous liquids

Preparations of porous liquids based on imine POCs presented before this work do not attempt to control the gas selectivity by tuning the molecular pore. Instead, they target structures with various vertex groups designed to improve solubility.[1–3] Further structural modification has been carried out *via* a variety of methods in microporous solids, in particular using the inclusion of sterically hindering groups to modify the binding and diffusion of small molecules in the porous material. Herein, this concept has been applied to a porous liquid, by investigating other POCs that introduce modified cage portals and cavity. The gas uptake in the materials was subsequently examined and NMR techniques were applied to further elucidate the gas uptake behaviour and properties of these porous liquids.

2.1   Controlling pore size in microporous solids

Modifying and controlling pore diameter and functionality in microporous solids has been carried out in a multitude of ways. Some MOFs can be prepared in such a way that they have continuously adjustable pore diameters, making a single material potentially applicable to a variety of separations.[4] More commonly, synthetic or post-synthetic modification techniques have been used in MOFs and COFs to allow for the modification and tuning of pore diameter in these microporous materials. In the case of 2- and 3-dimensional microporous framework solids, the use of reticular chemistry; i.e. modification of the linking, repeating units in a material; allows for a hugely diverse range of different materials based on the same base network topology.[5] Alternatively, introduction of appended groups to the linkers in COFs and MOFs has been used frequently to control the pore diameter and chemical properties of the pore interior. For example, isoreticular analogues of MOF-5 can be prepared with a huge number of pendant groups, which not only reduce the available space in the pore network but also introduce different chemical functionality within the pore.[6] In this study, Eddaoudi *et al.* found introduction of alkoxy groups to the MOF linkers greatly reduced total pore volume in the produced MOFs (Figure 2.1) and very significantly hindered accessibility by reducing the size of the portals in the pore network.

A similar effect was observed by Tilford *et al.* in an isoreticular COF series by including increasing sized alkyl groups which occupy more and more volume within the pore network.[7] As the incorporated alkyl chain increased in size, the
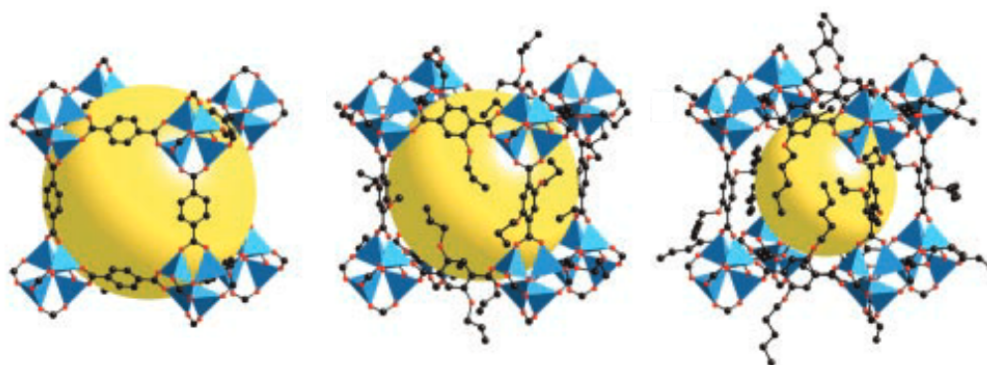
Figure 2.1: Eddaoudi's isoreticular MOFs: MOF-5, IRMOF-3 and IRMOF-4.[6] Introduction of propoxy and pentoxy groups in IRMOF-3 and IRMOF-4 reduce the pore size (yellow sphere).

pore diameter decreased from 18 Å to 16 Å, 14 Å and 11 Å when methyl, ethyl and propyl groups were introduced, respectively (Figure 2.2 a). Introducing these groups and reducing the pore size greatly reduces the affinity of larger adsorbants, for example, tetrahydrofuran (THF) was found to be excluded from the cavity in the 14 Å and 11 Å COFs while it is retained in the 18 Å and 16 Å COFs. This also greatly impacted the N_2 and H_2 capacities, the larger cavity sized COFs taking up appreciably more N_2 while the smallest 11 Å COF adsorbed much more H_2 than all the COFs with larger pores (Figure 2.2 b).

This concept has been applied in the field of POCs in the preparation of isoreticular nanotubes[8] and isoreticular quasiracemates based on isostructural cages.[9] In the case of the nanotubes, the organic cages were prepared by varying the length of the tetraldehyde, while the quasiracemates vary in the alkyl group at the cage molecules' vertices. In the solid crystals prepared from these POCs, the
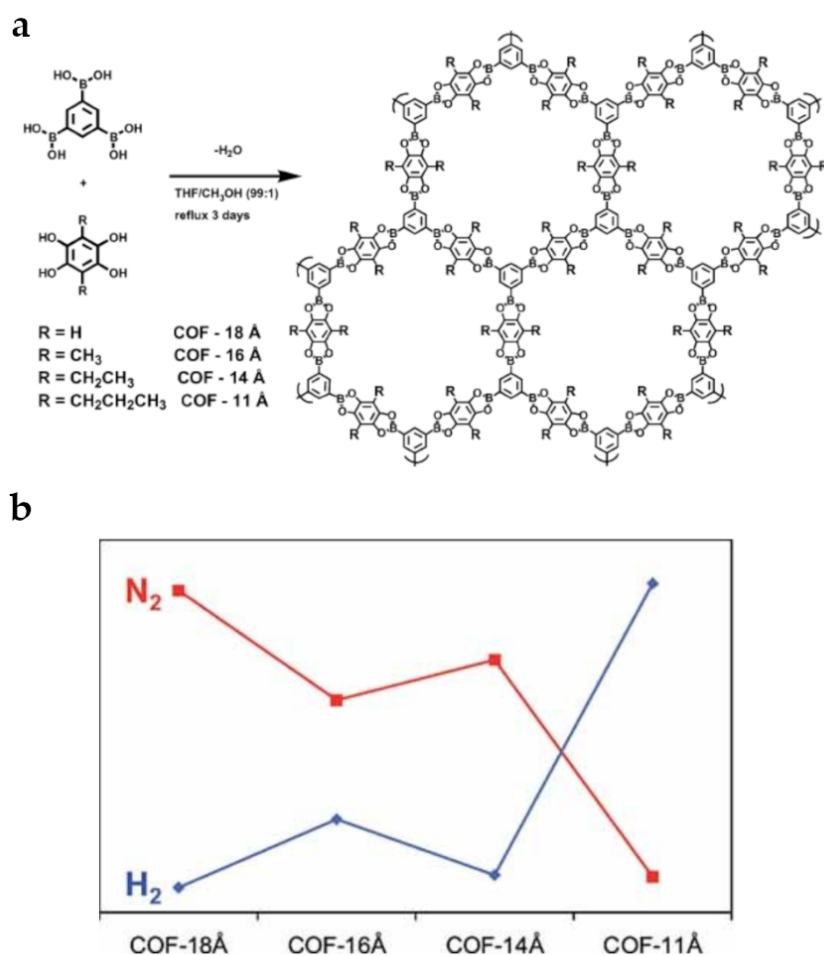
Figure 2.2:   Tilford's isoreticular boronate ester COFs.[7] (**a**) Synthesis and structure of the COF series with increasing sized R groups included in the pore cavity. (**b**) Normalised gas uptake of N_2 and H_2 for each of these COFs.

pore size varies along the axes of the crystals' unit cells. The nanotubes extend the pore dimension (Figure 2.3 a, left to right) in one direction with inclusion of longer linking groups. In the quasiracemates, the inclusion of cages with different vertex groups shrinks the unit cell size along all dimensions (Figure 2.3 b, left to right) due to the effect the vertex groups have on intermolecular packing. Despite the utility

of this type of structural modification, it relies ultimately on the crystal structure to modulate porosity, so cannot be imagined to transfer to a porous liquid.

a

b
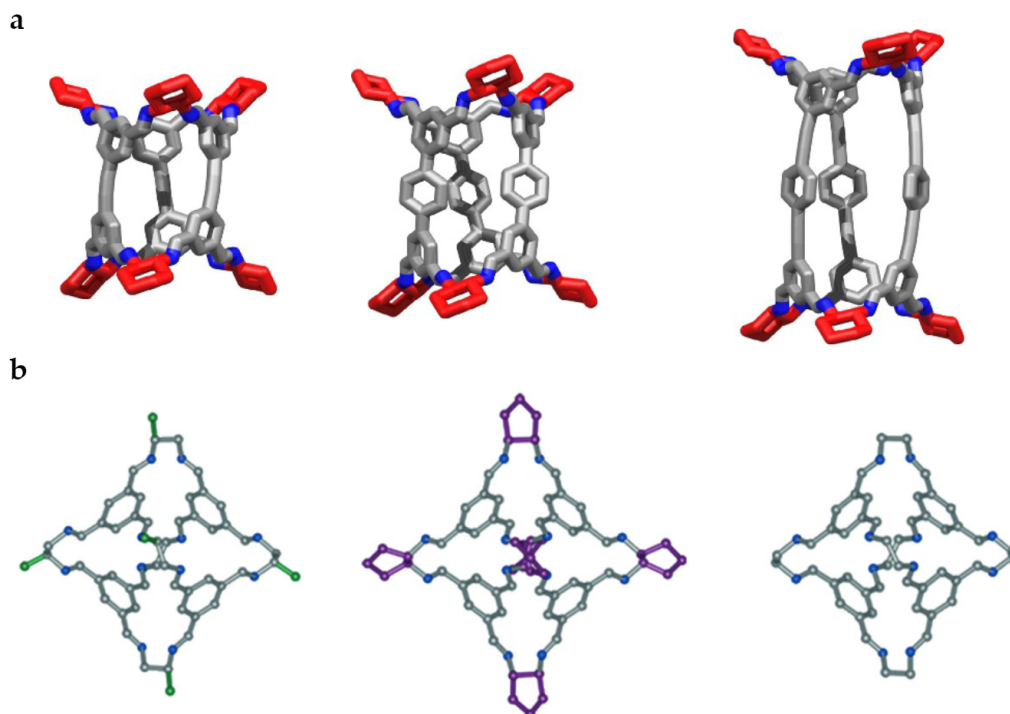
Figure 2.3: Isostructural cages used to prepare (**a**) Slater's nanorods[8] and (**b**) Tothadi's quasiracemic cocrystals[9], both solids have isoreticular structures as the crystal structures are extended or shortened along the length of the nanorods in (**a**) and in all three dimensions in (**b**) due to the bulk of the vertex groups.

Although the principles of isoreticular chemistry seem to not apply to the 0-dimensional molecular cages used in porous liquids, we have seen how these can be transferred to reticular chemistry in the multi-dimensional crystal structures that these molecules form. While this means we cannot directly apply the ideas of reticular chemistry to porous liquids, many of the pore-modification techniques employed allow us to understand how we can use different functionalities to

modulate gas uptake in microporous materials in general.

2.2   Type 2 porous liquids based on porous organic cages (POCs)

Of the type 2 porous liquids prepared before this work, the systems based on organic cages focus on using the tuneable vertex functionality to enable good solubility. Giri's porous liquid adds large crown-ether solubilising groups to the cage periphery,[1] Greenaway exploited the disrupted packing that arises due to 'scrambling' the vertices in POCs that enables good solubility,[2] and Jie *et al.* add potassium as a counter ion to a vertex group in their cage in order to introduce solubility.[3] In all these cases, the geometry of the cage molecular pore are unmodified. Conversely, in the solid state, introducing new functional groups to the inner structure of organic cages has been explored, and can lead to huge modifications to porosity, even allowing for reduction of pore size to the extent that these materials can be used for H_2/D_2 separations.[10] While the introduction of occluding groups to pores in solid microporous materials had been shown as an effective technique for tuning gas uptake, this has not been attempted in a porous liquid. Since the molecular pore in these organic cages is retained upon dissolution, these properties can be transferred to porous liquids.

2.3   Sterically altering the pore diameter in a porous liquid

In order to find an applicable system to test this effect in porous liquids we can look to POCs already used to demonstrate this in the solid state. In order to achieve this, we chose to take the porous liquid system originally developed by Greenaway *et*

al.[2] and selected structurally analogous POCs that could be used to modify the pore, namely **CC15**-*R* which includes window occluding methyl groups.[11] **CC15** was found to be soluble in the size excluded solvent perchloropropene (PCP) at up to 50 mg in 1 mL. While this is only 25% of that observed for Greenaway's scrambled cage, **CC3³:13³**-*R*, it is a high enough concentration to be investigated as a porous liquid. A sufficient concentration of cage in the porous liquids is needed for the gas uptake in the porous system to be significantly higher than the native solvent concentration so that the errors in measurements do not have a significant impact. Since the scrambled **CC3³:13³**-*R* mixture and Slater's POC **CC15**-*R* are both analogues of the same [4+6] structure, and are both highly soluble in PCP, we can use them to create type 2 porous liquids with differing pore windows. Both of these POCs were synthesised easily according to their preparations reported in the literature (Scheme 2.1).

Synthesis of a scrambled POC mixture analogous to **CC15**-*R* was attempted, combining the amine precursors used in the preparation of **CC3³:13³**-*R* with the triketone used to synthesise **CC15**-*R*, in an attempt to improve on solubility of **CC15**-*R* while retaining the CH_3 groups occluding the cage windows (Scheme 2.1). The reaction was carried out in $CHCl_3$ to allow for a higher reflux temperature to improve the effectiveness of using a reverse Dean-Stark apparatus to eliminate water (Scheme 2.2). high-performance liquid chromatography (HPLC) analysis revealed formation of only **CC15**-*R* in the crude reaction mixture, no other scrambled cage species was formed. This suggests that the CH_3 groups in the triketone, 1,3,5-triacetylbenzene, clash sterically with the two CH_3 groups in the diamine, 1,2-diamino-2-methylpropane, making formation of the imine bond
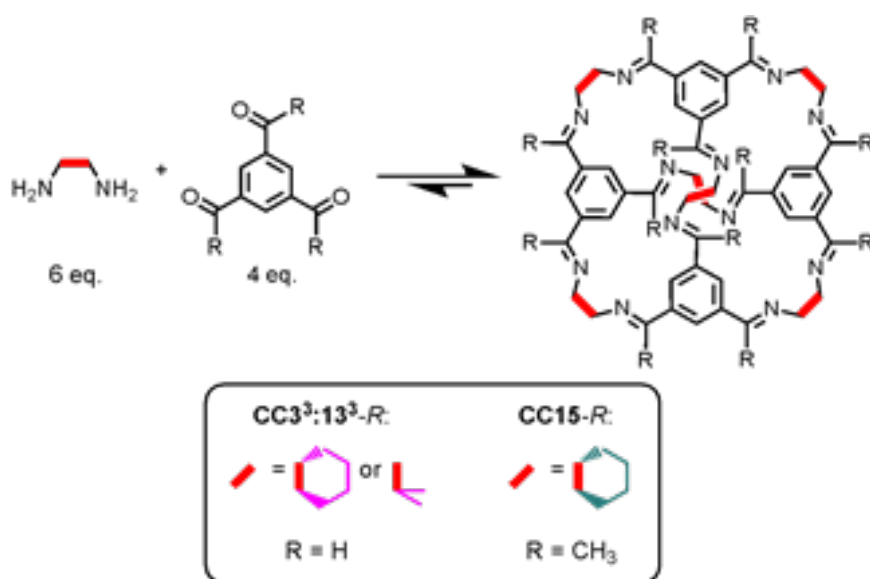
Scheme 2.1: Synthesis of POCs used to form type 2 porous liquids. Conditions: (**CC3³:13³-**
R) dichloromethane (DCM), room temperature, 72 h; (**CC15**-*R*) DCM, 3Å molecular sieves,
50 °C, reverse Dean Stark, 24 h.

highly unfavourable despite the harsher reaction conditions, inhibiting formation
of a POC based on the two incompatible precursors.
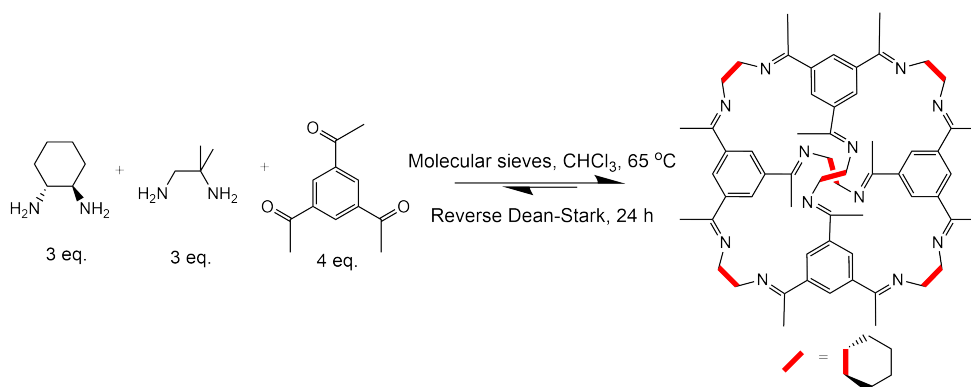
Scheme 2.2: Attempting the synthesis of a scrambled cage analogue of **CC15**-*R*: formation
of only **CC15**-*R* occurred.

Since the inclusion of additional methyls in **CC15**-*R* is the main difference
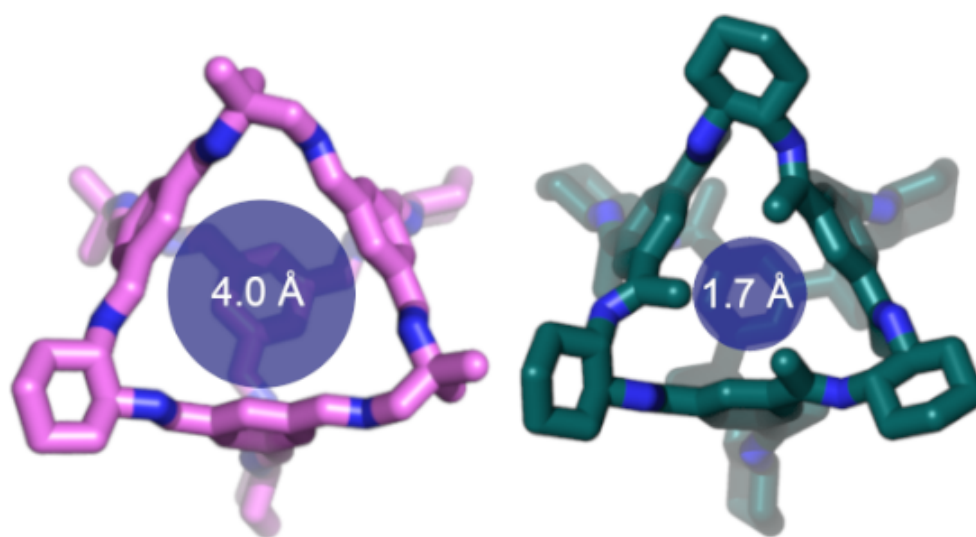
Figure 2.4: Structures of the *trans*-3^3:13^3 component of the scrambled cage mixture **CC3^3:13^3**-*R* (magenta, left) and **CC15**-*R* (teal, right) labelled with their respective pore window diameters calculated using the `pywindow` package.[12]

between the pores in these two POCs, appearing at the rim of each portal to the cage's cavity, we used `pywindow`[12] to determine the extent to which the cage windows and cavities are restricted. `pywindow` is an open source python package for analysing the structure of molecular pores. It was found that the addition of the methyl groups reduce the pore window size from 4.0 Å in **CC3^3:13^3**-*R* to just 1.7 Å in **CC15**-*R* (Figure 2.4). Moreover, the methyl groups also slightly restrict the inner cavity diameter (OPT pore size calculated: **CC3^3:13^3**-*R* 5.85 Å, **CC15**-*R* 4.61 Å).

An idea of the extent to which the gas uptake is modified by the inclusion of the CH$_3$ groups in **CC15**-*R* compared to **CC3^3:13^3**-*R* can be seen when comparing the N$_2$ sorption isotherms of the solid POCs at 77 K (Figure 2.5). In the solid state, N$_2$ uptake in **CC15**-*R* is effectively switched off when compared to **CC3^3:13^3**-*R*

(Figure 2.5). While this comparison is extreme, it should be noted that **CC3³:13³**-*R* and **CC15**-*R* have drastically different crystal packing structures, while **CC3³:13³**-*R* is amorphous, **CC15**-*R* packs in a configuration that also limits access of gas molecules to the molecular pore. **CC15**-*R* still absorbs smaller gas molecules, such as H_2. In order to compare these porous liquids directly, they were prepared at equimolar concentration in PCP (39 μmol$_{cage}$ in 1 mL$_{PCP}$): **CC3³:13³**-*R* at 4% w/v (40 mg$_{cage}$ in 1 mL$_{PCP}$) and **CC15**-*R* at 5% w/v (50 mg$_{cage}$ in 1 mL$_{PCP}$).
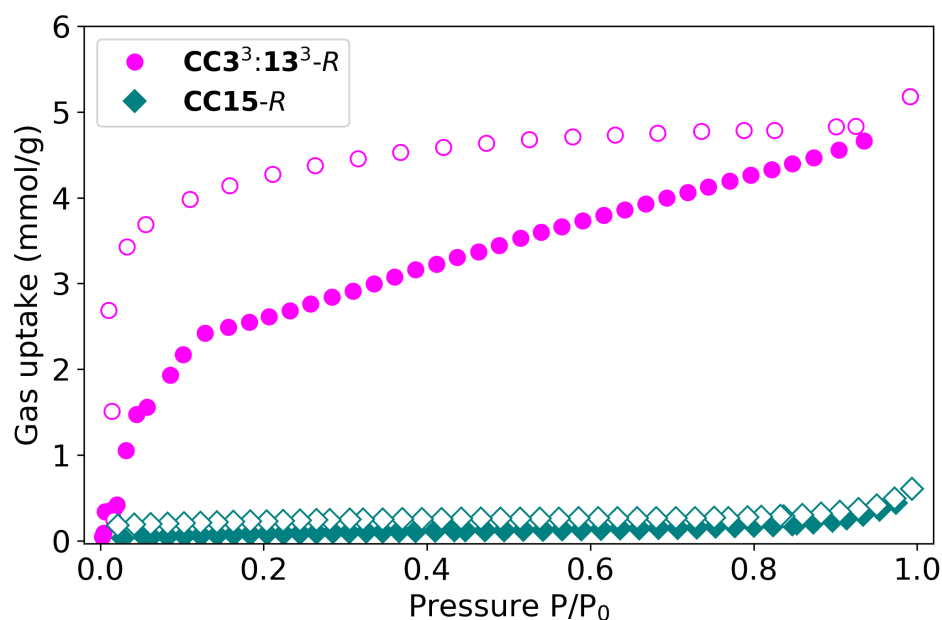
Figure 2.5: N_2 adsorption (filled) and desorption (empty) isotherms for **CC3³:13³**-*R* and **CC15**-*R* in the solid state at 77 K .

2.4   Gas uptake measurements

Gas evolution measurements were carried out on both of the new type 2 porous liquid systems to compare any accentuation of gas absorption and the differences between the two porous liquids. This was determined using the guest displacement method[2] where addition of a small guest, $CHCl_3$, to the gas loaded porous liquid triggers evolution of the gas contained within the cavities. The technique was verified previously using diffusion NMR experiments by Greenaway *et al.*,[2] showing that the chloroform molecule readily occupied the cavities in the POCs that constitute the porous liquids. This method was used to find the uptake capacity of CH_4, CO_2, Xe and N_2 initially to determine the effect changing the window diameter had on uptake of small gases (Figure 2.6). Due to the lower cage concentration in the porous liquids in this instance, the uptakes measured were significantly lower than those measured by Greenaway *et al.* previously. For example, the CH_4 uptake in the **CC3³:13³**-*R* porous liquid at 4% w/v was 11.7 μmol/g_{PL}, *ca.* 4 times less than the uptake in this porous liquid at 20% w/v.

Nitrogen uptake improvement in both porous liquids was low when compared to the neat solvents, reflecting observations at higher cage concentrations (Figure 2.6). When comparing the **CC3³:13³**-*R* and **CC15**-*R* porous liquids, the difference between the two in N_2 uptake improvement compared to solvent is negligible. For the other gases, even at this lower cage concentration, the gas solubilities were much higher. Gas uptake improvement was up to 5.5 fold over the neat solvent in the case of Xe in the **CC3³:13³**-*R* porous liquid, with significant differences between
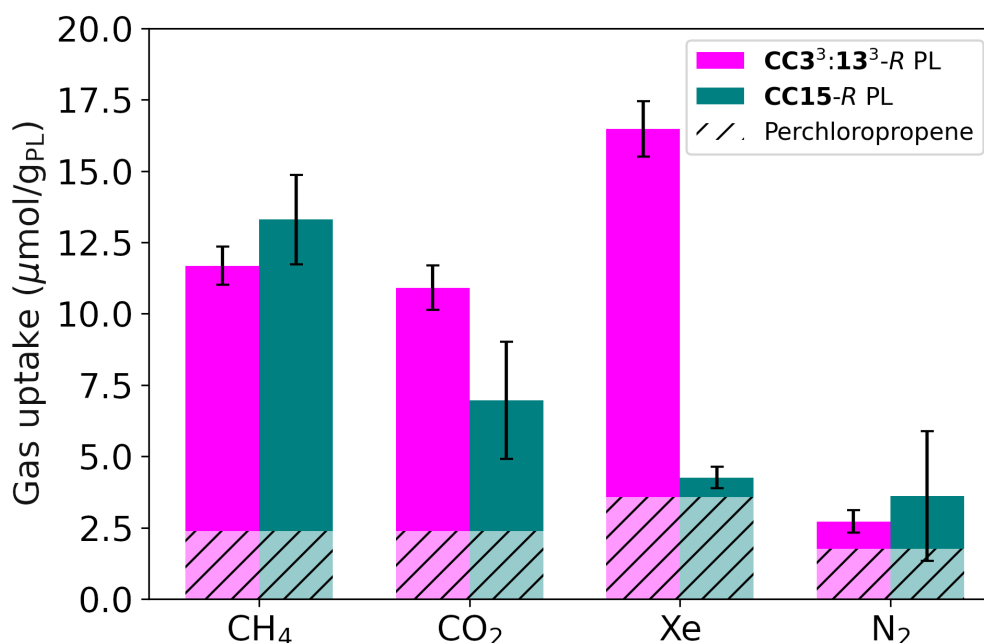
Figure 2.6: Gas uptake, as measured by the volumetric gas evolution technique, for CH_4, CO_2, Xe and N_2 in the **CC3^3:13^3**-*R* (magenta) and **CC15**-*R* (teal) porous liquids compared with the native gas uptake in the neat solvent, PCP. **CC3^3:13^3**-*R* porous liquid at 4% w/v and **CC15**-*R* porous liquid at 5% w/v. Each value is the average of 3 measurements with standard error shown as error bars.

the two systems.

Of the small gases investigated here, the **CC3^3:13^3**-*R* porous liquid absorbed more Xe than the other gases, mirroring the strong thermodynamic preference for Xe observed previously in these POCs.[13] In the **CC15**-*R* porous liquid however, this is completely lost. The Xe uptake in the **CC3^3:13^3**-*R* porous liquid (16.6 μmol/g$_{PL}$) was almost 4 times greater than in the **CC15**-*R* porous liquid (4.3 μmol/g$_{PL}$), indicating that the absorption of Xe that occurs in the pores of the **CC3^3:13^3**-*R* porous liquid does not in the **CC15**-*R* porous liquid. This is due to the presence of

the methyl groups around the cage portals, which both restricts the access to the internal cavity of the POCs in solution and reduces the cavity volume.

To confirm this was not a kinetic effect, where the Xe gas can occupy the cage cavities if exposed for an extended period of time, a **CC15**-*R* porous liquid sample was saturated repeatedly over 6 hours while in a sealed vial to ensure Xe exposure was maximised and allowed to equilibrate (Table 2.1). Even after this longer exposure, no more gas was absorbed than after a single exposure.

Table 2.1: Measured gas release for Xe from the **CC15**-*R* porous liquid when saturated once *vs.* several times.

Saturation	Volume Evolved (mL)	Mean Volume Evolved (mL)	Gas Uptake (μmol/g$_{PL}$)
Single	0.55		
	0.5	0.55 ± 0.05	4.25 ± 0.39
	0.6		
Hourly over 6 hours	0.5	0.5	3.87

Beyond this, the **CC15**-*R* porous liquid absorbs CH_4 most preferentially of the gases studied and at a higher capacity than the **CC3³:13³**-*R* porous liquid. While the **CC3³:13³**-*R* PL has preference for Xe, the **CC15**-*R* porous liquid shows uptake preference for CH_4. In order to investigate this further, ^{1}H and [129]Xe NMR spectroscopy were used to characterize the chemical environment of the gases in both of the porous liquids and in the neat solvent. This enabled the probing of the
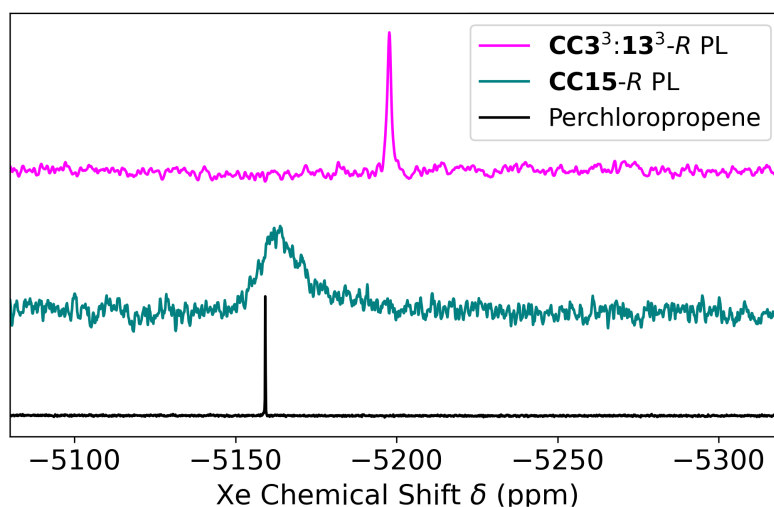
Figure 2.7: ^{129}Xe NMR spectra for Xe gas in **CC3^3:13^3**-*R* and **CC15**-*R* porous liquids compared to in neat PCP. **CC3^3:13^3**-*R* porous liquid at 4% w/v and **CC15**-*R* porous liquid at 5% w/v.

extent of gas binding in each porous liquid as these nuclei are highly sensitive to their chemical environment, leading to large shifting of peaks in the NMR spectra when the nuclei are occupying the cage cavity. In the spectra of ^{129}Xe in the porous liquids (Figure 2.7), significant shifting occurs in the **CC3^3:13^3**-*R* porous liquid relative to in neat PCP ($\Delta\delta$ = -38.6 ppm), whereas the change in shift of Xe in the **CC15**-*R* porous liquid is much less ($\Delta\delta$ = -4.7 ppm). This shows that the Xe gas cannot easily occupy the pores in the **CC15**-*R* porous liquid, while the peak broadening indicates there may be some exchange, the lack of strong shifting show this is not favourable. In contrast, the large upfield shift of Xe in the **CC3^3:13^3**-*R* porous liquid is due to the gas readily occupying the cage cavities, allowing for the very high gas uptake observed in this system.

This correlation between the amount of gas absorbed and upfield chemical shift
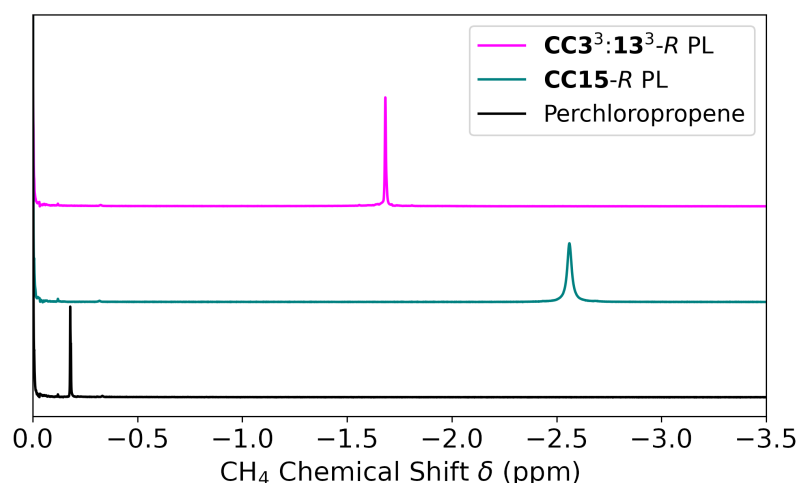
Figure 2.8: ^{1}H NMR spectra for CH_4 gas in **CC3^3:13^3**-*R* and **CC15**-*R* porous liquids compared to in neat PCP. **CC3^3:13^3**-*R* porous liquid at 4% w/v and **CC15**-*R* porous liquid at 5% w/v.

also occurs with CH_4 uptake in both of the porous liquids. In both porous liquids there is a significant shift in the ^{1}H NMR spectrum of CH_4 corresponding to the CH_4 gas occupying the cavities compared to in neat PCP (Figure 2.8). The change in shift relative to in neat PCP in the **CC15**-*R* porous liquid ($\Delta\delta$ = -2.38 ppm) is larger than that observed in the **CC3^3:13^3**-*R* porous liquid ($\Delta\delta$ = -1.50 ppm), indicating that CH_4 in the **CC15**-*R* system is experiencing a larger shielding effect due to more preferentially occupying the cage cavities. This effect corresponds to the greater uptake in the **CC15**-*R* porous liquid as it can better bind the gas molecules, manifesting as a larger uptake.

The CH_4 uptake quantity in these porous liquids can also be measured quantitatively using ^{1}H NMR spectroscopy using a sealed and calibrated DCM-d_2 and tetramethylsilane (TMS) capillary. Measured this way, the uptake of CH_4 in the porous liquids (17.5 μmol/g_{PL} in **CC3^3:13^3**-*R* porous liquid, 21.5

μmol/g$_{PL}$ in **CC15**-*R* porous liquid) is comparatively higher than measured by the displacement method (11.6 μmol/g$_{PL}$ in **CC3^3:13^3**-*R* porous liquid, 13.3 μmol/g$_{PL}$ in **CC15**-*R* porous liquid). This reflects the disparity in the measurements carried out by Greenaway *et al.* in the 20% w/v **CC3^3:13^3**-*R* porous liquid, where the amount of CH$_4$ soluble in the PCP (6.7 μmol/g$_{PCP}$)[2] approximately corresponds to the gap between these measurements. The guest displacement method largely displaces the gas molecules bound in the cage cavities and doesn't release the gas dissolved in the solvent upon addition of the displacing guest.

The loss of CH$_4$ over time was also measured using ^{1}H NMR spectroscopy. Multiple measurements were carried out at set time intervals over 2.5 days to give more information on the preference for CH$_4$ in the **CC15**-*R* porous liquid. Both the **CC3^3:13^3**-*R* and **CC15**-*R* porous liquids were fully saturated with CH$_4$ before leaving open to air with a calibrated d$_2$-DCM/TMS capillary, recording ^{1}H NMR spectra to determine how the CH$_4$ concentration changes over time. After normalising both resulting curves (Figure 2.9) we observe that the **CC15**-*R* porous liquid retains 23% more of it's initial CH$_4$ absorption after 1 day than the **CC3^3:13^3**-*R* porous liquid. Over the entire 2.5 days, CH$_4$ was also lost more slowly from the **CC15**-*R* porous liquid. This shows that the preference for binding CH$_4$ in this porous liquid also enables better retention of gas in the entire system.

The utility of diffusion, or pulsed field gradient (PFG) NMR spectroscopy for comparing the two porous liquid systems was also investigated. PFG NMR measurements relate to the translational diffusion of species within the sample being analysed.[14] All the species in an NMR tube can be spatially encoded along the length of the probe using a gradient pulse, where the magnetisation increases
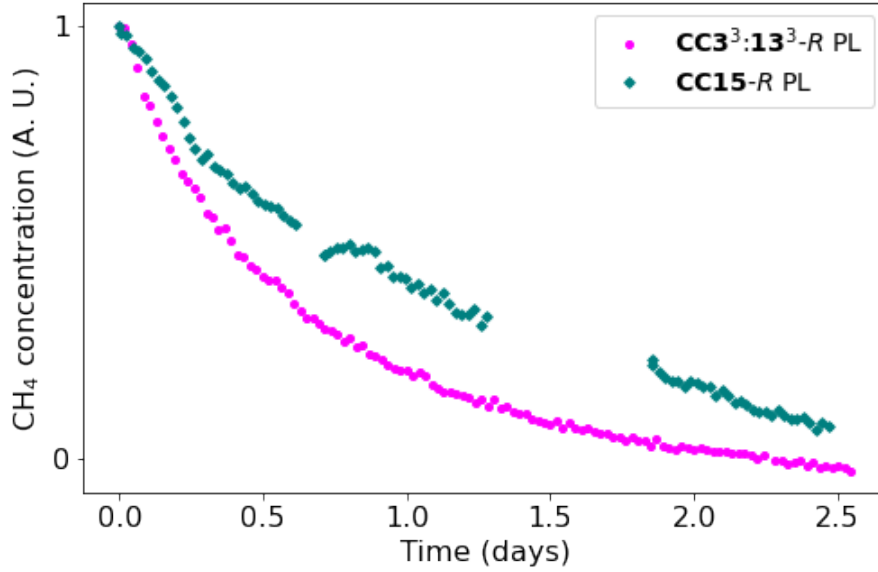
Figure 2.9: Normalised kinetic loss curves for CH_4 in **CC3³:13³**-*R* and **CC15**-*R* porous liquids measured by ¹H NMR spectroscopy. **CC3³:13³**-*R* porous liquid at 4% w/v and **CC15**-*R* porous liquid at 5% w/v.

along this length. After some diffusion time, attenuation in the signal acquired relates to the extent that the magnetisation gradient in the sample has decayed due to diffusion of the species within the NMR sample. The diffusion coefficient of species in an NMR sample can be calculated using the Skejskal-Tanner equation (Equation 2.1) where I/I_0 is the signal attenuation, g is the gradient field strength, δ is the length of the gradient pulse, and D is the diffusion coefficient:[15]

$$\frac{I}{I_0} = e^{-D\gamma^2 g^2 \delta^2 (\Delta - \frac{\delta}{3})} \tag{2.1}$$

Different species in a mixture have different diffusion coefficients based on their apparent solvodynamic radii, for mixtures with many components, Fourier

Figure 2.10: diffusion ordered spectroscopy (DOSY) plots of the diffusion NMR experiments carried out on CH_4 in the **CC3³:13³**-*R* (left) and **CC15**-*R* (right) porous liquids. **CC3³: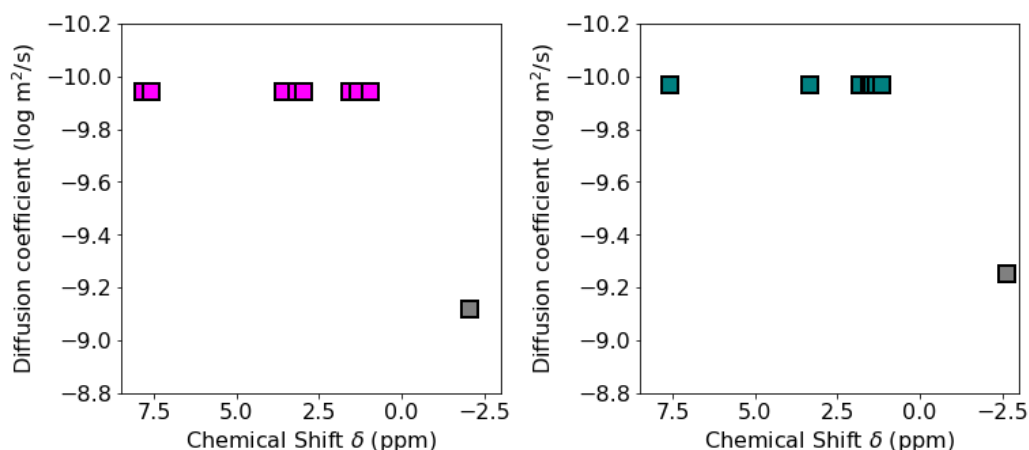13³**-*R* porous liquid at 4% w/v and **CC15**-*R* porous liquid at 5% w/v. The cage signals are coloured magenta for **CC3³:13³**-*R* and teal for **CC15**-*R* while the CH_4 signal is grey.

Transform PFG NMR experiments can be carried out to deconvolute complex data sets,[16] though this is not necessary in the samples analysed here. Diffusion NMR spectra were acquired for the **CC3³:13³**-*R* and **CC15**-*R* porous liquids when saturated with CH_4 and diffusion coefficients were determined for each cage and the CH_4 in the samples.

The measured diffusion coefficients (D) for the two cages were measured as 6.14×10^{-11} m^2/s for **CC3³:13³**-*R* and 6.33×10^{-11} m^2/s for **CC15**-*R* in PCP. These values cannot be directly related to the two cages, as the diffusion is heavily dependant on the sample viscosity, which varies between these samples (4.36 mPa s in the **CC3³:13³**-*R* porous liquids *vs.* 4.18 mPa s in the **CC15**-*R* porous liquid). In the two porous liquids, the values of D for CH_4 (5.43×10^{-10} m^2/s in **CC3³:13³**-*R*

and 4.58×10^{-10} m^2/s in **CC15**-*R*) are much lower than in the neat PCP (1.34×10^{-9} m^2/s). This effect occurs when a small molecule is enclosed in a molecular capsule, like the POCs used in these porous liquids, where the associated small molecule is observed as diffusing more slowly due to its effective solvodynamic radius being that of the occupied host molecule.[17] In the case of porous liquids where the small gas molecule is in dynamic equilibrium between occupying the POC cavities and being free in solution, the measured value of D corresponds to the average of these two states depending on the equilibrium constant.[2] This manifests as significant decreases in D compared to the neat liquid, indicating the diffusion is significantly frustrated as CH_4 is occupying the cavities.

Once diffusion coefficients are calculated based on the signal decay due to diffusion in the sample, in order to confirm the identity of the species, solvodynamic radii can be calculated using the Stokes-Einstein equation for Brownian motion (Equation 2.2), where D is the diffusion constant for the species, kT is the thermal energy ($k = 1.38 \times 10^{-23}$ Nm/K, $T = 298$ K), η is the sample viscosity, and R_s is the solvodynamic radius of the species.

$$D = \frac{kT}{6\pi\eta R_s} \tag{2.2}$$

In the **CC3^3:13^3**-*R* porous liquid sample, the diffusion corresponds to a solvodynamic radius of 8.2 Å, and in the **CC15**-*R* porous liquid diffusion corresponds to a radius of 8.3 Å. The values agree well with the expected size of these [4+6] imine cages.[18]

Furthermore, the diffusion coefficients can be used to calculate the proportion

of gas molecules in the system that are occupying the cage cavities (X_{occ}), this can be done by normalising for the differing sample viscosities.[19] This is shown in Equation 2.3, where D_G is the diffusion coefficient of free CH_4 in the solution, D_{obs} is the observed diffusion coefficient of CH_4, D_{HG} is the diffusion coefficient of the POC-CH_4 complex, assumed equal to the diffusion coefficient of the cage and CH_4 is bound internally, and η_{PCP} and η_{PL} are the viscosities of the neat solvent and the porous liquid.

$$X_{occ} = \frac{D_G \times \eta_{PCP} - D_{obs} \times \eta_{PL}}{D_G \times \eta_{PCP} - D_{HG} \times \eta_{PL}} \tag{2.3}$$

In the **CC3³:13³**-*R* porous liquid, this results as X_{occ} = 0.49, while with **CC15**-*R* the result is X_{occ} = 0.60. This indicates that in the **CC15**-*R* system CH_4 has a slightly higher affinity for the cage cavity than with **CC3³:13³**-*R*. Similarly, association constants (K_a) for the binding of CH_4 in the cage cavity in the porous liquids can be calculated from these values.[19] Equation 2.4 below shows this, $[POC]_0$ and $[G]_0$ are the cage and guest (CH_4) concentrations in the sample, respectively.

$$K_a = \frac{X_{occ}}{(1 - X_{occ})([POC]_0 - X_{occ}[G]_0)} \tag{2.4}$$

The computed values for the association constants for CH_4 in each of the porous liquids also reflected the measured uptake and retention. In the **CC3³:13³**-*R* porous liquid K_a = 2.71 × 10⁴ dm³/mol and in the **CC15**-*R* porous liquid K_a = 4.36 × 10⁴ dm³/mol. The values confirm that CH_4 occupies the cavity in the **CC15**-*R* porous liquid more preferentially than in the **CC3³:13³**-*R* porous liquid, reflecting the gas uptake measurements where the **CC15**-*R* porous liquid has a greater absorption

capacity for CH_4 (Figure 2.6).

2.5   Comparing gas uptake in solid POCs and porous liquids

Next, in order to compare gas uptake in the porous liquids with their solid POC counterparts, gas sorption experiments were carried out on the two solid POCs. Extensive solid state gas uptake studies have been carried out previously for this family of POC materials, particularly for **CC3**,[20] the uptake behaviour of which has been characterised extensively.[13,21–28] Amorphous scrambled POCs analogous to **CC3³:13³**-*R* have similar gas uptake capacity to porous crystalline cage materials, in that the amorphous packing still allows gas uptake to occur.[29] In **CC15**-*R* the gas uptake in the solid is modulated by the presence of the window-occluding methyl groups and the poorly connected pore network in the crystal packing structure.[30]

By comparing the gas uptake in these two porous liquids with that of the solid POCs, the difference in the pore structure should become much more apparent. Many solid POCs have large extrinsic pores in their extended crystal packing structure, allowing for gas adsorption to occur at multiple different shaped sites in the pore network. The comparison can be carried out by adjusting the gas uptake to account for the gas dissolved in the neat solvent and normalising to the mass of cage present in the porous liquids. This was done using the following equation (Equation 2.5):

$$[G]_{norm} = \frac{[G]_{PL} - [G]_{PCP}}{[POC]_{PL}} \tag{2.5}$$

Where $[G]_{norm}$ is the normalised gas uptake, $[G]_{PL}$ is the gas concentration in the

porous liquid, $[G]_{PCP}$ is the gas concentration in the neat solvent, and $[POC]_{PL}$ is the cage concentration in the porous liquid. This removes the effect of the solvent from the measured value, allowing for comparison of the gas uptake due to the presence of POCs in both the solid and liquid states (Figure 2.11).

N_2 was not included in this comparison as sorption measurements of the solids were carried out at 77 K, whereas all other measurements were carried out at ambient temperature. Both solid POCs have a similar gas capacity trend (Figure 2.11), that is Xe > CO_2 > CH_4 for **CC3³:13³**-*R* and Xe ≈ CO_2 > CH_4 for **CC15**-*R*. **CC3³:13³**-*R* gas uptakes correlate with the isoteric heats of adsorption of **CC3**-*R* calculated previously (Xe 31.31 kJ/mol > CO_2 27.73 kJ/mol > CH_4 22.05 kJ/mol).[2] In contrast, **CC15**-*R* shows a much weaker correlation, the CO_2 and Xe uptakes are more close in value and both are less that that measured in **CC3³:13³**-*R*. In **CC3**-*R*, CO_2 is favoured to occupy the cage portals in the solid, as electrostatic interactions occur here between the imine bonds in the POC structure and CO_2.[25] The reduced CO_2 capacity in **CC15**-*R* relative to in **CC3³:13³**-*R* is due to the window-occluding methyl groups infringing upon the most favourable adsorption site for CO_2 and reducing the extent of the electrostatic interaction available were it to occupy this smaller void. It should be noted that the molecular weight of **CC15**-*R* is greater than the average molecular weight of **CC3³:13³**-*R*, when calculating based upon the moles of POC present these values would be further shifted towards larger gas capacities in **CC3³:13³**-*R*.

The Xe uptake in the two solid POCs can be explained by comparing with solid **CC3**-*R*. Xe adsorbs strongly in solid **CC3**-*R* as it fits perfectly inside the pore cavities present.[13] This explains the reduced Xe capacity in solid **CC15**-*R* (1.283
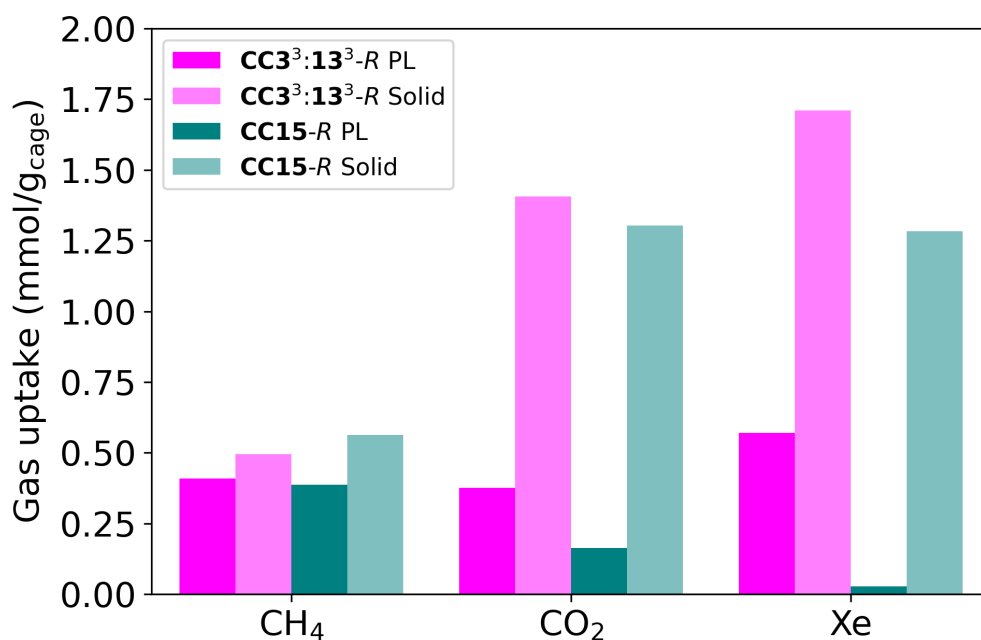
Figure 2.11: Gas uptake in the solid state POCs compared to the porous liquids. Uptake for the porous liquids is adjusted by subtracting the native gas capacity of PCP from the total uptake before normalizing to the mass of POC present in the sample. **CC3^3:13^3-**R porous liquid at 4% w/v and **CC15-**R porous liquid at 5% w/v.

mmol/g$_{cage}$) over solid **CC3^3:13^3-**R (1.710 mmol/g$_{cage}$), as **CC3^3:13^3-**R has a very similar internal cavity diameter to **CC3-**R due to its analogous structure, whereas in **CC15-**R the methyl groups reduce the cavity diameter sufficiently to reduce the ability of Xe to occupy the molecular pore. Porosity is not entirely lost in the solid **CC15-**R, these occluding groups mainly impact the intrinsic porosity, while the extrinsic pores in the material remain intact. This explains why the values for uptake in the solids greatly exceed that of the porous liquids (0.568 mmol/g$_{cage}$ for **CC3^3:13^3-**R porous liquid, 0.027 mmol/g$_{cage}$ for **CC15-**R porous liquid)

The CH$_4$ uptake is comparable across both of the solid materials as well as in the

porous liquids. The normalized uptake, accounting for gas absorption due to cages in the porous liquids, are 0.409 mmol/g_{cage} for **CC3^3:13^3**-*R* and 0.386 mmol/g_{cage} for **CC15**-*R* *vs.* 0.495 mmol/g_{cage} for **CC3^3:13^3**-*R* and 0.562 mmol/g_{cage} for **CC15**-*R* in the solids (Figure 2.11). The implication is that CH_4, like Xe and CO_2, has a lower preference to occupy the extrinsic pores in the porous solids. The kinetic diameter of CH_4 is 3.8 Å, smaller than the available cavities in the cages (**CC3^3:13^3**-*R*: 5.85 Å, **CC15**-*R*: 4.61 Å).

For CO_2, as with Xe, there is a large disparity between the uptake in the porous solids compared to the corrected uptake in the porous liquids. In the solid POCs, the CO_2 uptake (1.407 mmol/g_{cage} in **CC3^3:13^3**-*R*, 1.304 mmol/g in **CC15**-*R*) is *ca.* one order of magnitude greater than the adjusted uptakes for the two porous liquids (0.375 mmol/g_{cage} in **CC3^3:13^3**-*R* porous liquid, 0.164 mmol/g_{cage} in **CC15**-*R* porous liquid). This is due to the fact that CO_2 adsorption in the the solid materials occurs in both the the intrinsic molecular pore and the extrinsic interstitial cavities. This reflects the previous understanding of CO_2 binding in solid POCs, where a favourable electrostatic interaction between the gas molecule and imine groups that exist around the cage portal.[31] In the porous liquids, this portal site does not exist as the cage windows are partially occupied by the molecules of the solvent. Furthermore, this also relates to the reduced uptake in the **CC15**-*R* porous liquid compared to the **CC3^3:13^3**-*R* porous liquid, where any more minor electrostatic interactions and the cage are inhibited by the presence of the methyl groups in **CC15**-*R* further reducing the gas capacity.

2.6 Uptake of larger alkanes

Since they have not been investigated previously, and with the knowledge that CH_4 uptake behaviour is different for these two porous liquids, we next chose to investigate uptake of larger alkane gases. ^1H NMR spectroscopy was also used with ethane and propane to investigate whether altering the cage window diameter would have an effect on the uptake of these alkanes. For these experiments, the higher concentration was used for the **CC3³:13³**-*R* porous liquid (20% w/v) in order to maximise any possible selectivity contribution from the cage, a five-fold increase in pore concentration. However, for both porous liquids the alkane gas uptake was largely dependent on each gas' solubility in PCP, although in each case the uptake was improved marginally with the presence of the POC (Figure 2.12).

Despite an improvement in uptake being observed for these gases, no change to the uptake trends or selectivity could be achieved due to the inherent high solubility of the alkanes in PCP. It is not possible to compare measurement for each gas between the two porous liquids as these experiments were carried out at different cage concentrations. In the 20% w/v porous liquid significant selectivity or a size cut-off for uptake improvement was not observed. The largest uptake disparity is observed with C_2H_6, but the uptake enhancement compared to PCP in each of the porous liquids is *ca.* fivefold, proportional to the concentration of cage in the porous liquids (157 μmol/g for **CC3³:13³**-*R*, 67 μmol/g for **CC15**-*R vs.* 47 μmol/g for PCP; increase of 110 μmol/g and 20 μmol/g respectively). The same experiment was also attempted with butane but the very high solubility of the gas
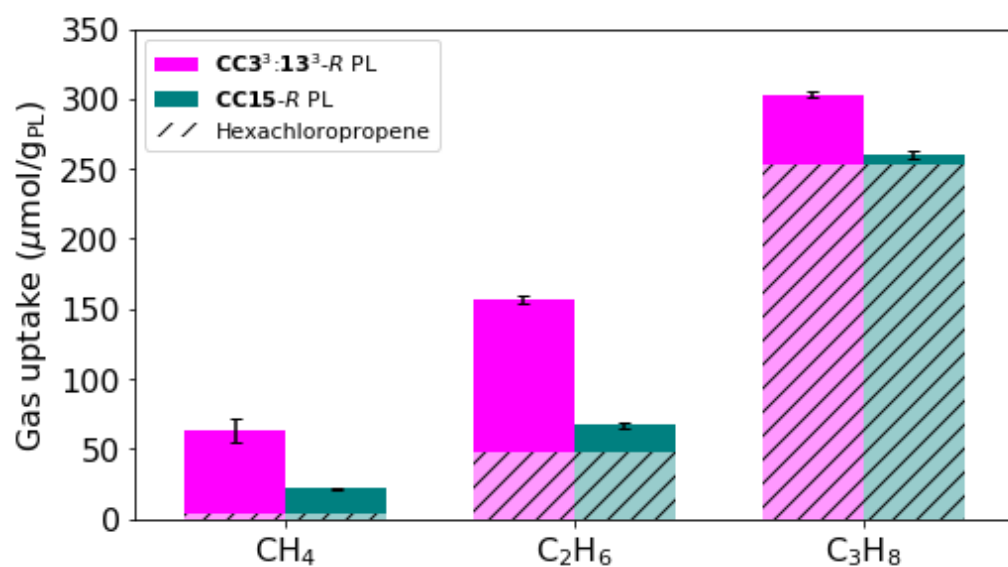
Figure 2.12:   Gas uptakes measured by ^{1}H NMR spectroscopy for CH_4, C_2H_6 and C_3H_8 for the **CC3^3:13^3**-*R* and **CC15**-*R* porous liquids. **CC3^3:13^3**-*R* at 20% w/v and **CC15**-*R* at 5% w/v.

in PCP meant it behaved as an anti-solvent, causing precipitation of the POC.

The chemical shift of each alkane peak in the porous liquids compared to in the neat PCP (Table 2.2, Figures 2.25, 2.26 and 2.27) also mirrors this effect. The chemical shifts for the ethane and propane in the porous liquids do all change, indicating the gas molecules are able to occupy the cage cavity, but are closer to the shifts observed in the neat solvent due to higher solubility in the solvent. Only C_2H_6 in the **CC3^3:13^3**-*R* porous liquid (-2.156 ppm) approaches the same shift as observed with CH_4 (-2.423 ppm), as it is in more of a balance between the concentration of gas occupying the cavities and dissolved in the solvent.

Table 2.2: Chemical shift measured by NMR spectroscopy for the alkane gases in **CC3^3:13^3**-*R* porous liquid and **CC15**-*R* porous liquid relative to the chemical shift of the alknes in PCP when saturated with the respective gas.

Gas	$\Delta\delta$ in CC3^3:13^3-*R* porous liquid (ppm)	$\Delta\delta$ in CC15-*R* porous liquid (ppm)
CH_4	-2.423	-2.025
C_2H_6	-2.156	-0.715
C_3H_8	-0.93[a] -0.701[b]	-0.168[a] 0.142[b]

[a]Shift for **CH$_2$** environment in propane. [b]Shift for 2**CH$_3$** environment in propane. **CC3^3:13^3**-*R* porous liquid at 20% w/v and **CC15**-*R* porous liquid at 5% w/v.

For comparison, gas evolution experiments for the alkane gases were also carried out to measure the gas uptake. While there is reasonable agreement between measurements for CH_4, there was a large disparity between the gas
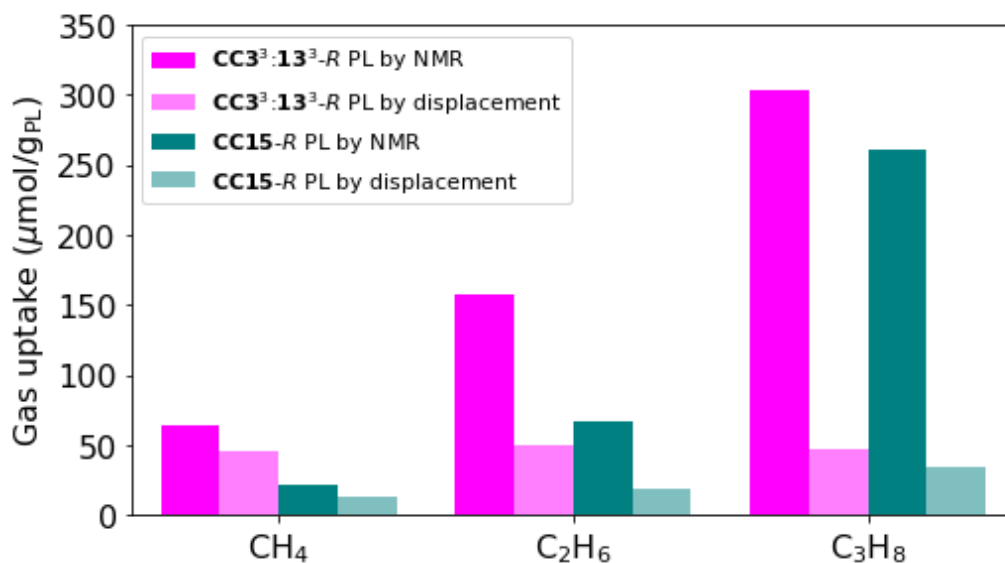
Figure 2.13:   Comparing measurements of CH_4, C_2H_6 and C_3H_8 gas uptake by NMR spectroscopy and by guest displacement in the **CC3^3:13^3**-*R* and **CC15**-*R* porous liquids. **CC3^3:13^3**-*R* porous liquid at 20% w/v and **CC15**-*R* porous liquid at 5% w/v.

evolution and NMR measurements for C_2H_6 and C_3H_8 (Figure 2.13). Therefore, it is worthwhile to note that although measuring uptake by displacement can be a useful technique for gases that cannot be easily measured spectroscopically, it is limited in determining an accurate gas uptake for the whole system, rather indicating the amount of gas occupying the cavities in a porous liquid. In porous liquids where a large proportion of the gas absorbed is not occupying the cavities, but is instead dissolved in the solvent, this volume of gas will not be evolved - this means the measurement will not reflect the amount of gas absorbed in a porous liquid.

2.7 Conclusions

Through the course of this study, the concepts used in reticular chemistry in solid microporous materials were transferred to porous liquids; modification of the POC structure can be used to modulate gas selectivity in these materials, showing how key design principles discovered in porous solids can be used in the liquid state. In this example, we successfully demonstrated that Xe gas uptake can be effectively shut off through narrowing of the cage window and reducing the pore diameter in th **CC15**-*R* porous liquid. Moreover, we observe some differences between the porous solids and liquids: CO_2 capacity is significantly lower in the porous liquids, pore for pore, when compared to the solids. This is largely due to the loss of well defined intermolecular pores found in solid POCs that enable the adsorption of larger quantities of gases and intermolecular interactions at sites not available in the liquid. Furthermore, it is demonstrated that the volumetric, guest displacement technique breaks down when used with larger, less volatile gases, no longer providing useful information about the entire system's capacity, though still a reasonable indicator for uptake enhancement.

The outlook from this work is promising, indicative that gas-selective porous liquids can be designed for use as flowable sorbents for gas separation processes. Selectivity in these materials can be increased further by designing analogous cages with even higher solubility, or by removing the solvent altogether as a type 1 porous liquid, though much increased viscosity may become an important limiting factor.

2.8   Experimental details

2.8.1   Materials

1,3,5-Triformylbenzene was purchased from Manchester Organics (UK), (*R,R*)-cyclohexyl-1,2-diamine was purchased from Fluorochem, and all other chemicals were purchased from Sigma-Aldrich or TCI UK. Perchloropropene was purchased from Sigma-Aldrich. Other solvents were reagent or HPLC grade and purchased from Fisher Scientific. All materials were used as received unless stated otherwise.

Gases were purchased from BOC of the following grades: carbon dioxide (N5.0), methane (N4.5), xenon (N5.0), and nitrogen (N4.8).

2.8.2   General analytical techniques

NMR: ^{1}H NMR spectra were acquired using an internal deuterium lock for the residual protons in $CDCl_3$ (δ = 7.26 ppm) or CD_2Cl_2 (δ = 5.32ppm) at ambient probe temperature on the following instruments: Bruker Avance400 (400 MHz) or Bruker DRX500 (500 MHz) spectrometers. In order to avoid mixing of porous liquids with deuterated solvents or TMS, NMR studies with the porous liquids were conducted using in-house calibrated CD_2Cl_2/TMS capillaries so that there was no effect on the porous liquid.

Data are presented as follows: chemical shift, integration, peak multiplicity (s = singlet, m = multiplet), and assignment. Chemical shifts are expressed in ppm on a δ scale relative to δ_{TMS}(0 ppm) or δ_{CDCl3}(7.26 ppm).

^{13}C NMR spectra were recorded using an internal deuterium lock using $CDCl_3$ (δ = 77.16 ppm) or CD_2Cl_2 (δ = 54.00ppm) at ambient probe temperatures on the

following instruments: Bruker Avance 400(101 MHz) or Bruker DRX500 (126 MHz) spectrometers.

^{129}Xe NMR Spectra were recorded using an internal deuterium lock using a sealed capillary of TMS in CD_2Cl_2 at ambient probe temperature on the following instrument: Bruker DRX500 (138.3 MHz).

HRMS: High resolution mass spectrometry (HRMS) was carried out using an Agilent Technologies 6530B accurate-mass QTOF Dual ESI mass spectrometer (capillary voltage 4000 V, fragmentor 225 V) in positive ion detection mode. The mobile phase was MeOH + 0.1% formic acid at a flow rate of 0.25 mL/min.

PXRD: Laboratory powder X-ray diffraction data were collected in transmission mode on samples held on thin Mylar film in aluminium well plates on a Panalytical X'Pert PRO MPD equipped with a high throughput screening XYZ stage, X-ray focusing mirror and PIXcel detector, using Ni-filtered Cu Kα radiation. Data were measured over the range 4–40° in 0.013° steps over 60 minutes.

2.8.3   Synthesis of porous organic cages (POCs)

Synthesis of scrambled [4+6] imine POC mixture CC3^3:13^3-*R*
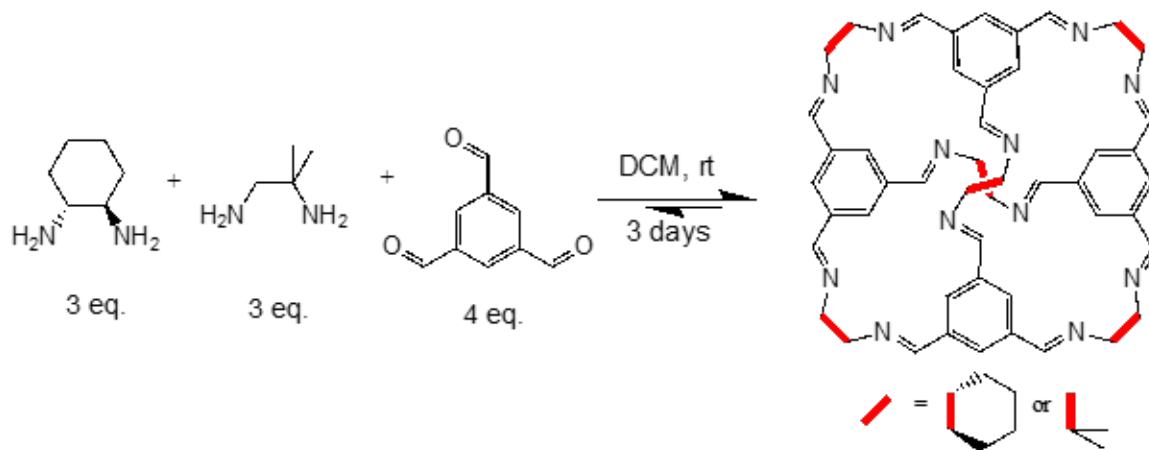
Scheme 2.3: Reaction scheme for synthesis of scrambled imine cage **CC3^3:13^3**-*R*.

(*R,R*)-Cyclohexyl-1,2-diamine (*R,R*-CHDA, 1.637 g, 14.3 mmol, 3 eq.), 1,2-diamino-2-methylpropane (DAMP, 1.264 g, 14.3 mmol, 3 eq.), and 1,3,5-triformylbenzene (TFB, 3.099 g, 19.1 mmol, 4 eq.)   were dissolved in dichloromethane (DCM, 1.35 L). The reaction mixture was stirred at room temperature for 3 days. The solution was filtered to remove insoluble precipitate before the DCM was removed by rotary evaporation. The resulting crude cream solid was washed with ethyl acetate (3 × 150 mL) before being re-dissolved in the minimum amount of DCM (ca. 35 mL), filtered, and recovered by rotary evaporation, to afford a cream solid which was dried in a vacuum oven overnight (5.1 g, 4.9 mmol, 85%).

^{1}H NMR (400 MHz, CDCl3) δ_H (ppm) 8.17–7.81 (24H, m, N=C*H* and Ar*H*), 3.94–3.35 (12H, m, C*H*N=CH), 1.91–1.32 (42H, m, C*H$_2$* and C*H$_3$*); **^{13}C NMR** (126 MHz, CDCl$_3$) δ_C (ppm) 160.9, 159.2, 155.3, 137.1, 136.6, 129.4, 74.8, 72.3, 61.2, 33.1,
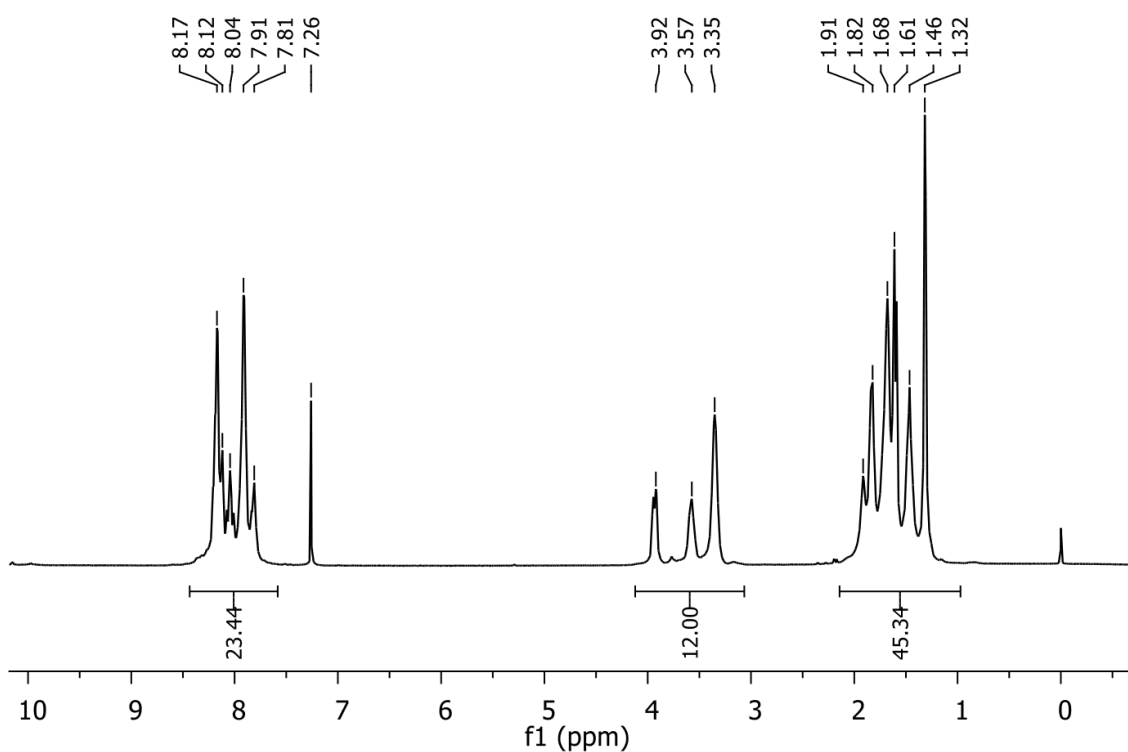
Figure 2.14: ^{1}H NMR (CDCl$_3$) spectrum of scrambled [4+6] imine cage **CC3^3:13^3**-*R*.

29.5, 24.4, 22.1; **HRMS** (ES+) calc. for scrambled cages **3^{0}13^6** C$_{60}$H$_{72}$N$_{12}$ 960.6003, **3^{1}13^5** C$_{62}$H$_{74}$N$_{12}$ 986.6159, **3^{2}13^4** C$_{64}$H$_{76}$N$_{12}$ 1012.6316, **3^{3}13^3** C$_{66}$H$_{78}$N$_{12}$ 1038.6472, **3^{4}13^2** C$_{68}$H$_{80}$N$_{12}$ 1064.6629, **3^{5}13^1** C$_{70}$H$_{82}$N$_{12}$ 1090.6785, **3^{6}13^0** C$_{72}$H$_{84}$N$_{12}$ 1116.6942; found [M+H]$^+$ 961.5756, 987.6111, 1013.6307, 1039.6470, 1065.6622, 1091.6768, and [M+2H]$^{2+}$ 481.2969, 494.3127, 507.3215, 520.3295, 533.3370, 546.3443. Data in accordance with literature values.[2]

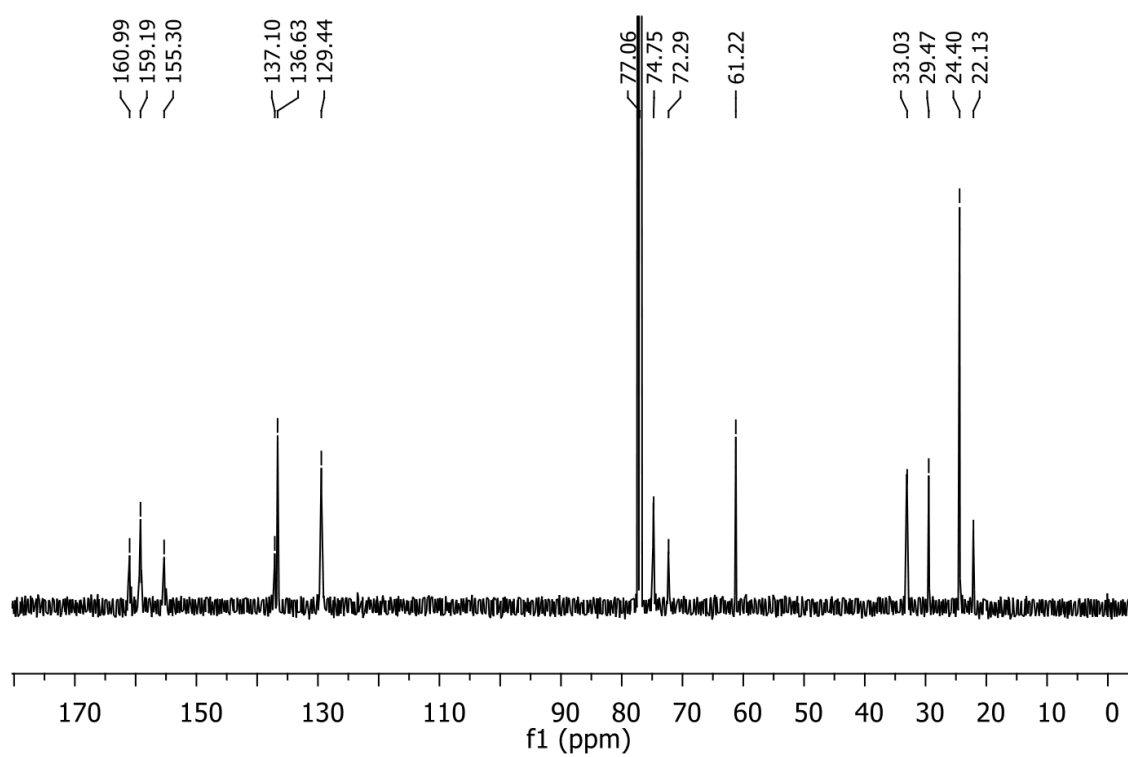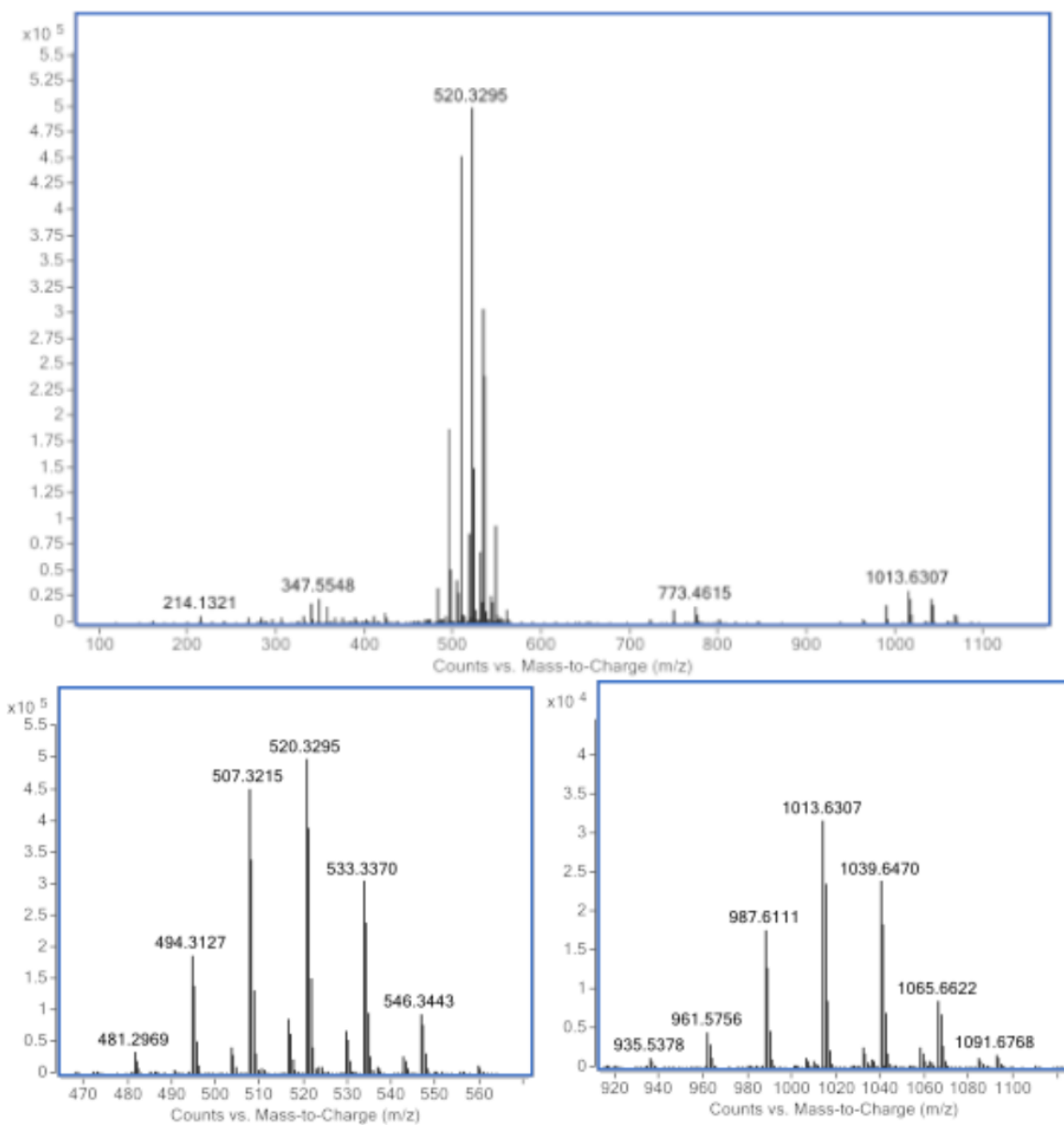**Figure 2.15:** ^{13}C NMR (CDCl$_3$) spectrum of scrambled [4+6] imine cage **CC3^3:13^3**-*R*.

Figure 2.16: HRMS spectra of scrambled [4+6] imine cage **CC3³:13³**-*R*: full spectrum (top), [M+H]⁺ species (bottom right) and [M+2H]⁺ (bottom left).
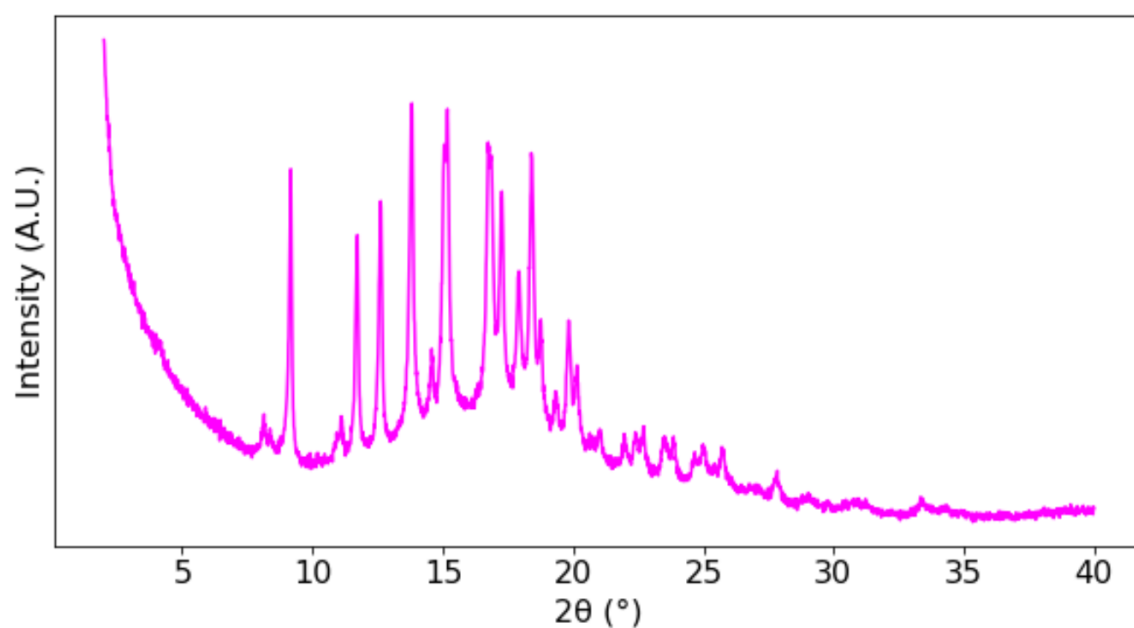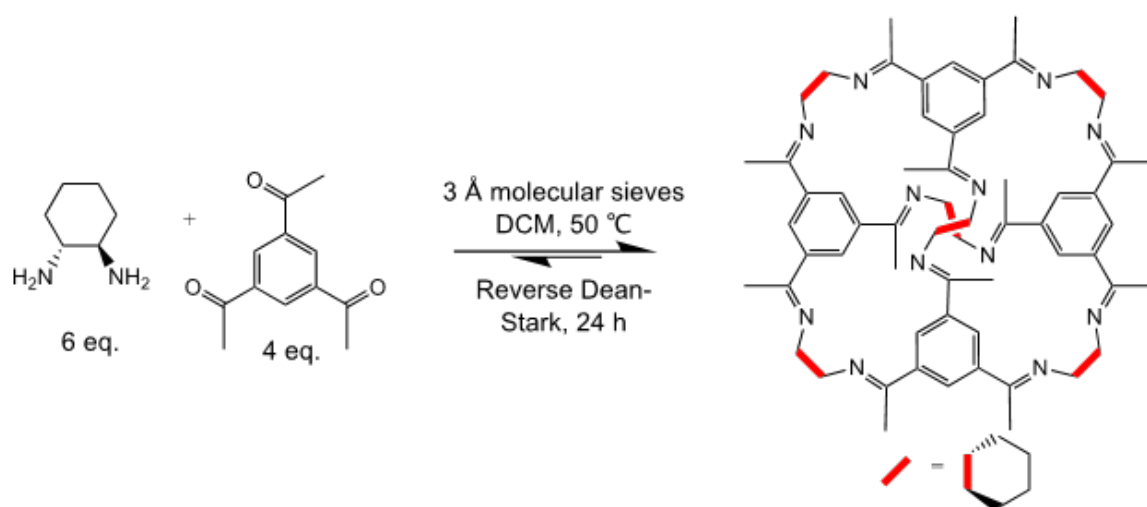
Figure 2.17: PXRD pattern of scrambled [4+6] imine cage **CC3³:13³**-*R*.

Synthesis of [6+4] Imine POC CC15-*R*

Scheme 2.4: Reaction scheme for synthesis of **CC15**-*R*.

A mixture of *R,R*-CHDA (4.28 g, 37.5 mmol, 6 eq.) and 1,3,5-triacetylbenzene

(TAB, 5.10 g, 24.9 mmol, 4 eq.) were dissolved in DCM (50 mL) in a round

bottomed flask with 3 Å molecular sieves. The vessel was fitted with reverse Dean-Stark apparatus and an air condenser. The reverse Dean-Stark apparatus was charged with DCM, and the reaction mixture was heated at 50 °C with stirring for 3 days. The reaction was allowed to cool to room temperature before being filtered to remove the molecular sieves, and the solvent removed by rotary evaporation to afford the crude product. The crude product was washed with diethyl ether (3 × 100 mL) before being dissolved in the minimum amount of 1:1 DCM/hexane and concentrated in vacuo to precipitate the product. The resulting solid (6.07 g, 4.7 mmol, 75 %) was recovered by vacuum filtration and dried in a vacuum oven overnight.

¹H NMR (500 MHz, CDCl$_3$) δ_H (ppm) 8.05 (12H, s, ArH), 3.82 (12H, m, N-CH), 2.19 (36H, s, CH_3), 1.84 (12H, m, CH_2), 1.69 (12H, m, C$H2$), 1.65 (12H, m, CH_2), 1.49 (12H, m, CH_2); **¹³C NMR** (126 MHz, CDCl$_3$) δ_C (ppm) 161.6, 140.3, 126.2, 65.3, 32.2, 24.7, 15.1; **HRMS** (ES+) calc. for C$_{84}$H$_{108}$N$_{12}$ 1284.8820; found [M+H]$^+$ 1285.8786, [M+2H]$^{2+}$ 643.4462, and [M+3H]$^{3+}$ 429.3005. Data in accordance with literature values.[30]
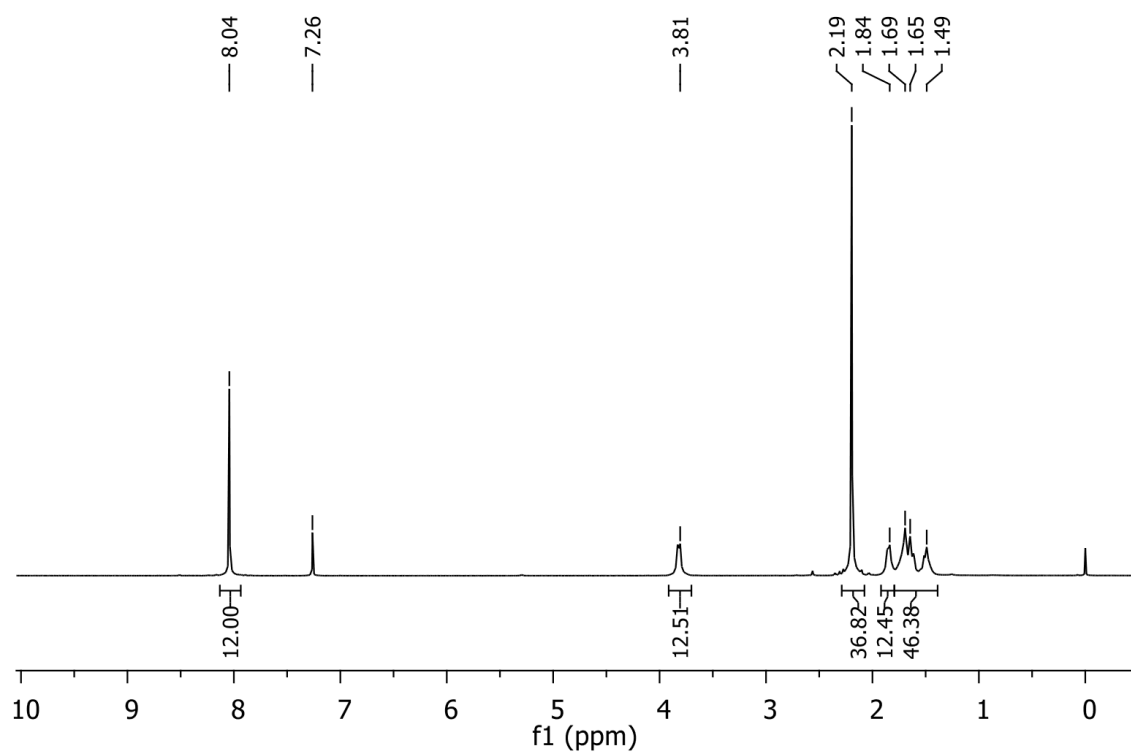
Figure 2.18: ^{1}H NMR (CDCl$_3$) spectrum of scrambled [4+6] imine cage **CC15**-*R*.
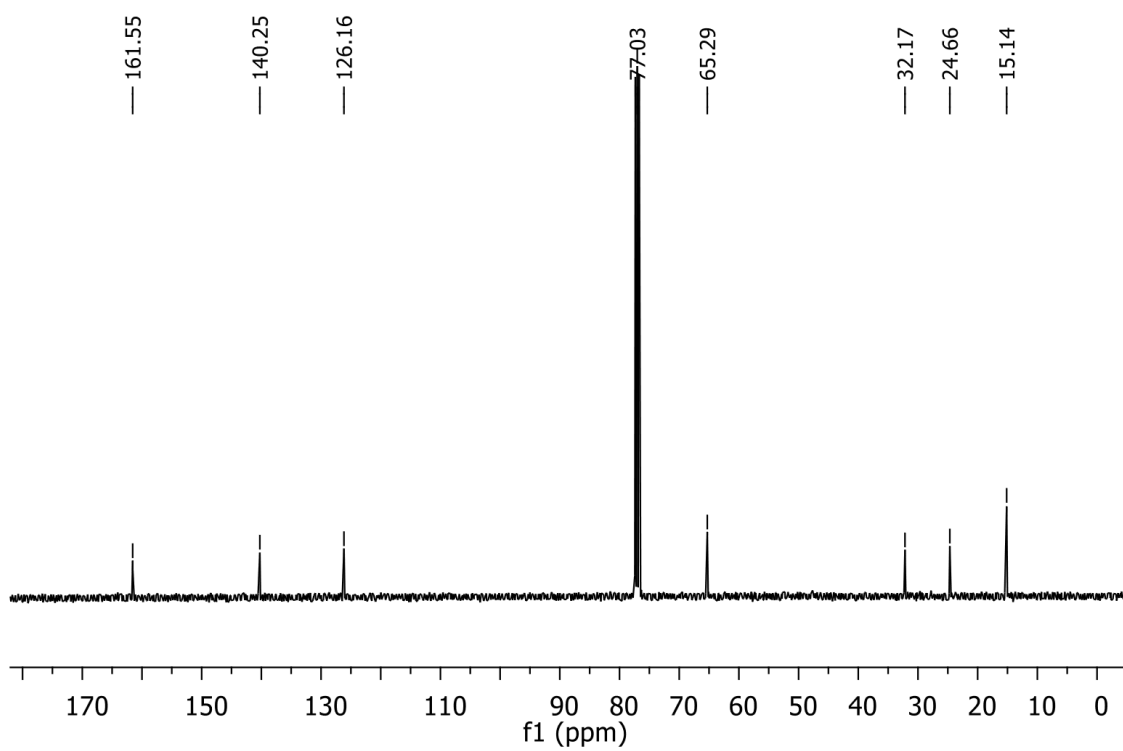
Figure 2.19: ^{13}C NMR (CDCl$_3$) spectrum of scrambled [4+6] imine cage **CC15**-*R*.
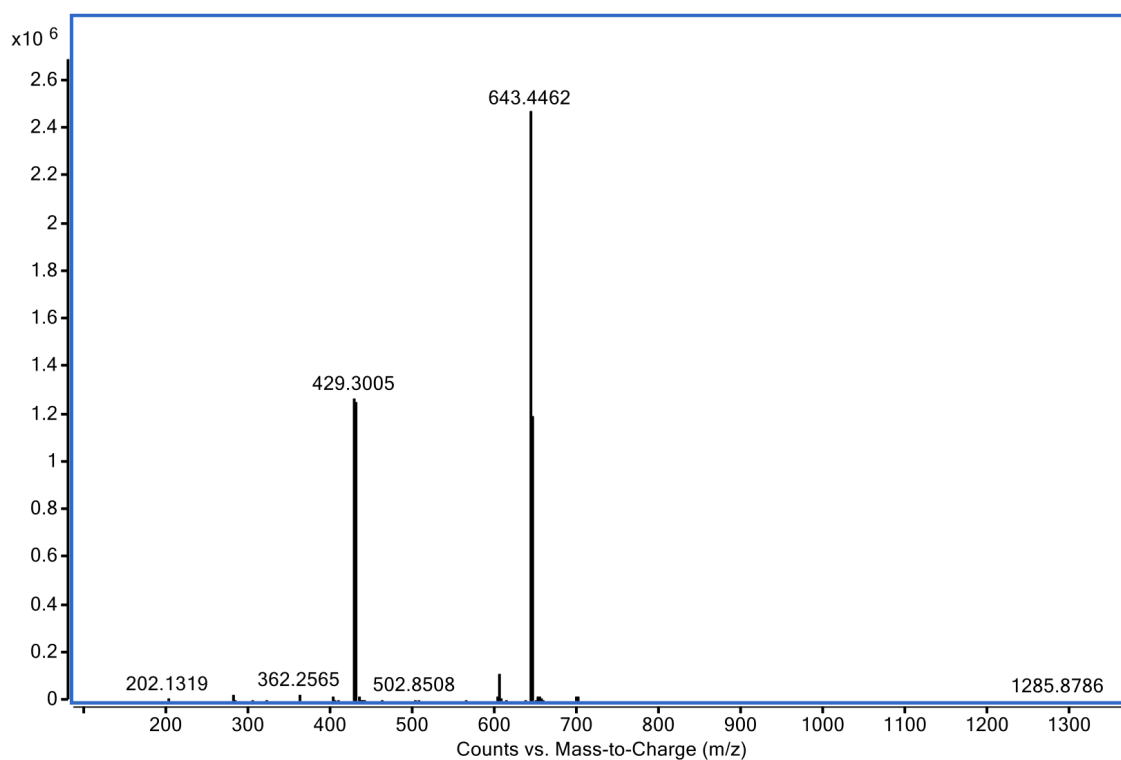
Figure 2.20: HRMS spectra of scrambled [4+6] imine cage **CC15**-*R*.
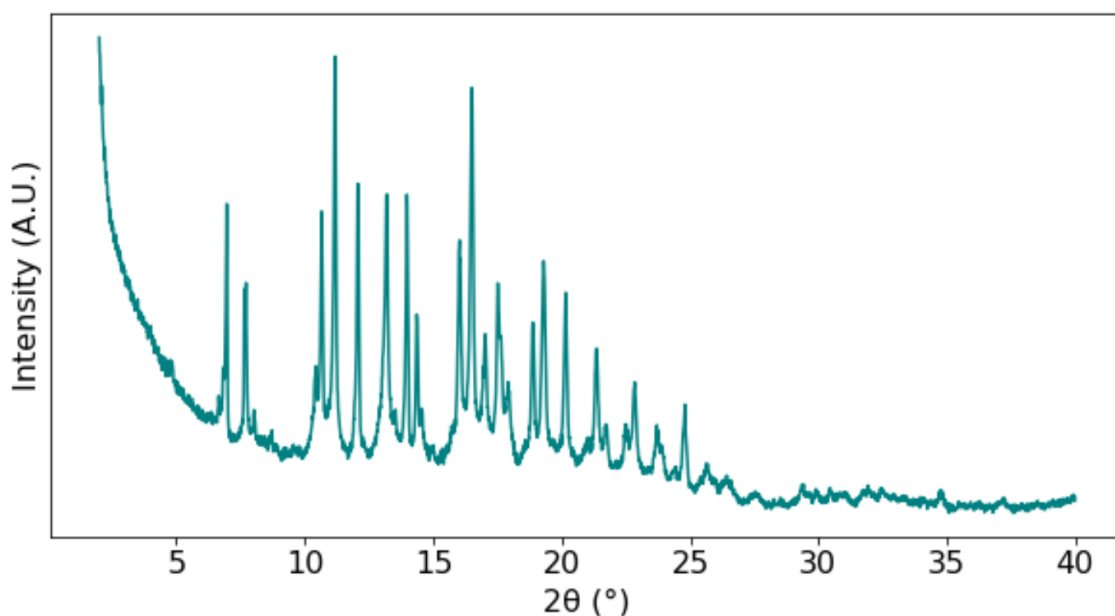
Figure 2.21: PXRD pattern of scrambled [4+6] imine cage **CC15**-*R*.

Attempted synthesis of scrambled [4+6] imine POC mixture analogous of CC15-*R*

R,R-Diaminocyclohexane (R,R-CHDA, 0.4282 g, 3.75 mmol, 3 eq.) and 1,2-diamino-2-methylpropane (DAMP, 0.3306 g, 3.75 mmol, 3 eq.) were dissolved in DCM (10 mL) and added to triacetylbenzene (TAB, 1.0212 g, 5 mmol, 4 eq.) and 3 Å molecular sieves (0.20 g) in a round bottomed flask. The flask was equipped with reverse Dean-Stark apparatus charged with DCM and was stirred at 45 °C until reaction completion as monitored by HPLC.
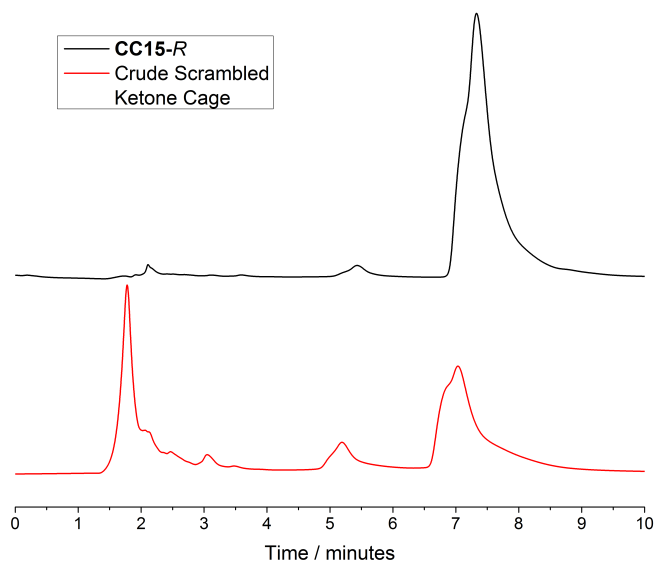
Figure 2.22: Chromatograph of HPLC analysis of the reaction mixture of attempted synthesis of scrambled cage analogue of **CC15**-*R* compared to pure **CC15**-*R*.

2.8.4   Purification of perchloropropene (PCP)

PCP, as provided from the supplier, often contains significant impurities which could behave competitively in the porous liquid when a guest is added. Each batch of PCP was analysed and purified before use as reported previously:[2]

PCP (800 g) was passed 5 times through columns packed with basic alumina (5 × 150 g) using positive N_2 pressure. Pure PCP (171.4 g, 21%; 387.3, 48%) was recovered.

^{13}C NMR (126 MHz, CD_2Cl_2/TMS capillary) δ_C (ppm) 132.1, 127.2, 92.8.
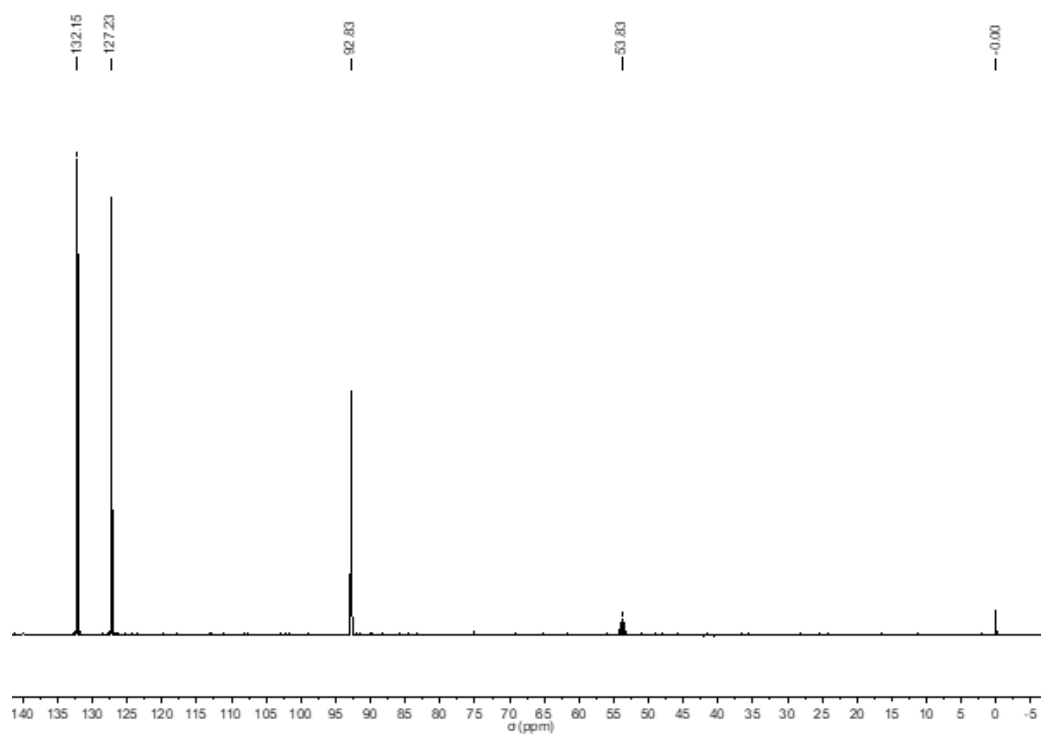
Figure 2.23: ^{13}C NMR (CD$_2$Cl$_2$/TMS) spectrum for purified PCP.

2.8.5   Gas uptake measurements in porous liquids

All samples had gas addition and measurements conducted between 20 and 25 °C in a temperature-controlled laboratory. The flow rate of gas addition was measured using a Gilmont calibrated/correlated flowmeter (tube size 0, Gilmont EW-03201-22) with a stainless steel float on a scale of 1-100, as reported previously.[2] The flow of each gas was calculated from the supplied correlated flow table for air, and general correction equation (Equation 2.6) for approximating gas flow from air using the density of each gas in g/mL at standard conditions taken from the NIST Chemistry WebBook[32] (Gilmont flowmeter calibrated at 1 atm, 294 K), with corrections for temperature and pressure. After optimisation, each gas was maintained at 50-60 mL/min flow rate by setting the regulator output pressure to 0.5 bar and fine-controlling the flow with a needle valve to the calculated scale readings.

$$q_G^2 = q_G^1 \sqrt{\frac{\rho_G^1}{\rho_G^2}} \tag{2.6}$$

q_G^1 and q_G^2 are the flow rates of the two gases being interconverted, and ρ_G^1 and ρ_G^2 are the densities of the respective gases.

Table 2.3: Calculated flow meter readings for gases used in this work using Equation 2.6.

Gas	Density ρ_G (g/mL)[32]	Equivalent air flow q_G (mL/min)	Corresponding flowmeter scale reading
Air	0.00120	50-60	39-43
N_2	0.00116	49.19-59.03	39-43
CO_2	0.00184	61.81-74.17	45-49
Xe	0.00547	106.77-128.13	61-67
CH_4	0.00066	37.26-44.71	32-37
C_2H_6	0.00126	51.16-61.38	39-45
C_3H_8	0.00186	62.23-74.68	44-50
C_4H_{10}	0.00249	71.99-86.39	48-54

2.8.6   Gas uptake in porous liquids measured by NMR

In order to determine the gas uptake concentration in NMR experiments, NMR capillaries were prepared by sealing a glass capillary containing 0.1 mL of a solution prepared by dissolving 10 µL of TMS in 0.5 mL CD_2Cl_2. Desolvated **CC3^3:13^3**-*R* (25 mg, 50 mg, 100 mg, 150 mg, 175 mg, and 200 mg) was dissolved in purified PCP (0.8 mL) in glass vials. Each of the resulting solutions were transferred to a 1 mL volumetric flask using a 1 mL syringe and needle. The vial was washed with PCP (0.1 mL) which was then transferred to the volumetric flask. Each solution was made up to the 1 mL mark with PCP before 0.5 mL samples of the resulting solutions were added to an NMR tube and fitted with a sealed NMR capillary. A ^{1}H NMR spectrum was then recorded for each solution using the same capillary. Using integrations of the NMR signals (TMS = 1, 0.016 to -0.016 ppm; 12NC**H**, 3.819 to 2.682 ppm) from the spectra, the NC**H** integration relative to TMS was plotted against the concentration to give a calibration curve (Figure 2.24). The equation for the curve was used to calculate concentrations of species relative to the TMS peak in spectra, adjusting for the ^{1}H occupancy of their environments.

Desolvated **CC3^3:13^3**-*R* (200 mg or 40 mg), or **CC15**-*R* (50 mg), was dissolved in PCP (1 mL) and an aliquot of the resulting porous liquid (0.6 mL) was added to an NMR tube. ^{1}H NMR spectra were recorded for the solution both before and after gas addition using a calibrated CD_2Cl_2/TMS capillary to quantify concentration using the calibration curve (Figure 2.24). For uptake of the alkane gases, the calibrated capillary was removed from the tube and the porous liquid was exposed to the gas by bubbling through a needle inserted into the NMR tube at 50-60
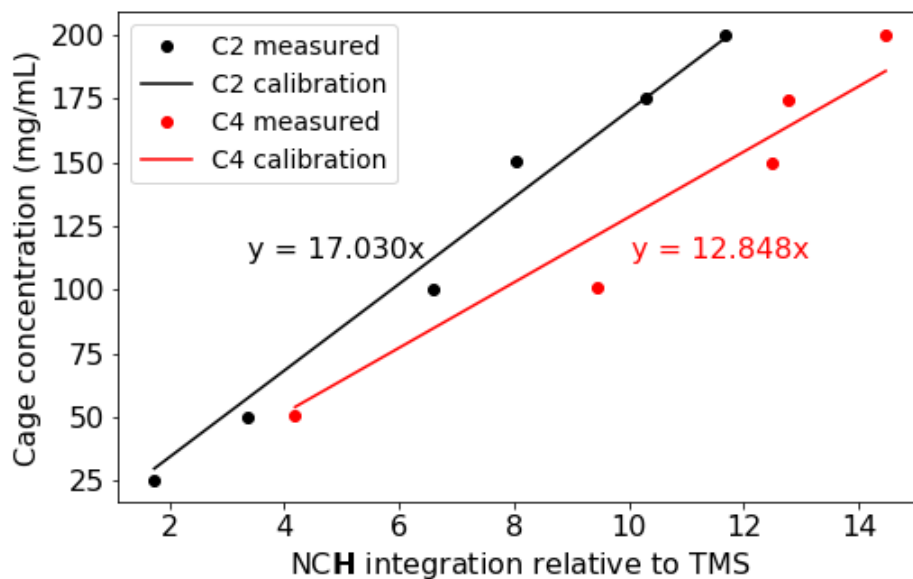
Figure 2.24: Representative calibration curves for CD_2Cl_2/TMS NMR capillaries used in this study.

mL/min.

Each alkane gas was bubbled through the samples in 3 minute increments with ^{1}H NMR spectra being recorded immediately after gas addition in order to produce gas concentration saturation curves (Figure 2.28). Once the saturation time was determined on an initial sample, saturations were carried out on a further 2 samples. This procedure was repeated for each sample, i.e., two porous liquids and the neat PCP. For the gas loss kinetics experiments with CH_4, the same sample preparation was carried out as above, the NMR tube was fitted with on open-top cap and spectra were recorded at 10 minute intervals over 2-3 days.
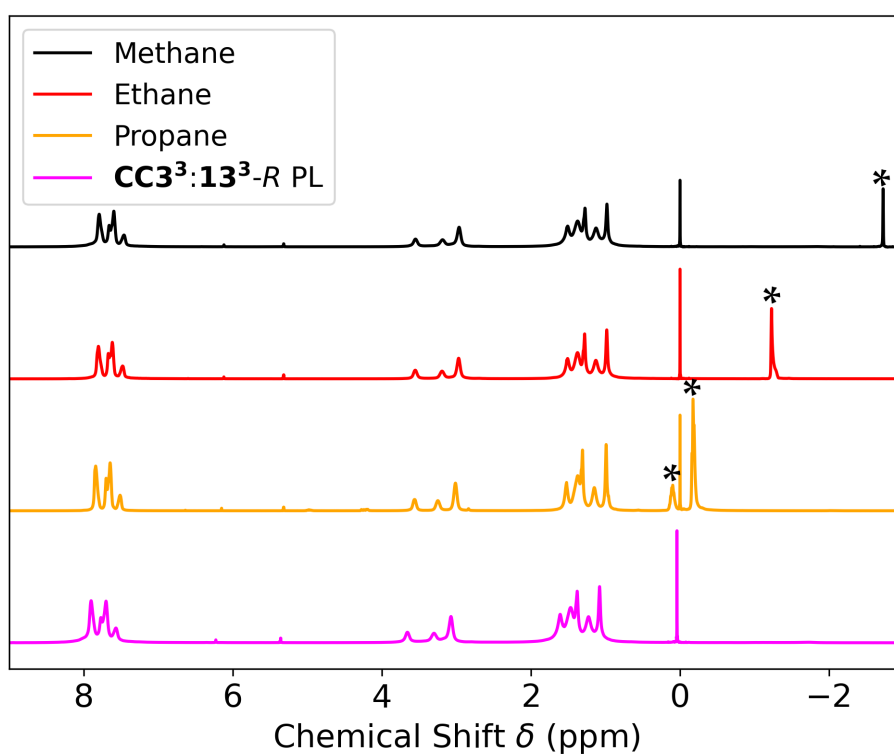
Figure 2.25: Stacked ^{1}H NMR spectra of alkane gases dissolved in the **CC3^3:13^3**-*R* porous liquid at at 20% w/v. Alkane peaks are labelled with asterisks.
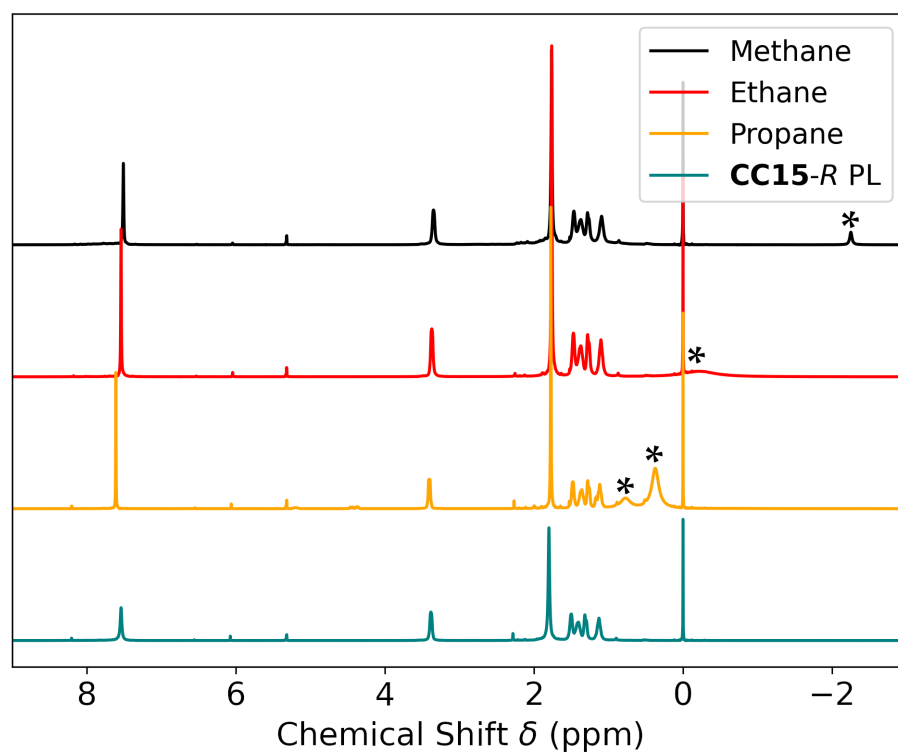
Figure 2.26: Stacked ^{1}H NMR spectra of alkane gases dissolved in the **CC15**-*R* porous liquid at 5% w/v. Alkane peaks are labelled with asterisks.
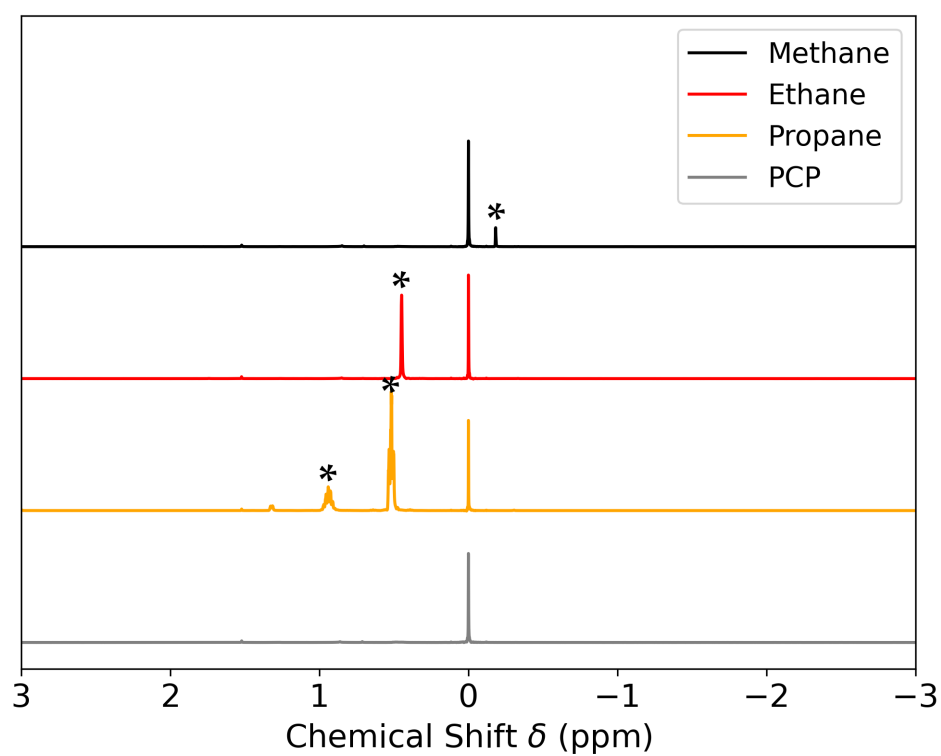
Figure 2.27: Stacked [^1]H NMR spectra of alkane gases dissolved in neat PCP. Alkane peaks are labelled with asterisks.
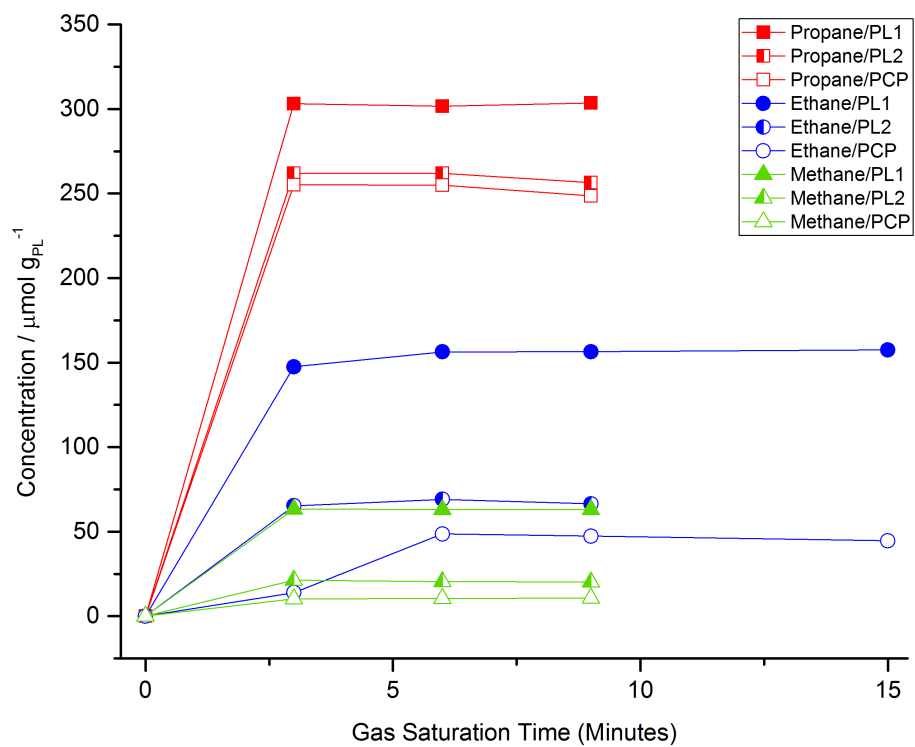
Figure 2.28: Saturation curves of the three alkane gases in **CC3³:13³**-*R* porous liquid (PL1), **CC15**-*R* porous liquid (PL2) and PCP. **CC3³:13³**-*R* porous liquid at 20% w/v and **CC15**-*R* porous liquid at 5% w/v.

Table 2.4: Summary of alkane gas chemical shifts in Figures 2.25, 2.26 and 2.27 measured by NMR spectroscopy for the alkane gases in **CC3^3:13^3**-*R* porous liquid, **CC15**-*R* porous liquid and PCP when saturated with the respective gas.

Gas	δ in CC3^3:13^3-*R* porous liquid (ppm)	δ in CC15-*R* porous liquid (ppm)	δ in PCP (ppm)
CH_4	-2.606	-2.208	-0.183
C_2H_6	-1.657	-0.216	0.449
C_3H_8	0.010[a] -0.184[b]	0.772[a] 0.375[b]	0.940[a] 0.517[b]

[a]Shift for CH_2 environment in propane.[b]Shift for $2CH_3$ environment in propane.

2.8.7 Gas uptake in porous liquids measured by gas evolution

Prior to use, **CC3³:13³**-*R* and **CC15**-*R* were desolvated in a vacuum oven at 90 °C overnight. **CC3³:13³**-*R* (120 mg), or **CC15**-*R* (150 mg), were dissolved in purified PCP (3 mL) in a GC headspace vial. Once saturation was complete, a screw-cap was tightly secured onto each vial, and a cannula was inserted into the cap to connect the internal headspace volume to an inverted burette pre-filled with water sat in a beaker of water. Chloroform (1 eq. relative to the amount of POC present) was added to the vial using a 100 μL microsyringe. The volume of gas evolved was captured in the burette and the water level change was recorded to calculate the amount of gas evolved using the ideal gas law. Gas evolution was measured by displacement of water in an inverted Rotaflo stopcock 10 mL burette (0.1 mL graduations) in a beaker of water connected to the GC vial containing the sample via a needle/tubing cannula. Measurements were repeated a total of three times at the same temperature to obtain a mean gas evolution and corresponding standard deviation.

Table 2.5: Gas evolution data and calculated gas uptake values for the **CC3^3:13^3**-*R* porous liquid (4% w/v) at 298 K. The normalized uptakes are calculated using the measured uptake for PCP (CH$_4$ 2.4 μmol/g$_L$; CO$_2$ 2.4 μmol/g$_L$; Xe 3.6 μmol/g$_L$).[2]

Gas	Volume Evolved (mL)	Mean Volume Evolved (mL)	Gas Uptake (μmol/g $_{PL}$)	Normalised gas uptake μmol/g$_{cage}$
CH$_4$	1.4 1.55 1.55	1.5 ± 0.09	11.6 ± 0.7	0.408
CO$_2$	1.4 1.5 1.3	1.4 ± 0.1	10.9 ± 0.8	0.374
Xe	2.25 2.0 2.1	2.12 ± 0.13	16.5 ± 1.0	0.567
N$_2$	0.3 0.4 0.35	0.35 ± 0.05	2.72 ± 0.38	-

Table 2.6: Gas evolution data and calculated gas uptake values for C_2H_6 and C_3H_8 in the **CC3^3:13^3**-*R* porous liquid (20% w/v) at 298 K.

Gas	Volume Evolved (mL)	Mean Volume Evolved (mL)	Gas Uptake (μmol/g $_{PL}$)
C$_2$H$_6$	6.85		
	7.2	7.01 ± 0.25	50.1 ± 1.8
	7.0		
C$_3$H$_8$	7.75		
	8.05	6.6 ± 2.2	47 ± 15
	4.05		

Table 2.7: Gas evolution data and calculated gas uptake values for the **CC15**-*R* porous liquid (5% w/v) at 298 K. The normalized uptakes are calculated using the measured uptake for PCP (CH_4 2.4 μmol/g_L; CO_2 2.4 μmol/g_L; Xe 3.6 μmol/g_L).[2]

Gas	Volume Evolved (mL)	Mean Volume Evolved (mL)	Gas Uptake (μmol/g $_{PL}$)	Normalised gas uptake (μmol/g_{cage})
CH_4	1.5 1.9 1.75	1.72 ± 0.20	13.3 ± 1.6	0.386
CO_2	1.0 1.1 0.6	0.9 ± 0.26	7.0 ± 2.0	0.164
Xe	0.55 0.5 0.6	0.55 ± 0.05	4.25 ± 0.39	0.027
Xe (6 hours)	0.5	0.5	3.87	-
N_2	0.8 0.25 0.35	0.47 ± 0.29	3.61 ± 2.3	-
C_2H_6	2.65 2.6 2.1	2.45 ± 0.30	19.0 ± 2.4	-
C_3H_8	4.5 4.3 4.4	4.40 ± 0.10	34.1 ± 0.8	-

Table 2.8: Gas evolution data and calculated gas uptake values for C_2H_6 and C_3H_8 in PCP at 298 K.

Gas	Volume Evolved (mL)	Mean Volume Evolved (mL)	Gas Uptake (μmol/g $_{PL}$)
C_2H_6	2.25		
	1.9	1.71	13.7
	1.0		
C_3H_8	4.55		
	3.8	4.17	33.2
	4.15		

2.8.8   Gas sorption analysis

Powder samples were degassed offline at 90 °C for 15 h under dynamic vacuum (10^{-5} bar) before analysis, followed by degassing on the analysis port under vacuum, also at 90 °C. Isotherms were measured using a Micromeritics 2020 or 2420 volumetric adsorption analyzer. Gas uptake measurements for CH_4, CO_2, and Xe were taken at a temperature of 293 K, stabilized using a circulating water chiller/heater and N_2 were taken at a temperature of 77 K.
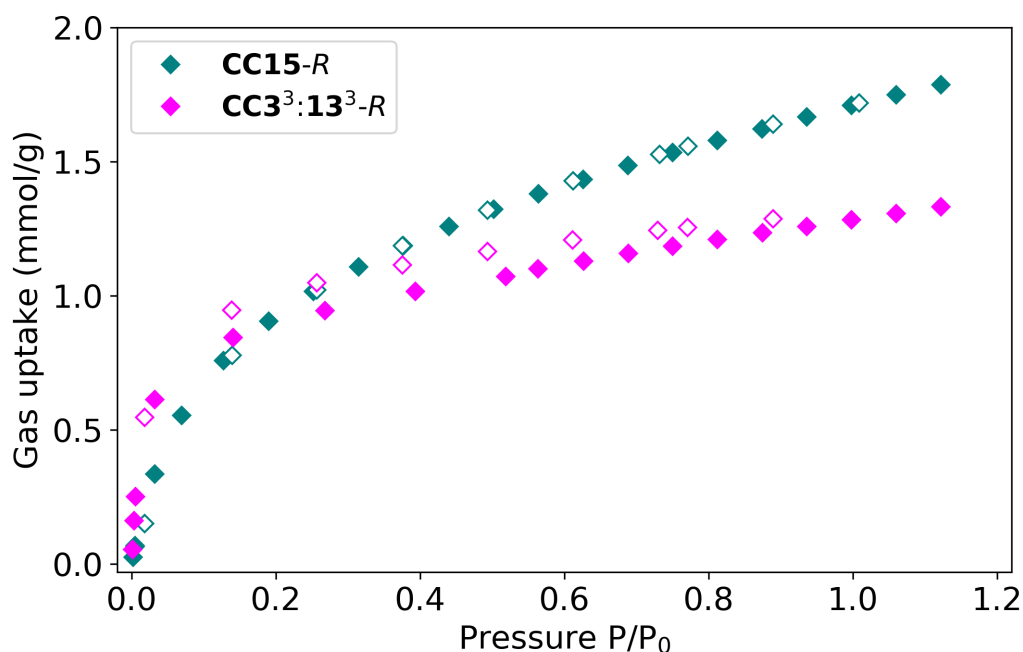
Figure 2.29: CH_4 adsorption (filled) and desorption (empty) isotherms for **CC3³:13³**-*R* and **CC15**-*R* at 298 K.
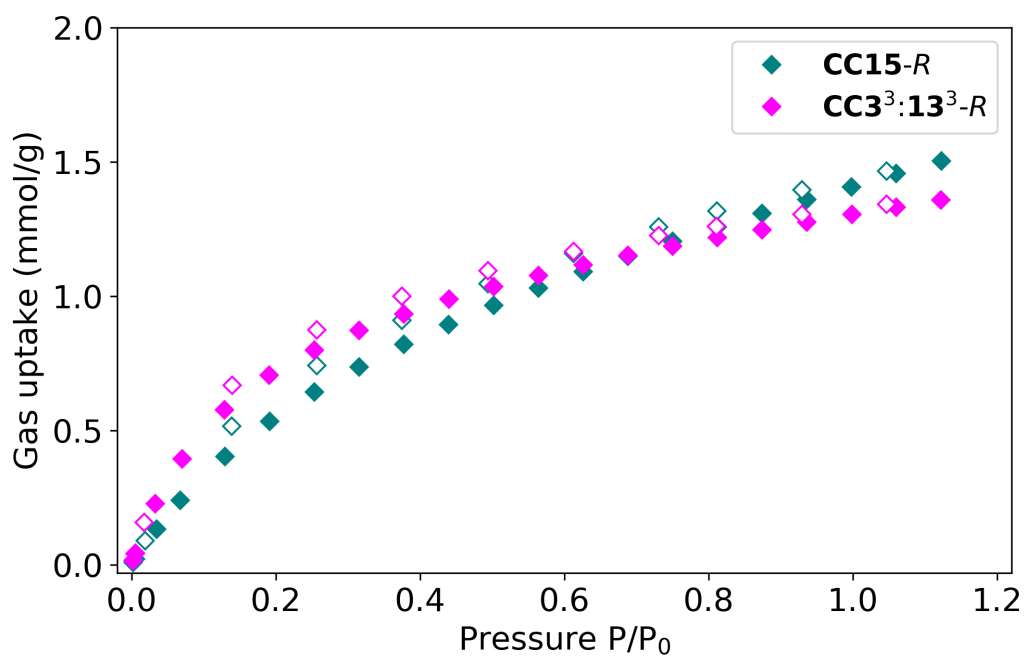
Figure 2.30: CO_2 adsorption (filled) and desorption (empty) isotherms for **CC3^3:13^3**-*R* and **CC15**-*R* at 298 K.
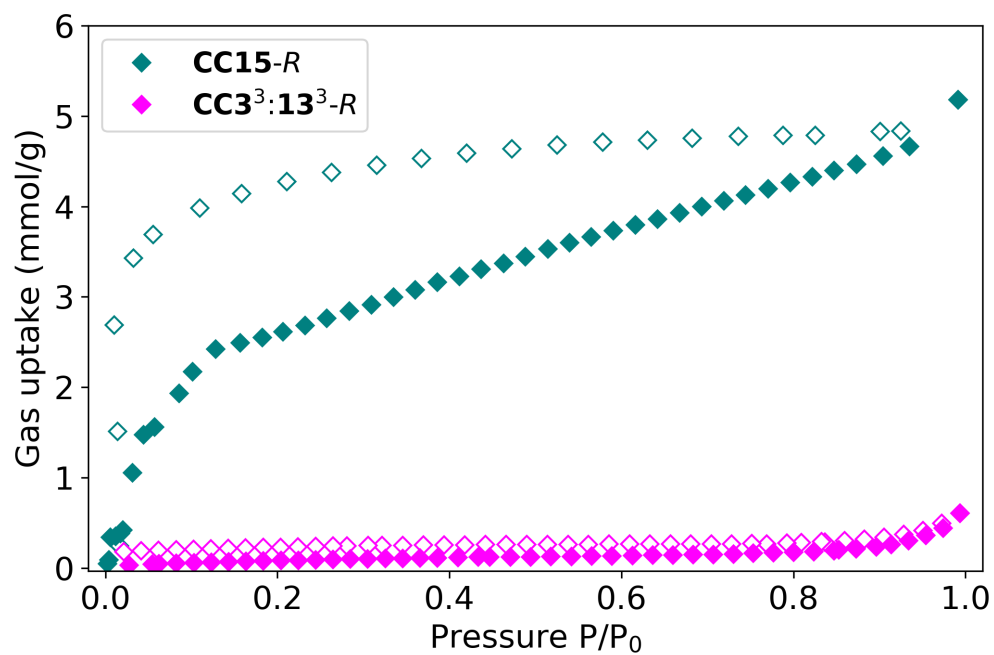
Figure 2.31: Xe adsorption (filled) and desorption (empty) isotherms for **CC3³:13³**-*R* and **CC15**-*R* at 298 K.
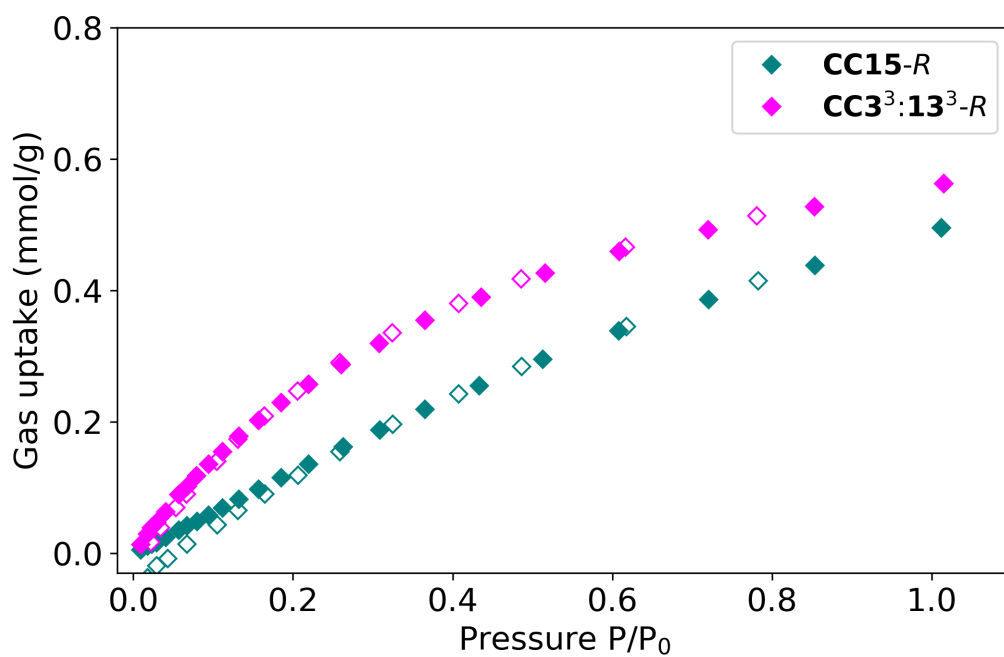
Figure 2.32: N$_2$ adsorption (filled) and desorption (empty) isotherms for **CC3^3:13^3**-*R* and **CC15**-*R* at 298 K.

2.8.9   Viscosity measurements

Viscosity measurements were carried out using a calibrated RheoSense μVISC viscometer (0.01-100 cP). Measurements were repeated a minimum of three times with the average viscosity reported.

Table 2.9: Measured viscosities of the porous liquids and PCP.

Sample	Viscosity, η (mPa s)
CC3^3:13^3-*R* porous liquid (4% w/v)	4.36
CC15-*R* porous liquid (5% w/v)	4.18
PCP	3.26

2.8.10   Diffusion NMR and DOSY experimental details

Samples were prepared and saturated with methane as outlined for the gas uptake experiments by ^{1}H NMR spectroscopy (Section 2.8.6).

All measurements were carried out non-spinning using a 5 mm indirect detection probe, equipped with a z-gradient coil producing a nominal maximum gradient of 34 G/cm. Diffusion data was collected using the Bruker longitudinal eddy current delay (LED) pulse sequence (ledgp2s). A diffusion encoding pulse δ of length 1–7 ms optimised for the diffusion of the solution species, and diffusion delay D of 0.1–0.25 s were used. Gradient amplitudes were equally spaced between 1.70 and 32.4 G/cm. Each FID was acquired using 16 k data points. All experiments were carried out at a nominal probe temperature of 298 K, with an air flow of 800 m^3/min to minimise convection. A sealed lock tube containing TMS
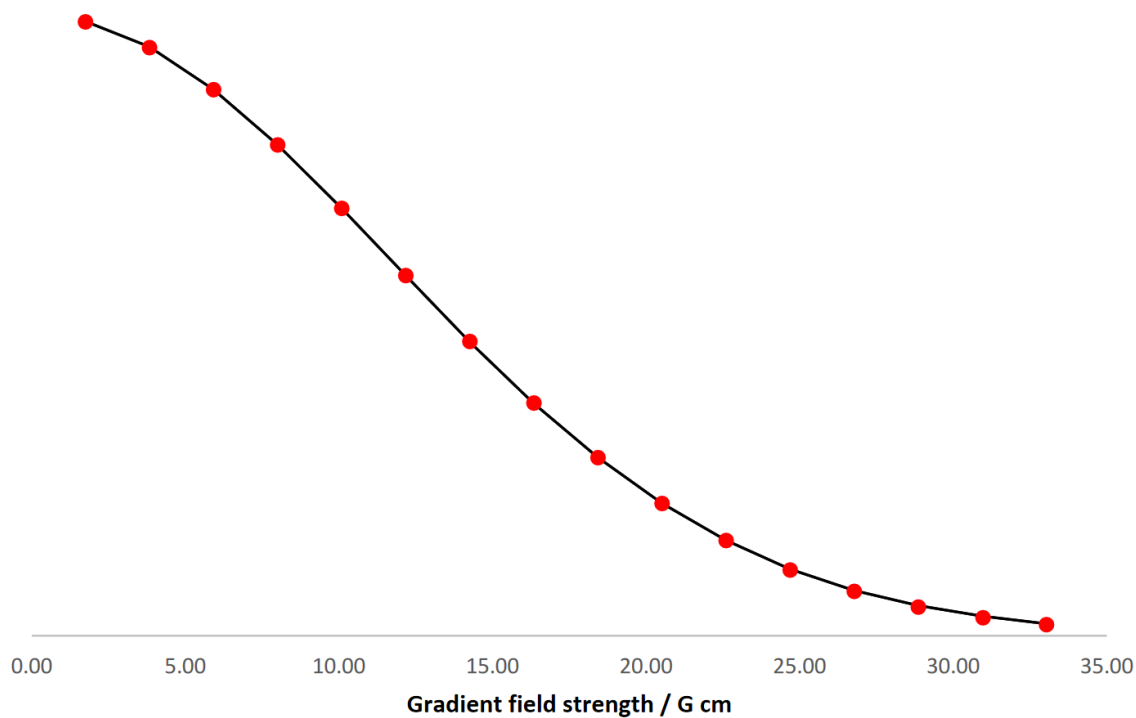
Figure 2.33: Typical signal decay curve at varied gradient amplitude for a well optimised diffusion NMR experiment (red) with fit (black).

in CD_2Cl_2 was used for an internal deuterium lock without affecting the chemical make-up of the porous liquid. Processing of the diffusion spectra was carried out using Bruker TopSpin.

Table 2.10: Summary of the diffusion co-efficients (D), viscosities, POC solvodynamic radii (R_S^{POC}, Equation 2.2), occupancies (X_{occ}, Equation 2.3), and association constants (K_a, Equation 2.4) for the porous liquids and PCP. **CC3^3:13^3**-R porous liquid at 4% w/v and **CC15**-R porous liquid at 5% w/v.

Sample	D_{CH4} (m^2/s)	$D_{\textbf{POC}}$ (m^2/s)	R_S^{POC} (Å)	X_{occ}	[POC] (mol/ dm^3)	[CH$_4$] (mol/ dm^3)	K_a (mol^{-1} dm^3)
PCP	1.34 × 10^{-9}	-	-	-	-	-	-
CC3^3:13^3-R porous liquid	5.43 × 10^{-10}	6.14 × 10^{-11}	8.2	0.49	3.90 × 10^{-5}	6.96 × 10^{-6}	2.71 × 10^4
CC15-R porous liquid	4.58 × 10^{-10}	6.33 × 10^{-11}	8.3	0.60	3.90 × 10^{-5}	7.78 × 10^{-6}	4.36 × 10^4

References

(1) N. Giri, M. G. Del Pópolo, G. Melaugh, R. L. Greenaway, K. Rätzke, T. Koschine, L. Pison, M. F. C. Gomes, A. I. Cooper and S. L. James, *Nature*, 2015, **527**, 216–220.

(2) R. L. Greenaway, D. Holden, E. G. B. Eden, A. Stephenson, C. W. Yong, M. J. Bennison, T. Hasell, M. E. Briggs, S. L. James and A. I. Cooper, *Chem. Sci.*, 2017, **8**, 2640–2651.

(3) K. Jie, N. Onishi, J. A. Schott, I. Popovs, D.-e. Jiang, S. Mahurin and S. Dai, *Angewandte Chemie*, 2020, **132**, 2288–2292.

(4) S. Ma, D. Sun, X.-S. Wang and H.-C. Zhou, *Angew. Chem. Int. Ed.*, 2007, **46**, 2458–2462.

(5) O. M. Yaghi, *Mol. Front. J.*, 2019, **03**, 66–83.

(6) M. Eddaoudi, J. Kim, N. Rosi, D. Vodak, J. Wachter, M. O'Keeffe and O. M. Yaghi, *Science*, 2002, **295**, 469–472.

(7) R. W. Tilford, S. J. Mugavero, P. J. Pellechia and J. J. Lavigne, *Adv. Mater.*, 2008, **20**, 2741–2746.

(8) A. G. Slater, M. A. Little, A. Pulido, S. Y. Chong, D. Holden, L. Chen, C. Morgan, X. Wu, G. Cheng, R. Clowes, M. E. Briggs, T. Hasell, K. E. Jelfs, G. M. Day and A. I. Cooper, *Nat. Chem.*, 2017, **9**, 17–25.

(9) S. Tothadi, M. A. Little, T. Hasell, M. E. Briggs, S. Y. Chong, M. Liu and A. I. Cooper, *CrystEngComm*, 2017, **51**, 7154–7157.

(10)   M. Liu, L. Zhang, M. A. Little, V. Kapil, M. Ceriotti, S. Yang, L. Ding, D. L. Holden, R. Balderas-Xicohténcatl, D. He, R. Clowes, S. Y. Chong, G. Schütz, L. Chen, M. Hirscher and A. I. Cooper, *Science*, 2019, **366**, 613–620.

(11)   A. G. Slater, P. S. Reiss, A. Pulido, M. A. Little, D. L. Holden, L. Chen, S. Y. Chong, B. M. Alston, R. Clowes, M. Haranczyk, M. E. Briggs, T. Hasell, G. M. Day and A. I. Cooper, *ACS Central Science*, 2017, **3**, 734–742.

(12)   M. Miklitz and K. E. Jelfs, *Journal of Chemical Information and Modeling*, 2018, **58**, 2387–2391.

(13)   L. Chen, P. S. Reiss, S. Y. Chong, D. Holden, K. E. Jelfs, T. Hasell, M. A. Little, A. Kewley, M. E. Briggs, A. Stephenson, K. M. Thomas, J. A. Armstrong, J. Bell, J. Busto, R. Noel, J. Liu, D. M. Strachan, P. K. Thallapally and A. I. Cooper, *Nat Mater*, 2014, **13**, 954–960.

(14)   E. O. Stejskal and J. E. Tanner, *The Journal of Chemical Physics*, 1965, **42**, 288–292.

(15)   D. Sinnaeve, *Concepts Magn. Reson. Part A*, 2012, **40A**, 39–65.

(16)   C. S. Johnson Jr., *Progress in Nuclear Magnetic Resonance Spectroscopy*, 1999, **34**, 203–256.

(17)   Y. Cohen, L. Avram and L. Frish, *Angew. Chem. Int. Ed.*, 2005, **44**, 520–554.

(18)   R. L. Greenaway, V. Santolini, M. J. Bennison, B. M. Alston, C. J. Pugh, M. A. Little, M. Miklitz, E. G. B. Eden-Rump, R. Clowes, A. Shakil, H. J. Cuthbertson, H. Armstrong, M. E. Briggs, K. E. Jelfs and A. I. Cooper, *Nature Communications*, 2018, **9**, 2849.

(19) K. S. Cameron and L. Fielding, *Journal of Organic Chemistry*, 2001, **66**, 6891–6895.

(20) T. Tozawa, J. T. a. Jones, S. I. Swamy, S. Jiang, D. J. Adams, S. Shakespeare, R. Clowes, D. Bradshaw, T. Hasell, S. Y. Chong, C. Tang, S. Thompson, J. Parker, A. Trewin, J. Bacsa, A. M. Z. Slawin, A. Steiner and A. I. Cooper, *Nature materials*, 2009, **8**, 973–978.

(21) T. Hasell, M. Schmidtmann and A. I. Cooper, *Journal of the American Chemical Society*, 2011, **133**, 14920–14923.

(22) T. Hasell, S. Y. Chong, M. Schmidtmann, D. J. Adams and A. I. Cooper, *Angew. Chem. Int. Ed.*, 2012, **51**, 7154–7157.

(23) T. Hasell, S. Y. Chong, K. E. Jelfs, D. J. Adams and A. I. Cooper, *Journal of the American Chemical Society*, 2012, **134**, 588–598.

(24) T. Hasell, M. Schmidtmann, C. A. Stone, M. W. Smith and A. I. Cooper, *Chemical Communications*, 2012, **48**, 4689.

(25) T. Hasell, J. a. Armstrong, K. E. Jelfs, F. H. Tay, K. M. Thomas, S. G. Kazarian and A. I. Cooper, *Chem. Commun.*, 2013, **49**, 9410–9412.

(26) D. Holden, K. E. Jelfs, A. Trewin, D. J. Willock, M. Haranczyk and A. I. Cooper, *Journal of Physical Chemistry C*, 2014, **118**, 12734–12743.

(27) T. Hasell, M. Miklitz, A. Stephenson, M. A. Little, S. Y. Chong, R. Clowes, L. Chen, D. Holden, G. A. Tribello, K. E. Jelfs and A. I. Cooper, *J. Am. Chem. Soc.*, 2016, **138**, 1653–1659.

(28)   S. Komulainen, J. Roukala, V. V. Zhivonitko, M. A. Javed, L. Chen, D. Holden, T. Hasell, A. Cooper, P. Lantto and V.-V. Telkki, *Chem. Sci.*, 2017, **8**, 5721–5727.

(29)   S. Jiang, J. T. a. Jones, T. Hasell, C. E. Blythe, D. J. Adams, A. Trewin and A. I. Cooper, *Nature communications*, 2011, **2**, 207.

(30)   A. G. Slater and A. I. Cooper, *Science*, 2015, **348**, 8075–8075.

(31)   S. Jiang, K. E. Jelfs, D. Holden, T. Hasell, S. Y. Chong, M. Haranczyk, A. Trewin and A. I. Cooper, *Journal of the American Chemical Society*, 2013, **135**, 17818–17830.

(32)   *Standard Reference Database Number 69*, DOI 10.18434/T4D303 can be found under https://webbook.nist.gov/chemistry/, National Institute of Standards and Technology (NIST), 2019.

3 Modifying porosity in type 3 porous liquids based on POCs

Until now, synthetic pore control in type 3 porous liquids hasn't been attempted. Since producing microporous dispersions by combining some microporous solid with an excluded silicone oil has been demonstrated as a relatively easy technique,[1] we chose to expand this to POCs. Preparation of POC nano- and microparticles *via.* a cocrystalisation technique was used to produce stable dispersions composed of POCs with altered pore structure. This resulted in the modification of the gas uptake in these type 3 porous liquids, demonstrating synthetic pore control, albeit not resulting in any change to the overall selectivity.

3.1 Type 3 porous liquids

A variety of type 3 porous liquids have already been presented in the literature since 2015, mainly prepared from MOFs, COFs and zeolites.[2,3] In all cases, these materials differ largely from type 1 and 2 porous liquids in that they are biphasic systems, consisting of a solid pore carrier dispersed in a fluid phase. Similar design considerations still apply here, the composing materials must be selected such that the molecules making up the fluid phase do not occupy all the pore spaces in the solid material. Type 3 porous liquids are in some ways easier to prepare than type 1 and 2 porous liquids, almost any microporous material can be dispersed in almost any fluid phase to some extent, showcased by Cahir *et al.* where a multitude of microporous materials were prepared as dispersions in a range of

polymeric and triglygeride oils, including silicone oils.[1] Rather than considering solubility, instead the dispersion stability must be accounted for to produce stable dispersions, depending on factors such as particle size, particle size polydispersity, and electrostatic interactions at the solid-liquid interface.[4]

3.2 Pore control in POCs by formation of cocrystals

Several examples of type 3 porous liquids developed so far were presented in Chapter 1, and have been based on selection of a suitable pore carrier that can be easily formulated into a porous dispersion. Little consideration has been taken to study the effects of synthetically controlling the porosity in porous liquids, *i.e.* carrying out fine tuning of pore size to influence gas uptake. Since cages have been effective as pore carriers in type 1 and type 2 porous liquids, it is important to also assess their ability as solid pore carriers in type 3 porous liquids. In type 1 and 2 porous liquids we have seen the loss of porosity relative to solid materials due to the loss of the extrinsic, 'between cage' voids. In type 3 porous liquids this porosity is retained as the solid is merely dispersed in a carrier liquid, retaining extrinsic porosity.[5]

Controlling POC pore structure to influence the gas uptake has been studied widely in the solid state, for example by introducing bulky groups to decrease the window or cavity sizes, as applied in Xe or hydrogen isotope separation.[7,8] Likewise, specific functional groups have been introduced into POCs to modulate the chemical environment for CO_2/CH_4 separations.[9] The modular formation of cocrystals from isostructural cage molecules has been demostrated as an effective
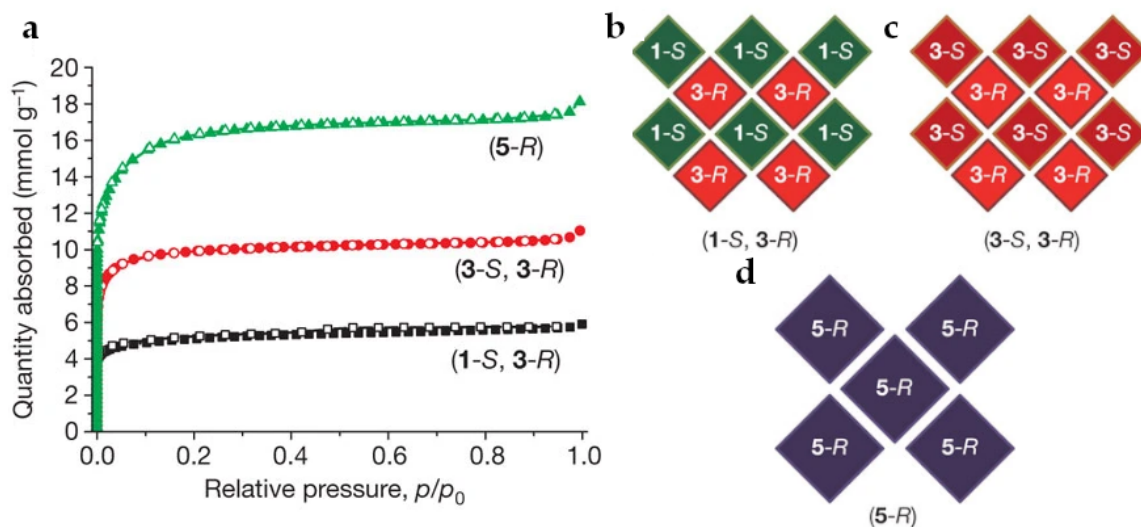
Figure 3.1: (**a**) N_2 uptake isotherms at 77 K of (**b**) quasiracemic POC **CC3**-*R*/**CC1**-*S* cocrystal, (**c**) racemic **CC3**-*R/S* cocrystal and enantiopure **CC5**-*R*, which did not form cocrystals, prepared by Jones *et al.*[6]

method for creating racemates and quasiracemates with varying pore network structure, as well as demonstrating certain cages would not favourably form cocrystals (Figure 3.1).[6] Cocrystal formation from chiral [4+6] imine POCs, like **CC3**, occurs due to the favourable interaction between the two enantiomers of these POCs. In the case of **CC3**, the window-to-window interaction that constitutes the crystal packing structure in the solid state is further enhanced when the two enantionmerically pure cages **CC3**-*R* and **CC3**-*S* are combined, resulting in a denser crystal structure and lower solubility of the product, **CC3**-*R/S*. This strong interaction can also be used to direct the packing with other POCs, when combining other chiral cages that do not form pore networks in the solid crystal with quasienatiomeric **CC3**, crystal packing can be directed to form the porous

diamondoid network found in enantiopure **CC3**.[6] This enables modulation of gas uptake in the solid crystal (Figure 3.1 a) and can even be extended to form ternary cocrystals of POCs, further tuning the porosity.[10]

Beyond control of gas selectivity, cocrystal formation can be exploited to control the particle size of solid POCs. Combination of solutions of each enantiomer of **CC3** leads to formation of nano- or microcrystalline particles forming rapidly due to a sharp reduction in the solublility of the cages upon mixing.[11] Changing the temperature and addition rate modifies the particle size and morphology, which can be used to control particle formation (Figure 3.2). The dispersions of these particles, as produced in DCM, were observed as stable for several months with no aggregation or change to particle size observed. Quasiracemic cocrystal microparticles can also be prepared in a similar manner, Jiang *et al.* demonstrated that core-shell cocrystals can be prepared by a similar technique.[9]

Here, we sought to transfer this concept to type 3 porous liquids by using POC quasiracemic cocrystals with modified pore structures.
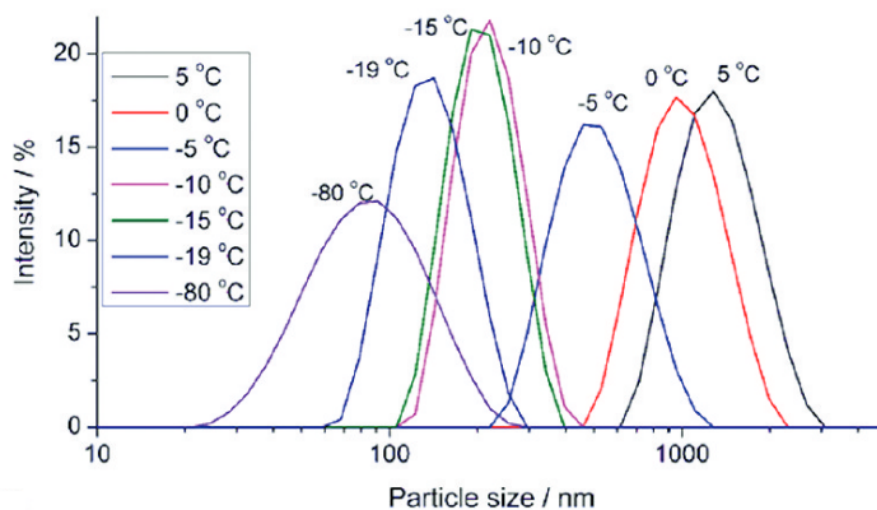
Figure 3.2: Temperature control of the formation of **CC3**-*R/S* POC nanocrystals. Temperature modulates the crystal growth rate.[11]

3.3 Modifying pore structure in POC microparticles for porous liquids

Preparing microcrystals from **CC3**-*R* and **CC3**-*S* has been developed previously, where the chiral recognition of **CC3**-*R* and **CC3**-*S* enables rapid crystallisation into nano- and microcrystals by combining solutions of each homochiral cage.[11] This can be used to either produce racemic cocrystals, as in **CC3**-*R* and **CC3**-*S* (Figure 3.3, or from isostructural cages, such as **CC19**-*R* containing the same underlying geometric structure to enable formation of quasi-racemates.[9,10]

3.3.1 Synthesis of POC microcrystals

As in Chapter 2, cages were selected which have restricted apertures compared to **CC3**. In this case we selected **CC15**-*S*[7] and **CC19**-*S*[9] to cocrystallise with **CC3**-
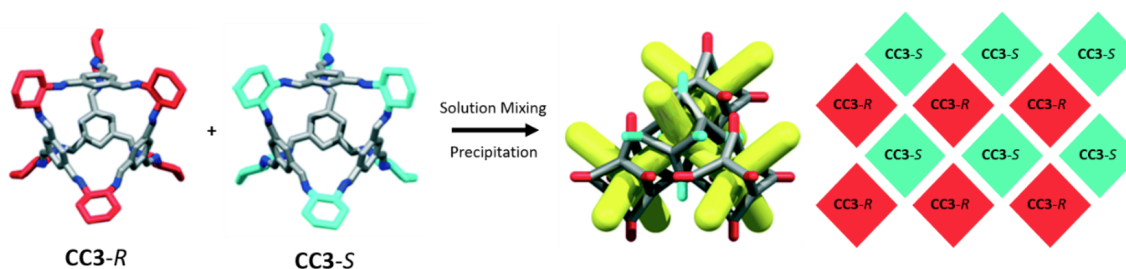
Figure 3.3: Enantiopure **CC3**-*R* and **CC3**-*S* are combined to form racemic **CC3**-*R/S* by mixing in solution to form a cocrystal composed of the two POCs.[6] The packing structure of the formed cocrystal has the interconnected diamondoid pore network found in **CC3**-*R* and is composed of alternating **CC3**-*R* and **CC3**-*S* molecules.

R (Figure 3.4). Here, solubility of the cages did not need to be considered as formation of stable dispersions of the solid POCs was required, in fact the lower solubility of POCs in these racemic mixtures helps to improve the stability of the prepared dispersions. By combining different cages in this way, the components can be selected based on whether they include functional groups that modify the pore network in the crystal structure. This can be used to restrict the pore and portal diameter or the chemical environment of the pore.

Following a method adapted from Hasell *et al.*, microcrystals of racemic **CC3**-*R/S* and the quasiracemates, **CC3**-*R*/**CC15**-*S* and **CC3**-*R*/**CC19**-*S*, were prepared.[11] The three cages used to prepare these microparticles, **CC3**-*R*, **CC15**-*S* and **CC19**-*S* all have differing pore window structure (Figure 3.4). **CC15**-*S* contains window-occluding methyl groups and **CC19**-*S* contains hydroxyl groups located on the aromatic rings, pointed into the cage windows. While **CC3**-*R/S* and **CC3**-*R*/**CC19**-*S* solid microparticles precipitated readily from dilute solutions in DCM

Figure 3.4: Molecular structures of **CC3**-*S*, **CC15**-*S* and **CC19**-*S*, the POCs combined with **CC3**-*R* to form the cocrystalline materials used in this study.

at room temperature, crystallisation did not occur when carrying out the same method with **CC3**-*R* and **CC15**-*S*. Slater *et al.* prepared crystals of **CC3**-*R*/**CC15**-*S* from DCM at a much higher concentration, but did not target reduced particle si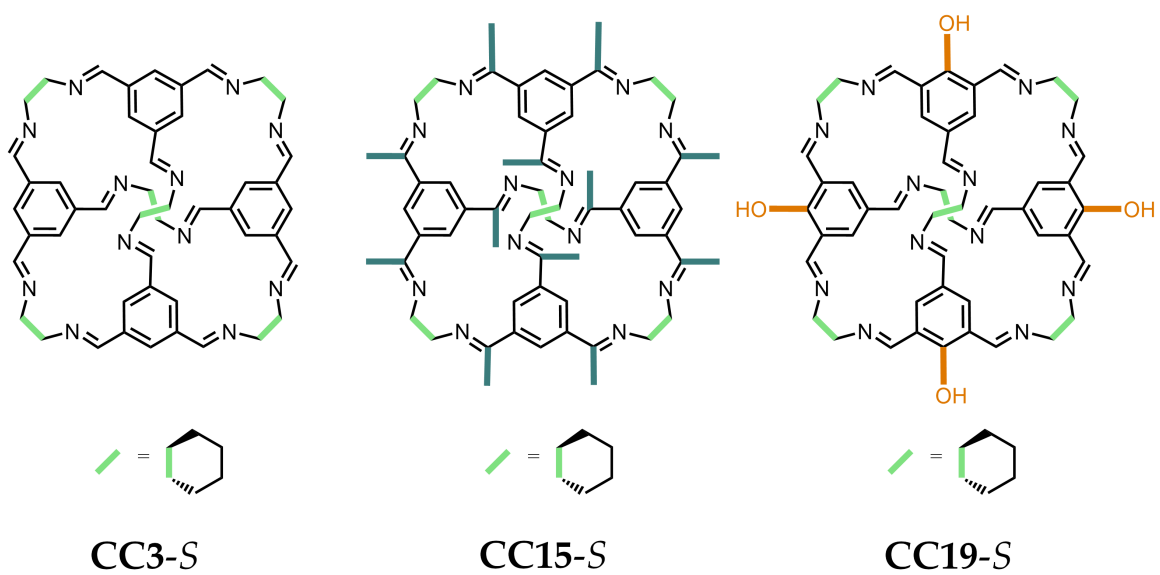ze.[7] Instead **CC3**-*R*/**CC15**-*S* could be prepared by precipitation from a 1:1 methanol/DCM mixture at the same very dilute concentration. This is attributed to the methyl groups reducing the favourable window-to-window interaction between the cages which enable the crystal formation, requiring a lower solubility of the cage mixture in the solvent phase to allow crystallisation.

3.3.2   Particle size determination

Since the formation of the POC cocrystals allows for control over the size of the crystallites, light scattering and scanning electron microscopy (SEM) were used to probe this effect. Previously, dynamic light scattering (DLS) was shown as a useful technique for determining the particle size distribution in dispersions of **CC3**-*R/S* nanoparticle dispersions, coupled with SEM to confirm particle size and provide information about the morphology of the particles.[11] DLS was carried out across several similar batches of **CC3**-*R/S* particles to confirm reproducibility of the particle preparation (Figure 3.5), batches 1-5 were prepared by rapid addition of solutions of **CC3**-*R* and **CC3**-*S* while batch 6 was prepared following the slow addition method employed by Hasell *et al.*[11] All batches varied in particle size, with the Z-average values ranging from 540 nm to 1200 nm, and the slow addition batch placed between the extremes (940 nm) (Figure 3.5).

With the **CC3**-*R*/**CC19**-*S* particles, the DLS measurements show a Z-average of 300 nm (Figure 3.6), while smaller than that measured for **CC3**-*R/S* paticles,
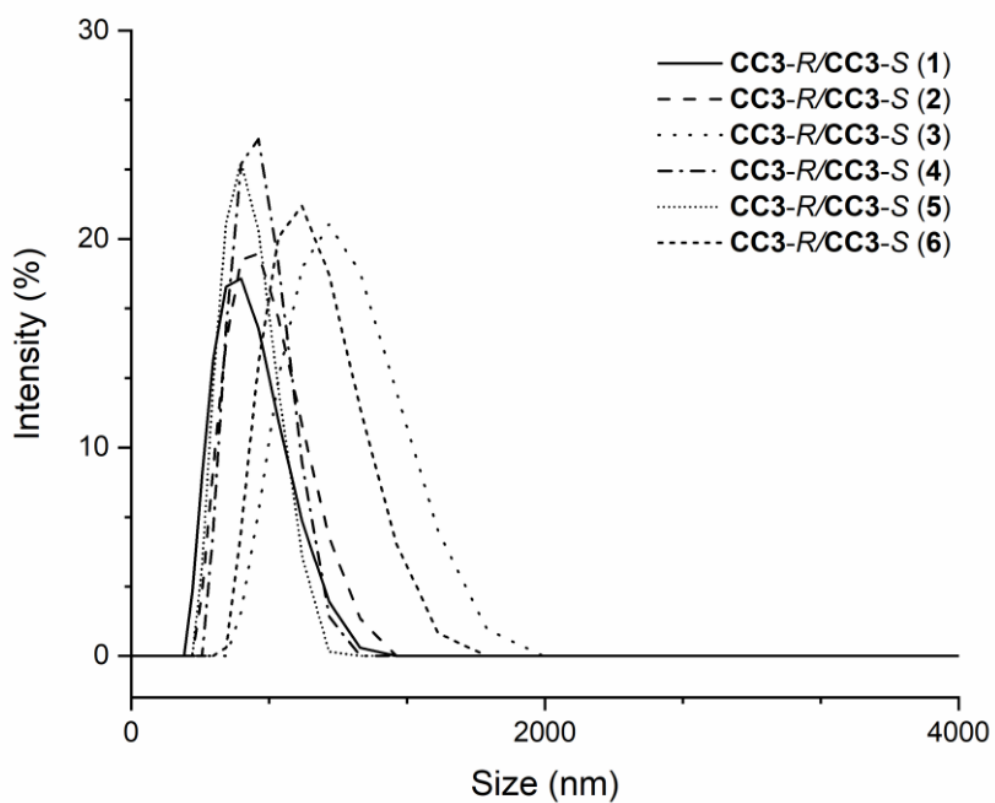
Figure 3.5: Representative DLS measurement of the six batches of **CC3**-*R/S* cocrystals prepared by rapid solution mixing, with Z-average values all within a similar range of particle sizes (540 nm to 1200 nm).
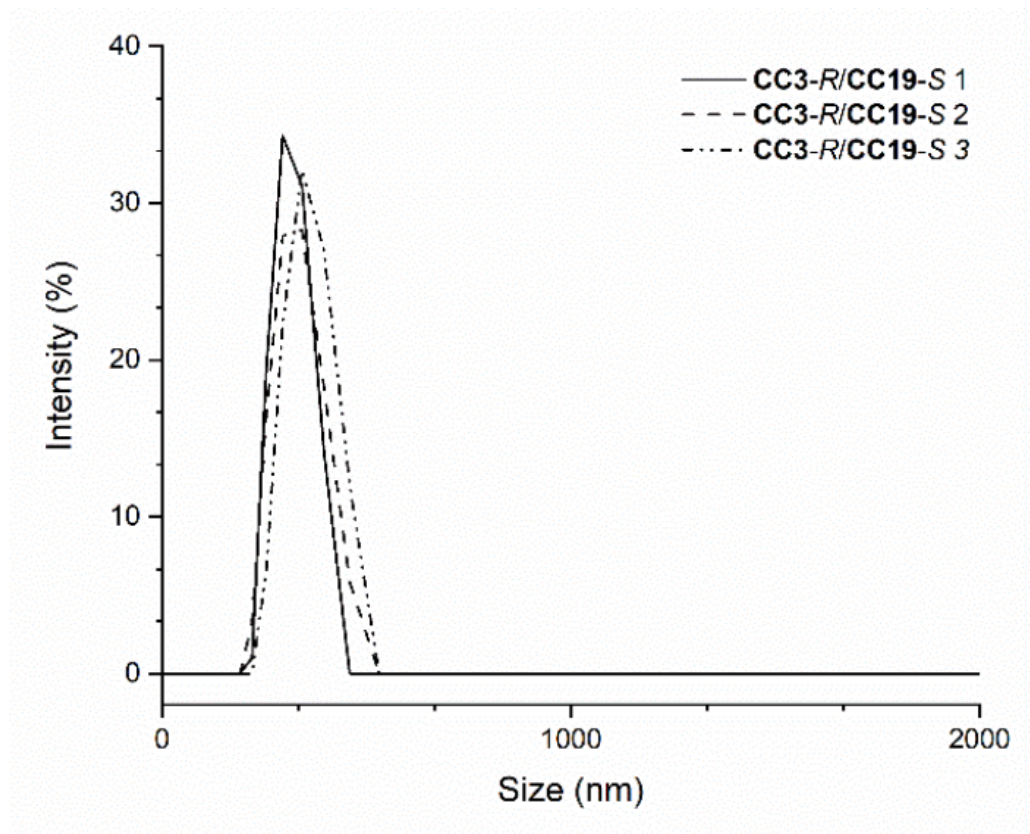
Figure 3.6: Representative DLS measurements of **CC3**-*R*/**CC19**-*S*.

the particles are in a similar range of magnitude and would be expected to form stable dispersions as with **CC3**-*R/S*. This was observed with the samples forming dispersions that were stable for at least several days, allowing for the DLS measurements to be carried out.

DLS measurements could not be carried out with the **CC3**-*R*/**CC15**-*S* cocrystals however, due to the settling of the dispersed particles being greater than the Brownian motion of the particles, the effect that DLS relies on.[12] Instead we employed static light scattering (SLS) to determine the particle size average for the prepared **CC3**-*R*/**CC15**-*S*; the instability of the dispersions already indicated

that the particle size was much larger than the other POC cocrystals. SLS is an alternative light scattering technique that measures the scattering across a range of scattering angles, allowing the use of stirring to maintain the dispersed particles in the light beam and not relying on measurement of the Brownian motion of the dispersion. The average particle size of the prepared **CC3**-*R*/**CC15**-*S* was determined to be 17 μm (Figure 3.7), much larger than for the other two cocrystals prepared. This indicates either that particle aggregation occurs significantly in the **CC3**-*R*/**CC15**-*S* cocrystals, or that the seeding rate of new crystallites from solution is much slower than with the other two cocrystals, despite use of an anti-solvent to aid crystallisation. This may be largely influenced by the weakening of the window-to-window interaction between **CC3**-*R* and **CC15**-*S*. Jiang *et al.* used **CC3**-*R/S* cocrystals to seed growth of **CC3**-*R*/**CC15**-*S* cocrystal shells, eliminating issues with slow seeding rate in crystallite formation in this application.

SEM images were acquired for the samples to confirm the particle size of the three POCs cocrystals, as well as determine the particle morphology. For **CC3**-*R/S*, on slow addition of the solutions octahedral crystals were formed (Figure 3.8 right) whereas upon rapid mixing of the solutions, spherical particles formed due to the much more rapid crystal growth (Figure 3.8 left). The particle size in the SEM images agrees well with the DLS measurements. In contrast to the **CC3**-*R/S* particles, in **CC3**-*R*/**CC15**-*S* and **CC19**-*R* (Figure 3.9 both of the prepared cocrystals have octahedral morphology, even **CC19**-*R* is prepared by the same process as **CC3**-*R/S*. The sizes of the particles also match that of the DLS and SLS.
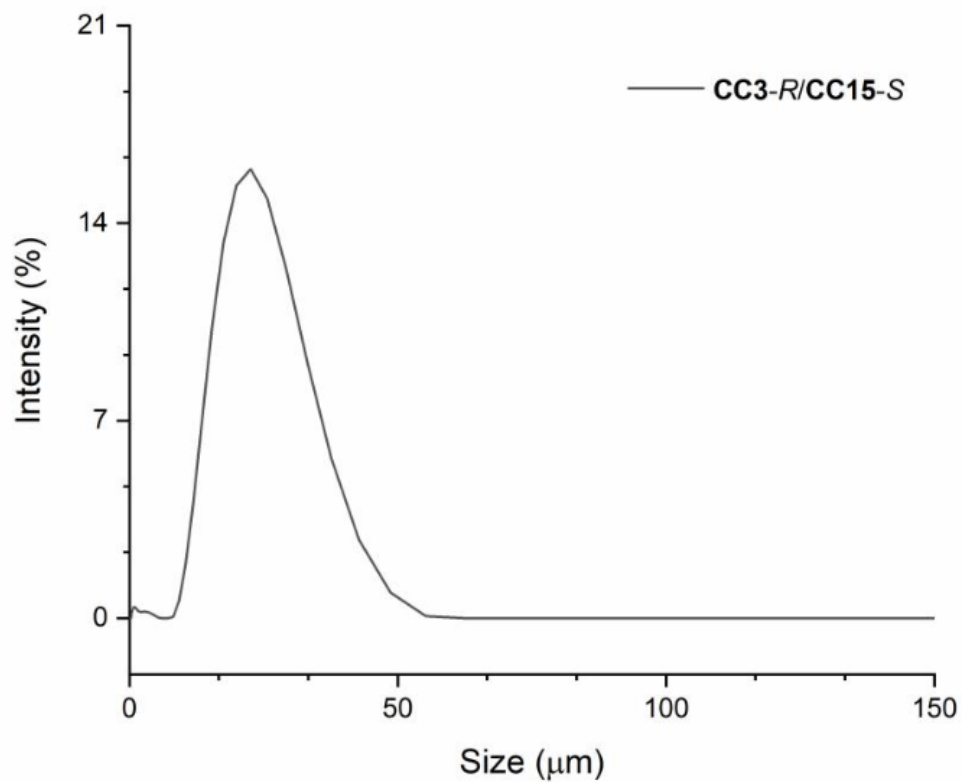
Figure 3.7: Representative SLS measurement of **CC3**-*R*/**CC15**-*S*.
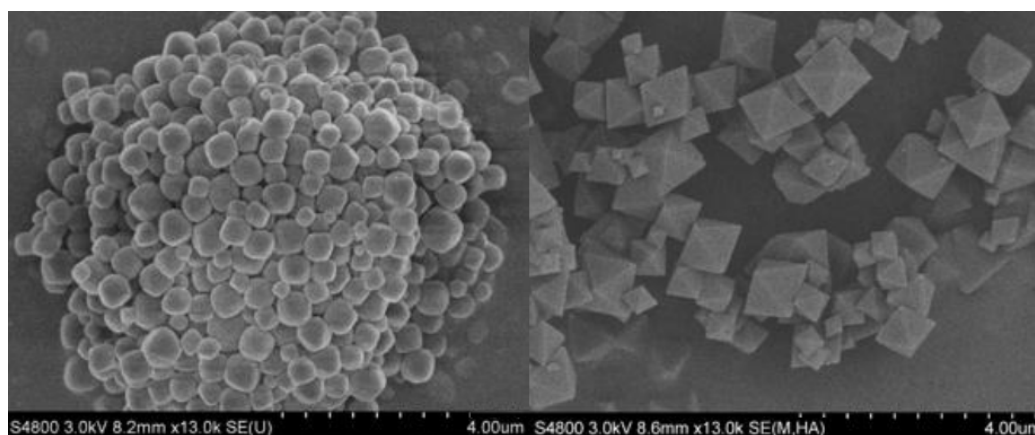
Figure 3.8: Representative SEM images of POC cocrystals of **CC3**-*R/S* prepared by rapid solution mixing (left) and slow addition (right). The product of rapid solution mixing of **CC3**-*R* and **CC3**-*S* produces spherical particles (left) while the slower addition enables formation of octahedral crystallites (right).
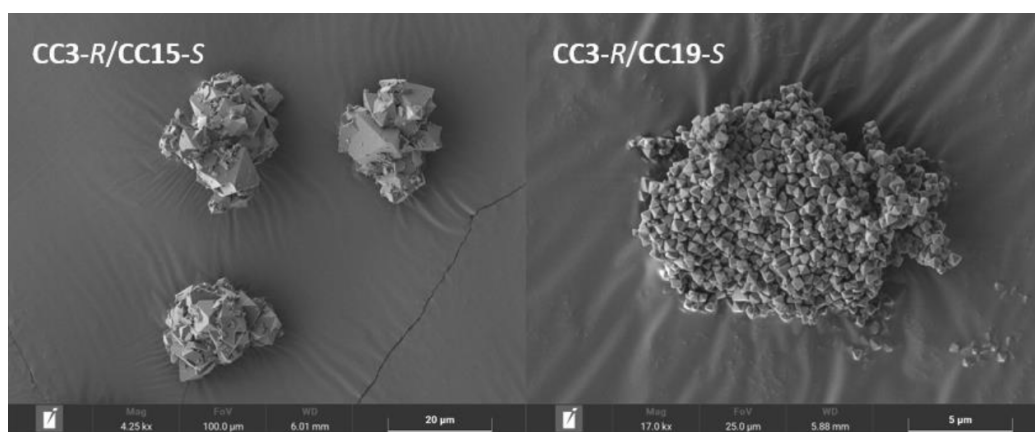
Figure 3.9: Representative SEM images of **CC3**-*R*/**CC15**-*S* (left) and **CC3**-*R*/**CC19**-*S* (right), in both cases the particles formed have octahedral morphology.

145

3.3.3   Structure determination

In order to confirm the identity of the prepared quasiracemic cocrystals, PXRD was employed to confirm the solid state packing and compared with literature patterns to find good agreement (Figure 3.10).[7,9,13] In enantiomeric **CC3**-*R* and **CC19**-*S*, each form the expected structures with window-to-window packing occuring in the solid, whereas **CC15**-*S* forms a window-to-arene packed structure; the presence of the methyl groups in **CC15** lead to loss of this favourable packing motif found in **CC3**. In the (quasi)racemates, all three form the **CC3**-α packing structure, even in **CC3**-*R*/**CC15**-*S* the presence of **CC3** guides the formation of this structure that gives rise to the diamondoid pore network (Figure 3.3). This is especially important in the case of **CC15** as now all three of the cocrystals have the same packing arrangement, with structural modification of the individual molecules.

Furthermore, the PXRD patterns also indicate the changing density of the crystals as the unit cell shrinks in the cocrystals, although **CC15**-*R* cannot be compared due to its differing packing arrangement (Figure 3.10). The reflection at *ca.* 12-13° has been used previously to indicate this in other POC cocrystals,[10] and the moving of all the peaks to greater angles is represented by this. In enantionmeric **CC19**-*S* and **CC3**-*R*, this peak is found at 12.28° and 12.16° respectively, while in the quasiracemic cocrystal **CC3**-*R*/**CC19**-*S* this reflection shifts to 12.42° and **CC3**-*R/S* shows the greatest contraction of the cell with the refection at 12.44°. In **CC3**-*R*/**CC15**-*S* this reflection is at 12.36°, showing the crystal density is not as great as in the other cocrystals, due to the methyl groups reducing the interaction between adjacent cages in the packing structure compared to the

interaction between **CC3**-*R* and **CC3**-*S* or **CC19**-*S*.
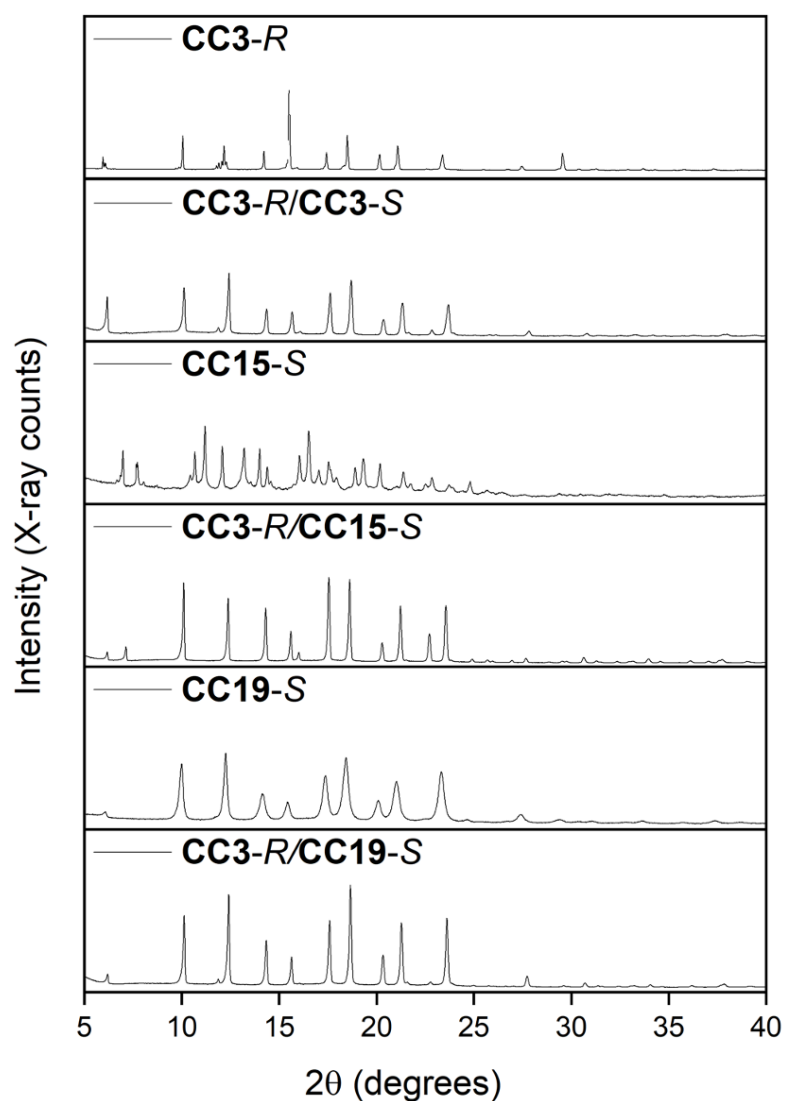
Figure 3.10: PXRD patterns of the enantiopure, racemic and quasiracemic POCs used in this study. **CC3**-*R*, **CC19**-*S*, **CC3**-*R/S*, **CC3**-*R*/**CC15**-*S* and **CC3**-*R*/**CC19**-*S* all have the same series of major reflections due to their matching window-to-window crystal packing structure, whereas **CC15**-*S* does not match due to the window-to-arene packing structure.

3.4   Type 3 porous liquids from POCs

Silicone oils have been used previously to prepare type 3 porous liquids with a variety of microporous materials.[1] Dispersions of **CC3**-*R/S* can be formed stably in silicone oil at up to 50 wt.% silicone oil.[14] In order to balance viscosity and pore concentration, 12.5 wt.% dispersions were prepared of the three cocrystals for comparison (13.22 mPa s in **CC3**-*R/S* porous liquid *vs.* 5.01 mPa s in neat silicone oil).[14]

We determined that the **CC3**-*R*/**CC15**-*S* microcrystals did not form a stable dispersion in DCM when carrying out DLS measurements, but combining the greatly increased viscosity of silicone oil (5 mPa s) with stirring to overcome the settling that occurs, it was possible to form a homogenous fluid at 12.5 wt.% with the **CC3**-*R*/**CC15**-*S* in order too compare the porosity with the other dispersions. All of these dispersions were visually stable after standing at room temperature for at least 24 hours. While the particle size is significantly greater in **CC3**-*R*/**CC15**-*S* than in **CC3**-*R/S* and **CC3**-*R*/**CC19**-*S*, the porosity of the dispersions is not expected to be related to surface area or particle size of the solid component of the dispersion. In the solid state adsorption in the bulk crystal and diffusion carries little bearing on volumetric adsorption experiments due to equilibration time being much greater than diffusion time.

3.5   Gas uptake in type 3 porous liquids

Gas uptake measurements in the type 3 porous liquids was carried out using a volumetric gas sorption instrument (Quantachrome Nova 4200e) modified to

allow stirring of samples during the experiment. CO_2 and CH_4 uptake was measured for the three systems to determine the effect of controlling the pore in POCs in type 3 porous liquids. A 30 minute equilibration time was used to minimise the impact of diffusion of the gases through the viscous silicone oil, and stirring was employed to further aid this.

For **CC3**-*R/S*, the CO_2 and CH_4 uptake at 1 bar in the porous dispersions was greater than in the neat liquid (Figures 3.11 and 3.12) showing that porosity is retained in the solid component of these dispersions, *i.e.* the silicone oil is excluded from the pores in the dispersed cocrystals. When comparing the dispersions to the uptake in the solid state, we can use the same calculation carried out in Chapter 2 (Equation 2.5) to calculate what contribution to the gas uptake is due to the presence of the cage in the dispersion, subtracting the uptake in the neat silicone oil. In the cases of both CO_2 and CH_4 the relative uptake enhancement per gram of cage is reduced in these dispersions to 50% of the CO_2 capacity (912 μmol/g_{cage} in the porous liquid *vs* 1792 μmol/g_{cage} in the solid) and 66% of the CH_4 capacity (704 μmol/g_{cage} in the porous liquid *vs* 1064 μmol/g_{cage} in the solid). This observed reduction in uptake is potentially due to the loss of some extrinsic porosity when **CC3**-*R/S* is dispersed, and possibly the viscosities of the dispersions affecting the diffusion of gas through the liquid phase of the porous dispersions.

The two additional systems were also studied, **CC3**-*R*/**CC15**-*S* and **CC3**-*R*/**CC19**-*S* (3.11 and 3.12). As outlined in Chapter 2, **CC15**-*S* is isostructural with **CC3**-*S* but methyl groups occupy the four windows and reduce the window size to 1.7 Å (from 4 Å in **CC3**-*S*, Figure 2.4). The reduced cage window size in **CC15**-*R* affects gas sorption in the internal cavities and in the portal sites, with

Figure 3.11: CO$_2$ uptake isotherms measured using adapted Quantachrome Nova 4200e in the three porous liquids prepared from **CC3**-*R/S*, **CC3**-*R*/**CC15**-*S* and **CC3**-*R*/**CC19**-*S* at 12.5 wt.% in silicone oil at 298 K.
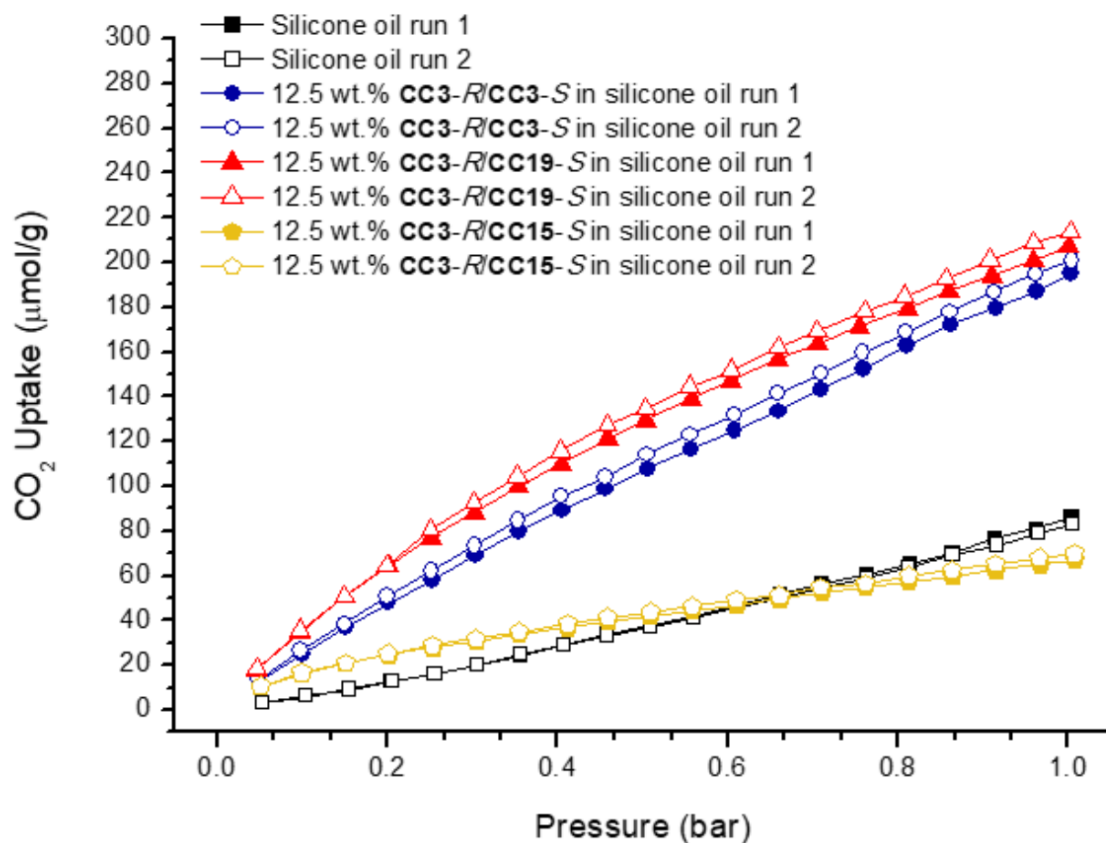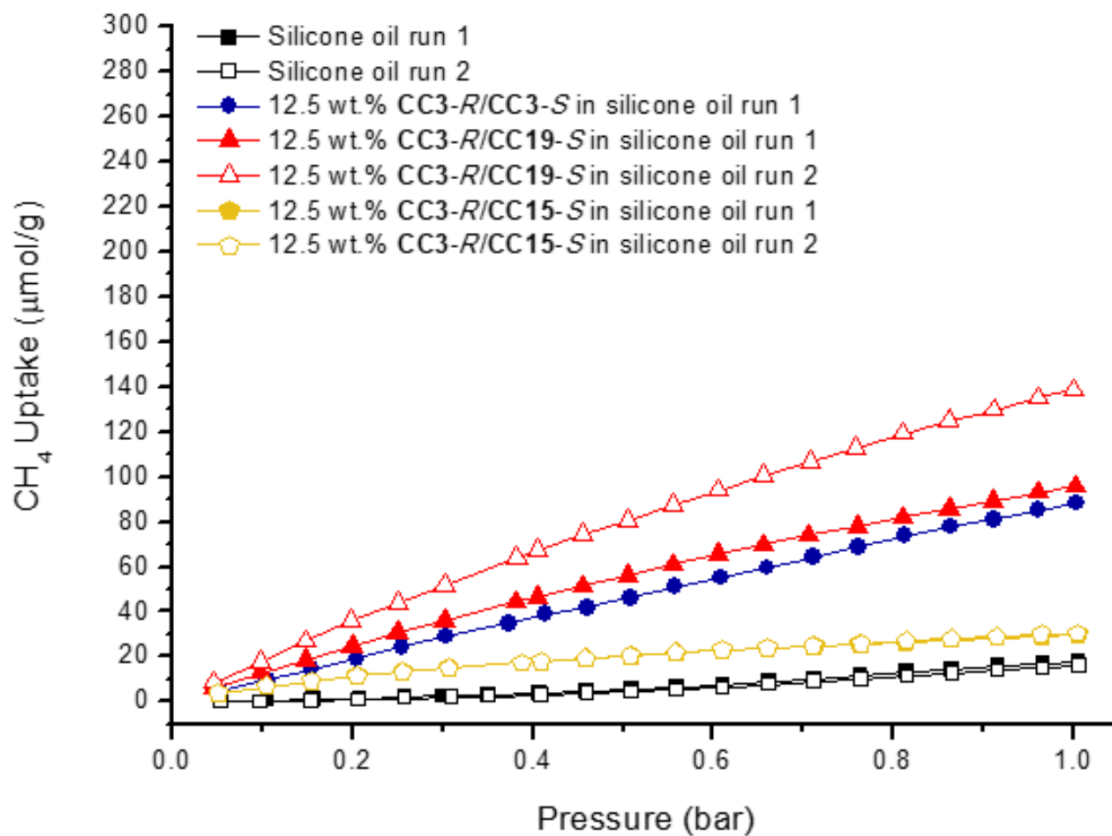
Figure 3.12: CH$_4$ uptake isotherms measured using adapted Quantachrome Nova 4200e in the three porous liquids prepared from **CC3**-*R/S*, **CC3**-*R*/**CC15**-*S* and **CC3**-*R*/**CC19**-*S* at 12.5 wt.% in silicone oil at 298 K.

the methyl groups both excluding larger guests and interfering with electrostatic interactions of guest molecules with the imine bonds.[7] **CC19**-*S* has an analogous molecular structure, but with one hydroxyl group attached to each of its four aromatic rings. The incorporation of these polar hydroxyl groups improves the CO_2 uptake in the solid state compared to **CC3**, while lowering CH_4 uptakes. Hence, by incorporating either **CC15**-*S* or **CC19**-*S* into the microparticles, there is an opportunity to tune the gas selectivity in the corresponding porous liquids.

As may have been expected, both the CO_2 (Figure 3.11) and CH_4 (Figure 3.12) uptakes in the 12.5 wt.% dispersions of **CC3**-*R*/**CC15**-*S* in silicone oil were significantly reduced compared to the **CC3**-*R/S* liquid (CO_2: 68.5 μmol/gL vs 198.0 μmol/g; CH_4: 30.2 μmol/g vs 105.2 μmol/g). In contrast, we observe slightly increased CO_2 uptake, and similar CH_4 uptake in the 12.5 wt.% dispersion of **CC3**-*R*/**CC19**-*S* in silicone oil (CO_2: 210.3 μmol/g; CH_4: 117.4 μmol/g). This reduction in porosity on introduction of **CC15**-*S* is likely based on the methyl groups blocking the cage windows and restricting access of the pore cavities. Incorporating **CC19**-*S* into the microparticles improved gas uptakes in these type 3 porous liquids, and no significant enhancement in CO_2/CH_4 selectivity was observed (Figure 3.13), unlike in the solid state. This is probably due to the fact that the **CC3**-*R*/**CC19**-*S* microparticles used here do not reflect the composition used in previous studies,[15] where CO_2/CH_4 selectivity was enhanced when the **CC19**-*S* was included in a core-shell particle. These core-shell crystals contained an internal **CC3**-*R/S* core that may have allowed for a difference in the capacity of gases while the **CC3**-*R*/**CC19**-*S* outer shell controlled the selectivity.
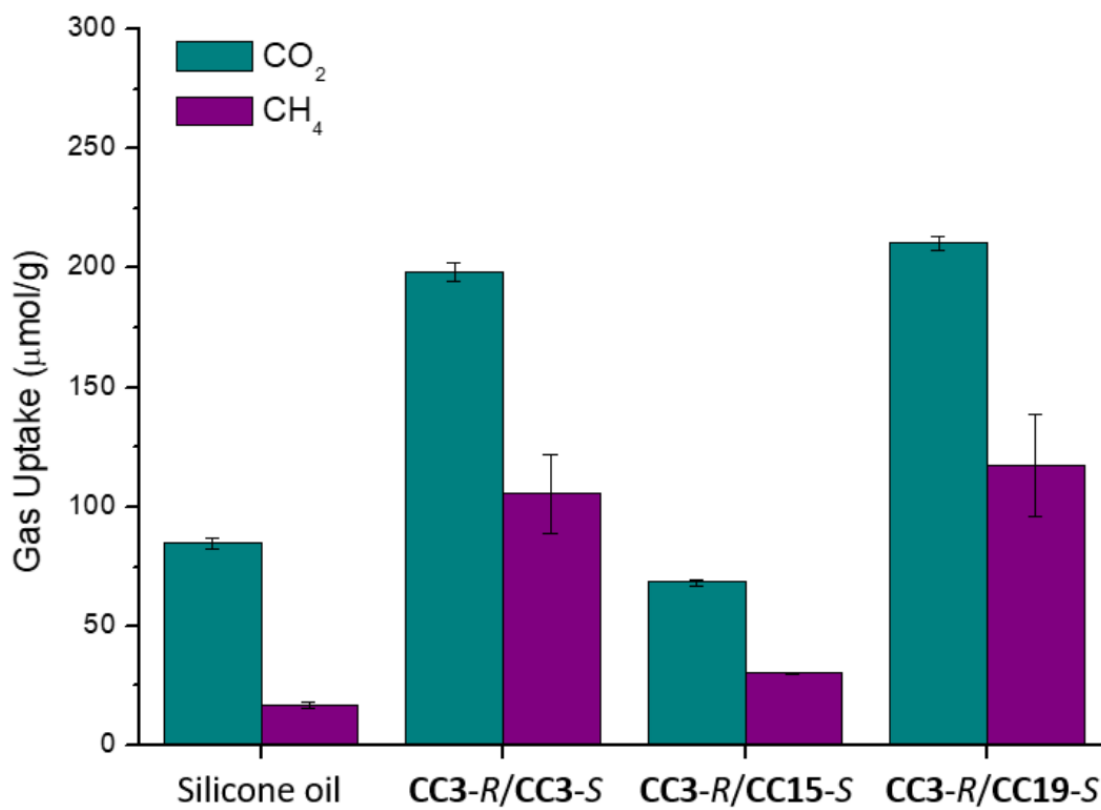
Figure 3.13: Comparison of of CO_2 and CH_4 uptake capacity at 1 bar in silicone oil and the three type 3 porous liquids at 12.5% w/v at 298 K.

3.6   Comparisons with type 3 porous liquids

When comparing these porous liquids to industrial solvents like Genesorb 1753, which is used in the Selexol natural gas sweetening process,[16] the CO_2 absorption capacity in these porous liquids is much greater at lower pressures.[17] However, the working capacity in the Selexol process is usually >30 bar. The higher uptake capacity that using POCs provides in these porous liquids at lower pressures (up to 210.3 μmol/g CO_2) is much greater than Genesorb 1753 (104.0 μmol/g CO_2, Figure 3.17), as well as introducing the ability to tune the porosity to improve selectivity, indicates that type 3 porous liquids may be a promising alternative to the Selexol process, potentially allowing for much lower working pressures and lower energy consumption of the process.

In Chapter 2, gas uptake in type 2 porous liquids based on similar POCs was investigated in depth. While comparisons cannot be made directly between these type 3 porous liquid systems and the type 2 porous liquids due to use of different POCs, we can note that there are different losses in capacity when comparing the adjusted uptakes in the liquids compared to the solids to account for the uptake in the neat solvents/liquids. In the type 2 porous liquids, CO_2 uptake capacity was greatly diminished in both the **CC3³:13³**-*R* and **CC15**-*R* porous liquids (**CC3³:13³**-*R*: 27%, **CC15**-*R*: 13% of the solid's capacity) whereas in the **CC3**-*R/S* based type 3 porous liquid, 50% of the capacity is retained. In these examples, when comparing with the CH_4 uptakes in the type 2 and 3 porous liquids, the solid POCs used in the type 2 porous liquids don't adsorb very much when compared to **CC3**-*R/S* used in the type 3 porous liquid, so it may be difficult to draw direct comparisons. The

type 2 liquids absorb 82% (**CC3³:13³**-*R*) and 68% (**CC15**-*R*) of the CH_4 compared to the respective solid POC's capacity, and the **CC3**-*R/S* type 3 porous liquid absorbs 66% as much CH_4 compared to the solid POC. These comparisons show how the retention of the extrinsic, interstitial pores, which interact favourably with the CO_2 molecule to aid adsoprtion,[18] in the dispersions allow the type 3 porous liquids to absorb a more significant proportion of the possible CO_2 uptake when compared to type 2 porous liquids. With CH_4, the differences are much less stark, showing how these extrinsic pores are of much less importance in the CH_4 absorption in porous liquids. This also shows how selection of the different types of porous liquids may have benefits over others, depending on the specific application or property requirement.

3.7   Conclusions

Presented herein are the first examples of transferring synthetic pore control in solid porous materials to type 3 porous liquids based on the dispersion of POC particles. The incorporation of **CC15**-*S* into the microparticles reduced the CO_2 and CH_4 uptakes significantly, while inclusion of **CC19**-*S* increases the uptake of the gases studied, indicating the possiblity of tuning gas sorption properties in type 3 porous liquids as previously demonstrated in the solid state. Other potential applications for the future include the separation of volatile organic compounds or chiral separations using POC porous liquids.[19,20] Using core shell crystals may help to enhance uptakes and selectivity in future designed type 3 porous liquids.[9] Understanding how uptake capacity varies with higher pressure will give us a

better indication of whether porous liquids can compete with industrial systems.

3.8 Experimental details

3.8.1 Materials

1,3,5-Triformylbenzene was purchased from Manchester Organics (UK), (*R,R*)-cyclohexyl-1,2-diamine was purchased from Fluorochem. Silicone oil 5 cSt was purchased from Sigma Aldrich. All other chemicals were purchased from Sigma-Aldrich or TCI UK. Solvents were reagent or HPLC grade and purchased from Fisher Scientific. All materials were used as received unless stated otherwise.

Gases were purchased from BOC of the following grades: carbon dioxide (N5.0), methane (N4.5).

3.8.2 General analytical techniques

NMR: ^{1}H NMR spectra were acquired using an internal deuterium lock for the residual protons in $CDCl_3$ (δ = 7.26 ppm) or CD_2Cl_2 (δ = 5.32ppm) at ambient probe temperature on the following instruments: Bruker Avance400 (400 MHz) or Bruker DRX500 (500 MHz) spectrometers.

Data are presented as follows: chemical shift, integration, peak multiplicity (s = singlet, m = multiplet), and assignment. Chemical shifts are expressed in ppm on a δ scale relative to δ_{TMS}(0 ppm) or δ_{CDCl3}(7.26 ppm).

PXRD: Laboratory powder X-ray diffraction data were collected in transmission mode on samples held on thin Mylar film in aluminium well plates on a Panalytical X'Pert PRO MPD equipped with a high throughput screening XYZ stage, X-ray focusing mirror and PIXcel detector, using Ni-filtered Cu Kα radiation. Data were measured over the range 4–40° in 0.013° steps over 60 minutes.

3.8.3   Synthesis of POCs

Synthesis of CC3-*R*

Dichloromethane (DCM, 100 mL) was added slowly onto solid 1,3,5-triformylbenzene (TFB, 5.0 g, 30.86 mmol) without stirring at room temperature. Trifluoroacetic acid (TFA, 100 μL) was added directly to this solution. (*R,R*)-Diaminocyclohexane (*R,R*-CHDA, 5.0 g, 44.64 mmol) was dissolved in DCM (100 mL) before adding slowly to the reaction vessel without disturbing the layers. The reaction was left to stand covered for 5 days to yield product in the form of white, octahedral crystals of **CC3**-*R*. The product was removed by fitration and washed with 95% ethanol/5% DCM to afford **CC3**-*R* or **CC3**-*S* (with *S,S*-CHDA) as off-white crystals (3.5 g, 81%). ^{1}H NMR (400MHz, CDCl$_3$) δ_H 8.13 (12H, s, C*H*=N), 7.85 (12H, s, Ar*H*), 3.34 (12H, m, C*H*N), 1.9-1.4 (48H, m, C*H* and C*H*$_2$ groups). The NMR data was in accordance with the literature values.[13]

Synthesis of CC15-*S*

CC15-*R* was synthesized according to a previously reported method.[7] A solution of *S,S*-CHDA (3.06 g, 26.8 mmol, 6 eq.) in DCM (35 mL) and molecular sieves (0.7 g, 3 Å) were added to 1,3,5-triacetylbenzene (TAB, 3.65 g, 17.9 mmol, 4 eq.) in a round bottom flask. The flask was equipped with reverse Dean-Stark apparatus, which was charged with DCM, and the solution was heated to 45 °C and kept stirring for 24 h before being allowed to cool to room temperature. The molecular sieves were removed by filtration and the resulting pale yellow solution was evaporated to obtain crude **CC15**-*S*. The crude product was washed with diethyl ether (3 x 50 mL) before dissolving in the minimum volume of

1:1 DCM/hexane possible, and the DCM was carefully removed under reduced pressure to precipitate **CC15**-*S*. The resulting pale cream solid was collected by filtration and dried in a vacuum oven to yield pure product (3.28 g, 82%). ^{1}H NMR (400 MHz, CDCl3) δ_H 8.05 (12H, s, Ar*H*), 3.82 (12H, m, N-C*H*), 2.1 (36H, s, C*H*$_3$), 1.84 (12H, m, C*H*$_{Hex}$), 1.69 (12H, m, C*H*$_{Hex}$), 1.65 (12H, m, C*H*$_{Hex}$), 1.49 (12H, m, C*H*$_{Hex}$). Data in accordance with literature values.[7]

Synthesis of CC19-*S*

2-Hydroxy-1,3,5-benzenetricarbaldehyde (3.19 g, 17.9 mmol, 4 eq.) and *S,S*-CHDA (3.06 g, 26.8 mmol, 6 eq.) were dissolved in methanol (500 mL) and stirred at room temperature for 3–5 days. Once the reaction had reached completion, **CC19**-*S* was obtained by filtration and washed with ethyl acetate (3 x 50 mL) before redissolving in DCM. The solvent was then removed under reduced pressure to afford pure **CC19**-*S* as a yellow solid (3.42 g, 65%). ^{1}H NMR (400 MHz, CDCl3) δ_H 8.58 (4H, m, N=C*H*), 8.26 (4H, m, N=C*H*), 8.06 (4H, m, N=C*H*), 7.87 (8H, m, Ar*H*), 3.30 (12H, m, N-C*H*), 1.75 (48H, m, C*H*$_{Hex}$), 1.45 (s(b), O*H*). Data in accordance with literature values.[9]

3.8.4 Formation of POC microparticles

Formation of CC3-*R*/*S* and CC3-*R*/CC19-*S* microparticles

A solution (1.5 mg/mL) of **CC3**-*R* (1.35 g) in DCM (900 mL) was poured directly into a solution (1.5 mg/mL) of **CC3**-*S* (1.35 g) in DCM (900 mL) or a solution (1.58 mg/mL) of **CC19**-*S* (1.43 g) in DCM (900 mL) with stirring. The mixture was stirred for a further 10 minutes to afford a colourless suspension (**CC3**-*R/S*) or yellow suspension (**CC3**-*R*/**CC19**-*S*). Fine particles (**CC3**-*R/S*: colourless, **CC3**-*R*/**CC19**-*S*:

yellow) were then collected by filtering the suspension through a nylon membrane with 0.45 μm pore diameter, and dried in a vacuum oven at 90 °C overnight (**CC3**-*R/S*: 2.32 g, 86%, **CC3**-*R*/**CC19**-*S*: 2.16 g, 78%).

Formation of CC3-*R*/CC15-*S* microparticles

CC3-*R*/**CC15**-*S* microparticles were prepared in a slightly modified way to **CC3**-*R/S*and **CC3**-*R*/**CC19**-*S*, with the solvent changed to DCM and methanol in 1:1 ratio. A solution (1.5 mg/mL) of **CC3**-*R* (1.35 g) in DCM/methanol (900 mL) was poured directly into a solution (1.73 mg/mL) of **CC15**-*S* (1.55 g) in DCM/methanol (900 mL) with stirring. After *ca.* 30 minutes a colourless suspension had formed. The fine particles were collected by filtration through a nylon membrane with 0.45 μm pore diameter, and dried in a vacuum oven at 90 °C overnight (2.24 g, 73%).

3.8.5 Particle size determination of POC microcrystals

Dynamic light scattering (DLS)

DLS measurements were performed on a Zetasizer instrument. Samples were prepared by dispersing and sonicating a small amount of nanocrystals (0.5 mg) in 20 mL dichloromethane (DCM).

Static light scattering (SLS)

SLS measurements were carried out using a Malvern Instruments Mastersizer 3000. Samples were dispersed in ethanol before dropping into sample chamber with constant stirring to ensure scattering intensity was within range.

Scanning electron microscopy (SEM)

SEM characterisation was performed either on a Hitachi S4800 SEM or a Tescan

S8000G SEM. Samples were prepared by depositing nanocrystals on high purity carbon tabs on aluminium stubs and coated with chromium before imaging.

Table 3.1: Comparison of the particle sizes and shapes in the different prepared cocrystals using light scattering measurements and SEM images.

Cocrystal	Size by light scattering (nm)	SEM size range (nm)	Particle shape
CC3-*R/S* (1)	540[a]	200-700	Spherical
CC3-*R/S* (2)	600[a]	300-800	Spherical
CC3-*R/S* (3)	1200[a]	300-1000	Spherical
CC3-*R/S* (4)	720[a]	300-1000	Spherical
CC3-*R/S* (5)	630[a]	200-800	Spherical
CC3-*R/S* (6)	940[a]	200-1500	Octahedral
CC3-*R*/**CC15**-*S*	17000[b]	8000-31000	Octahedral
CC3-*R*/**CC19**-*S*	300[a]	200-800	Octahedral

Table 3.2: [a] Particle size determined by DLS. [b] Particle size of **CC3**-*R*/**CC15**-*S* determined by SLS due to reduced dispersion stability.

3.8.6   Preparation of type 3 porous liquids from POCs

The cages or microparticles were desolvated at 90 °C overnight in a vacuum oven before the direct addition of the as bought liquids, and the resulting suspension was sonicated for 10 minutes until a homogenous dispersion was formed. 200 mg microparticles dispersed in 1.4 g liquid for 12.5 wt% dispersion. The dispersions
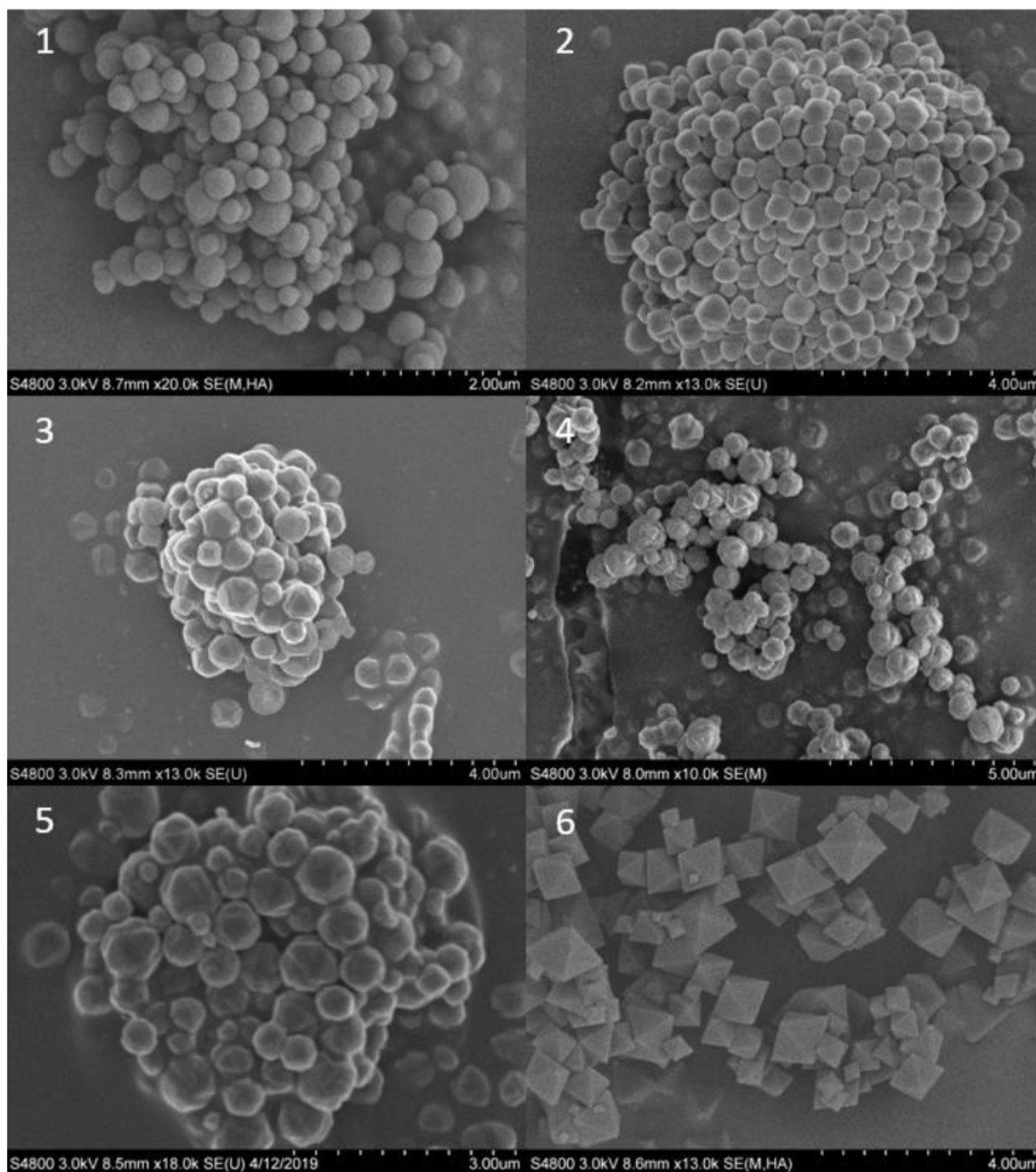
Figure 3.14: Representative SEM images of the batches of **CC3**-*R/S* prepared for use in this study.

were then transferred to sorption tubes using wide-bore needles fitted to a syringe for gas uptake measurements.

3.8.7   Gas Sorption

Gas uptakes of the type 3 porous liquids were measured on a Quantachrome Nova 4200e according to Kai *et al.*[14] Method for liquids - 0.5 mL sample was injected into a 9 mm sample cell with large bulb (P/N: 74064) and a glass-coated stirrer bar was added. The sample was degassed under vacuum with stirring overnight at room temperature and backfilled with helium before being removed from the degassing station. A filler rod (P/N: 74105-L) was used with the sample cell during sorption measurements at room temperature and the adsorption settings were as follows: 20 pressure points from 0.05 to 1.0 bar in 0.05 increments; pressure tolerance = 0.05 mmHg; equilibration time = 1800 seconds; equilibration timeout = 5400 seconds. Dispersions were kept stirring during all measurements.

Powder samples were degassed offline at 90 °C for 15 h under dynamic vacuum (10^{-5} bar) before analysis, followed by degassing on the analysis port under vacuum, also at 90 °C. Isotherms were measured using a Micromeritics 2020 or 2420 volumetric adsorption analyzer. Gas uptake measurements for CH_4, CO_2 were taken at a temperature of 293 K, stabilized using a circulating water chiller/heater and N_2 were taken at a temperature of 77 K.

Table 3.3: Gas uptake data and calculated normalised gas uptake values for CO_2 in the **CC3**-*R/S* solid and **CC3**-*R/S*, **CC3**-*R*/**CC15**-*S* and **CC3**-*R*/**CC19**-*S* porous liquids at 12.5 wt.% in silicone oil 5 cSt. The normalized uptakes are calculated using the measured uptake in silicone oil (84.8 μmol/g).

Solid	Loading (% w/v)	Average uptake (μmol/g)	Normalised gas uptake μmol/g$_{cage}$
CC3-*R/S*	100	1792 ± 72	-
CC3-*R/S*	12.5	199.5 ± 1.9	912
CC3-*R*/**CC15**-*S*	12.5	68.5 ± 1.3	-128
CC3-*R*/**CC19**-*S*	12.5	210.3 ± 3.3	1000

Table 3.4: Gas uptake data and calculated normalised gas uptake values for CO_2 in the **CC3**-*R/S* solid and **CC3**-*R/S*, **CC3**-*R*/**CC15**-*S* and **CC3**-*R*/**CC19**-*S* porous liquids at 12.5 % w/v in silicone oil 5 cSt. The normalized uptakes are calculated using the measured uptake in silicone oil (17.1 μmol/g).

Solid	Loading (% w/v)	Average uptake (μmol/g)	Normalised gas uptake (μmol/g$_{cage}$)
CC3-*R/S*	100	1064 ± 77	-
CC3-*R/S*	12.5	105.2 ± 16.5	704
CC3-*R*/**CC15**-*S*	12.5	30.2 ± 0.3	104
CC3-*R*/**CC19**-*S*	12.5	117.4 ± 21.4	800
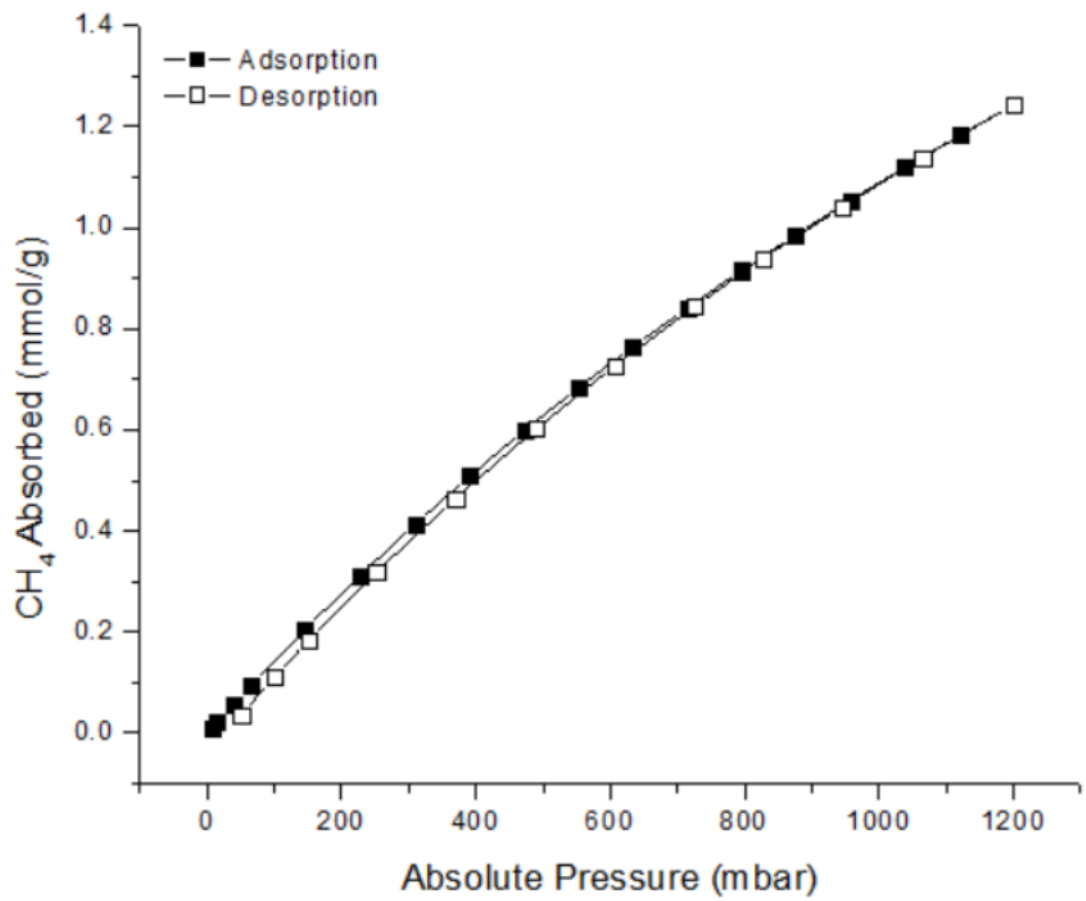
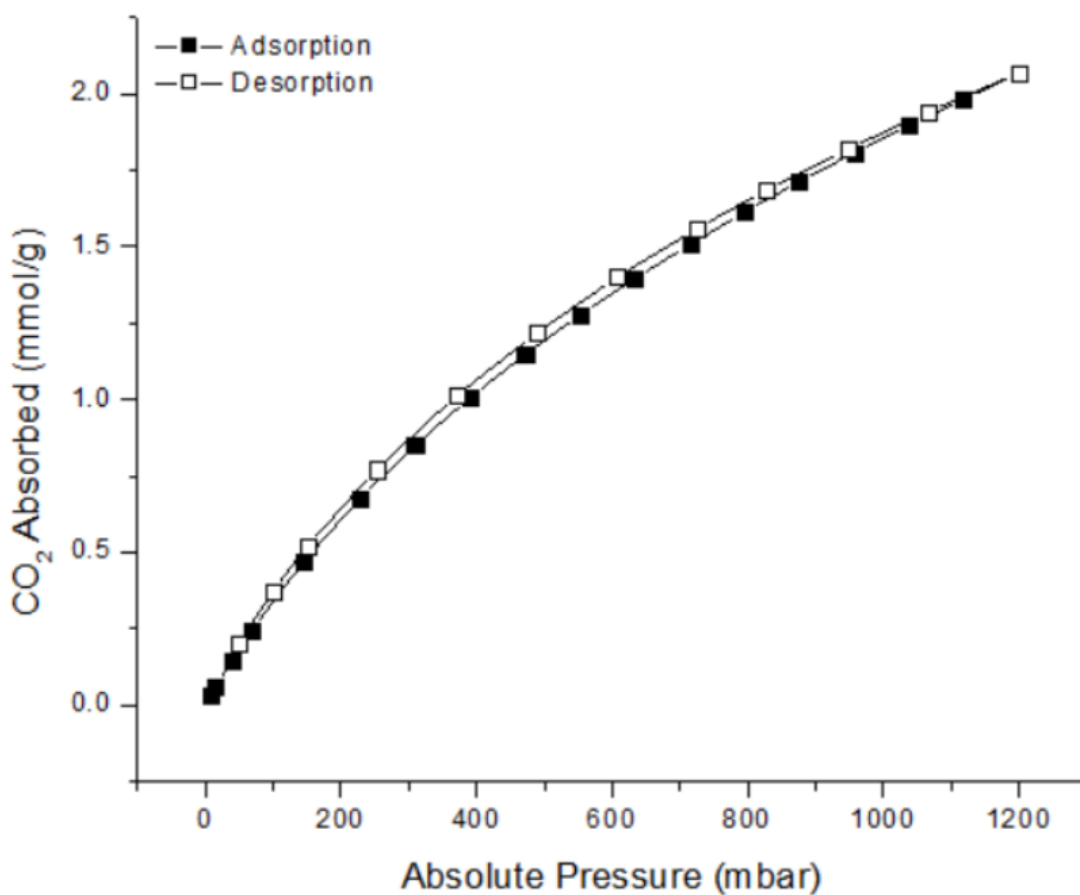**Figure 3.15:** CH_4 sorption isotherm for **CC3-R** at 298 K.

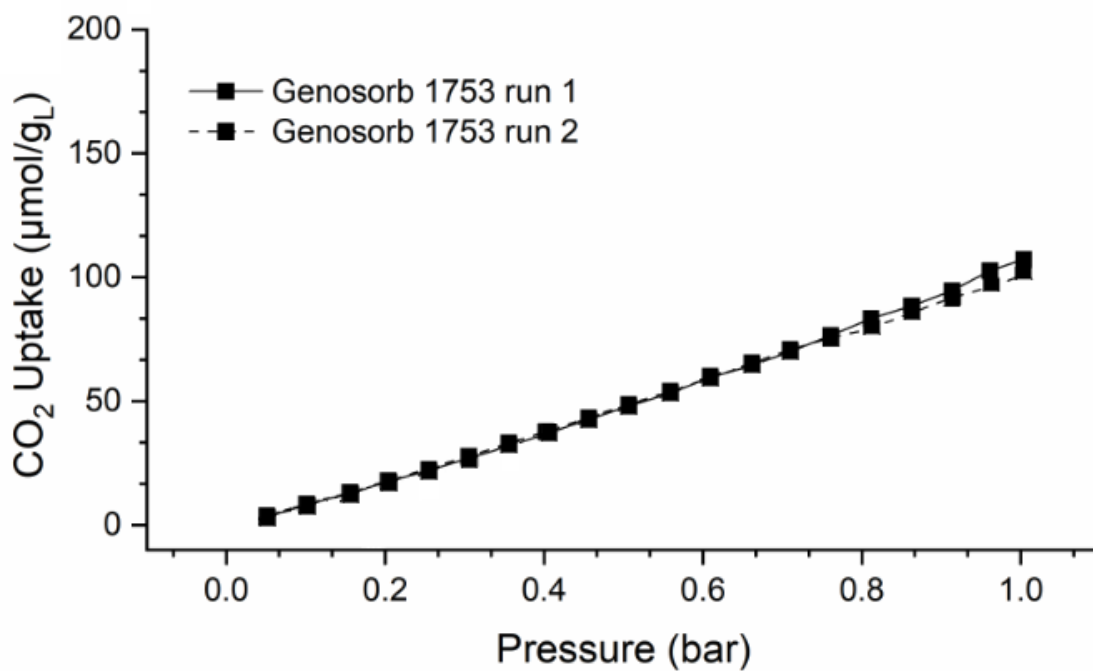**Figure 3.16:** CO_2 sorption isotherm for **CC3**-*R* at 298 K.

Figure 3.17: CO$_2$ sorption isotherms for Genesorb 1753 industrial gas sorbent used in Selexol process at 298 K.

References

(1) J. Cahir, M. Y. Tsang, B. Lai, D. Hughes, M. A. Alam, J. Jacquemin, D. Rooney and S. L. James, *Chem. Sci.*, 2020, **11**, 2077–2084.

(2) W. Shan, P. F. Fulvio, L. Kong, J. A. Schott, C. L. Do-Thanh, T. Tian, X. Hu, S. M. Mahurin, H. Xing and S. Dai, *ACS Applied Materials and Interfaces*, 2018, **10**, 32–36.

(3) R. E. Mow, A. S. Lipton, S. Shulda, E. A. Gaulding, T. Gennett and W. A. Braunecker, *J. Mater. Chem. A*, 2020, **8**, 23455–23462.

(4) T. Cosgrove, *Colloid science : principles, methods and applications.* Wiley, 2010.

(5) N. O'Reilly, N. Giri and S. L. James, *Chemistry - A European Journal*, 2007, **13**, 3020–3025.

(6) J. T. A. Jones, T. Hasell, X. Wu, J. Bacsa, K. E. Jelfs, M. Schmidtmann, S. Y. Chong, D. J. Adams, A. Trewin, F. Schiffman, F. Cora, B. Slater, A. Steiner, G. M. Day and A. I. Cooper, *Nature*, 2011, **474**, 367–371.

(7) A. G. Slater, P. S. Reiss, A. Pulido, M. A. Little, D. L. Holden, L. Chen, S. Y. Chong, B. M. Alston, R. Clowes, M. Haranczyk, M. E. Briggs, T. Hasell, G. M. Day and A. I. Cooper, *ACS Central Science*, 2017, **3**, 734–742.

(8) M. Liu, L. Zhang, M. A. Little, V. Kapil, M. Ceriotti, S. Yang, L. Ding, D. L. Holden, R. Balderas-Xicohténcatl, D. He, R. Clowes, S. Y. Chong, G. Schütz, L. Chen, M. Hirscher and A. I. Cooper, *Science*, 2019, **366**, 613–620.

(9)   S. Jiang, Y. Du, M. Marcello, E. W. Corcoran, D. C. Calabro, S. Y. Chong, L. Chen, R. Clowes, T. Hasell and A. I. Cooper, *Angewandte Chemie - International Edition*, 2018, **57**, 11228–11232.

(10) T. Hasell, S. Y. Chong, M. Schmidtmann, D. J. Adams and A. I. Cooper, *Angew. Chem. Int. Ed.*, 2012, **51**, 7154–7157.

(11) T. Hasell, M. Schmidtmann and A. I. Cooper, *Journal of the American Chemical Society*, 2011, **133**, 14920–14923.

(12) R. Pecora, *J. Nanopart. Res.*, 2000, **2**, 123–131.

(13) T. Tozawa, J. T. a. Jones, S. I. Swamy, S. Jiang, D. J. Adams, S. Shakespeare, R. Clowes, D. Bradshaw, T. Hasell, S. Y. Chong, C. Tang, S. Thompson, J. Parker, A. Trewin, J. Bacsa, A. M. Z. Slawin, A. Steiner and A. I. Cooper, *Nature materials*, 2009, **8**, 973–978.

(14) A. Kai, B. D. Egleston, R. Clowes, M. E. Briggs, Andrew and R. L. Greenaway, *ChemRxiv*, 2021, DOI: `10.26434/chemrxiv.14719503.v2`.

(15) H. Jiang, X.-C. Liu, Y. Wu, Y. Shu, X. Gong, F.-S. Ke and H. Deng, *Angewandte Chemie International Edition*, 2018, DOI: `10.1002/anie.201712872`.

(16) A. V. Rayer, A. Henni and P. Tontiwachwuthikul, *J. Chem. Eng. Data*, 2012, **57**, 764–775.

(17) A. V. Rayer, A. Henni and P. Tontiwachwuthikul, *Can. J. Chem. Eng.*, 2012, **90**, 576–583.

(18)   S. Jiang, K. E. Jelfs, D. Holden, T. Hasell, S. Y. Chong, M. Haranczyk, A. Trewin and A. I. Cooper, *Journal of the American Chemical Society*, 2013, **135**, 17818–17830.

(19)   A. Kewley, A. Stephenson, L. Chen, M. E. Briggs, T. Hasell and A. I. Cooper, *Chemistry of Materials*, 2015, **27**, 3207–3210.

(20)   L. Chen, P. S. Reiss, S. Y. Chong, D. Holden, K. E. Jelfs, T. Hasell, M. A. Little, A. Kewley, M. E. Briggs, A. Stephenson, K. M. Thomas, J. A. Armstrong, J. Bell, J. Busto, R. Noel, J. Liu, D. M. Strachan, P. K. Thallapally and A. I. Cooper, *Nat Mater*, 2014, **13**, 954–960.

# 4 Absorption in hydrophobic microporous solids in water

Previously, porosity in liquids had only been investigated in materials designed mainly considering the use of size, or steric, exclusion of the fluid phase from the microporous component of the material. In type 3 porous liquids, or microporous dispersions, O'Reilly *et al.* mainly focussed on the outlook for using highly crystalline microporous framework materials with well defined cavities as pore generators in these materials.[1] So far, the systems discovered have mirrored this prediction, mostly being based on either zeolites or MOFs.[2]

Here we wanted to explore other methods of liquid exclusion to produce either new porous liquids, or some new fluid material that can be used for liquid or gas absorption. Hydrophobicity has been explored as an important part of supramolecular binding. Recently, Barnett *et al.* observed a very strong solvophobic effect in cavitand host molecules, resulting in the de-wetting of the supramoleclar cavity.[3] The extreme hydrophobicity of the internal surface of the cavity caused the occupation of the internal cavity to spontaneously exclude water molecules. This work indicates that it may be possible to design materials which can contain unoccupied micropores when in water. This is an extension of the hydrophobic effect observed in many supramolecular systems, where the structure of the cavity on these molecules, as well as the apolar nature of the internal surface, leads to occupation with water being highly energetically unfavourable.[4]

4.1   Hypercrosslinked polymers (HCPs) from crosslinking of small monomers

Hypercrosslinked polymers (HCPs) are a class of microporous material prepared from small, rigid organic monomers.[5] The permanent porosity arises as a result of the extensive crosslinking that occurs during synthesis, introducing rigid bonds between the monomers to form 3D networks of polymer chains.[6] This rigidity and high extent of crosslinking prevents the pore network from collapsing on removal of solvent.

Synthetic routes to HCPs include 'knitting' of smaller aromatic monomers to form polyphenylene networks, which are a recently developed class of microporous polymer. In 2011, Li *et al.* demonstrated this method can be used to produce network polymers with high surface areas and micropore volumes very cheaply and easily.[7] Rather than using styrene derivatives, as are frequently used in preparing HCPs,[8] or monomers based on chloroxylenes for polycondensation reactions,[9] this method relies on combining aromatic precursors with a reactive external cross-linker. Phenylenes, such as benzene, toluene, phenol, biphenyl and 1,3,5-triphenylbenzene (TPB), can be crosslinked by combining with formaldehyde dimethyl acetal (FDA) and $FeCl_3$ to produce these 'knitted' HCPs by a Friedel-Crafts reaction (Scheme 4.1)[7] These materials can exhibit BET surface areas as high as 1980 m^2/g.[10] More recently, many examples have been reported using an even simpler method of preparing HCPs from phenylenes.[11,12] In these works, rather than using FDA and $FeCl_3$, $AlCl_3$ and a chlorinated reaction solvent, which also acts as a cross linker, is used to carry out a Scholl coupling reaction (Scheme
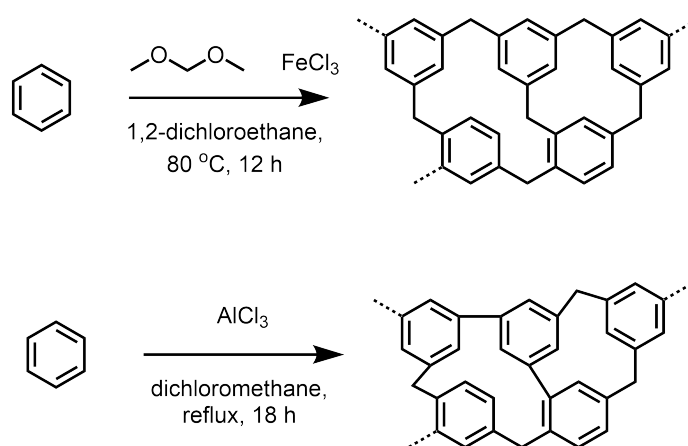
Scheme 4.1: Synthesis of Knitted HCPs (top) and Scholl-coupled HCPs (bottom) and prepared from various phenylenes.

4.1). These HCPs can be synthesized readily and inexpensively to produce very high surface area materials for CO_2 adsorption. One material, prepared by Scholl-coupling of TPB had a BET surface area as high as 2435 m^2/g with a significant CO_2 uptake of 5.9 mmol/g at 1 bar.[13]

One example of these materials has been shown to effectively adsorb CO_2 even without complete drying in order to 'activate' the HCP.[14] This is in huge contrast to other microporous materials, such as some MOFs and zeolites, which suffer an order of magnitude reduction in CO_2 uptake when not sufficiently activated in order to remove water. The HCP in particular was prepared from the 'knitting' reaction of benzene with $FeCl_3$ and formaldehyde dimethyl ether, producing a highly microporous network polymer with a BET surface area of 1228 m^2/g. In this case, the material retains 86% of its CO_2 uptake at 40 bar when not activated under vacuum (15.32 mmol/g dry, 13.17 mmol/g wet, Figure 4.1) whereas other microporous materials such as zeolite 13X and **HKUST-1** only retain 5.7% and 27%
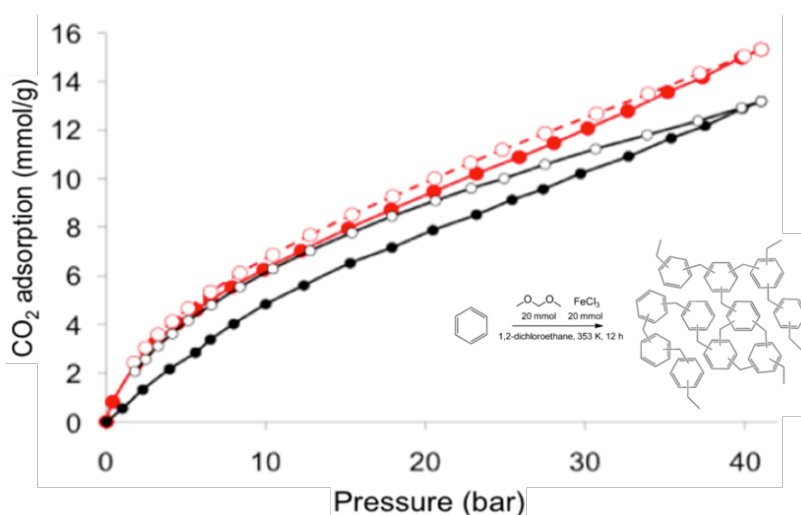
Figure 4.1: Gas adsorption (filled) and desorption (empty) curves for wet (black) and dry (red) knitted benzene HCP at 298 K.[14]

of their CO_2 uptake under these conditions.

This study intends to determine the viability of a different kind of porosity, or at least absorption, in a liquid where the porosity is retained not by size exclusion of a liquid from a porous materials' pores, but rather by the solvophobicity of the porous material. Further to this, one of the greatest draw backs to most PLs to date is the exotic nature of the bulky solvents or dispersants, leading to cost being prohibitively high to justify immediate industrial application. Instead, readily and cheaply available liquids should be targeted, tailoring the porous material to the liquid rather than using a specially designed solvent. An obvious choice for an accessible liquid is water. HCPs are highly hydrophobic and have been shown to adsorb CO_2 even under humid conditions;[14] they were selected as a candidate to investigate the possibility of a water based type 3 porous liquid.

4.2 Screening HCPs for hydrophobicity

A range of 'knitted' and Scholl-coupled HCPs prepared fomr vaious phenylenes (Figure 4.2), were analysed for their hydrophobicity to determine whether a single example was particularly hydrophobic when compared to the other HCPs. We were particularly interested in the knitted aromatic derivative polymers as they had been previously shown to adsorb CO_2 even when moisture wasn't removed in vacuum oven.[14]

Thermogravimetric analysis (TGA) is a useful analytical technique for determining the thermal stability of the components of a material by recording the mass of a sample as a function of temperature.[15,16] The temperature is controlled to change at a controlled rate under an inert atmosphere. This technique enables the determination of the temperatures at which a material will evaporate or decompose. When studying polymeric substances, TGA also provides useful information about the composition of the material, such as the presence of solvent used during synthesis, absorbed water and unreacted starting material.[17]

TGA was exploited in order to determine the water content of the selected microporous HCPs. The water content of the HCPs was determined at the following levels of exposure to water:

- Immediately after desolvation.

- After being exposed to the conditions for several days.

- Immediately after being mixed with water.

- After being left under air for 30 minutes after being mixed with water.

175

These were chosen to provide a range of conditions which could be used to differentiate between the materials based on how much water they will adsorb in each case. More hydrophobic HCPs will contain less water due to the energetic unfavorability of water adsorping at the surface of the pores. We applied a temperature programme to ramp to 300 °C in order to ensure all moisture present had been desorbed during the length of the experiment. The TGA curves of knitted benzene is shown in Figure 4.3 as a representative example of the the generally observed phenomena. For the immediately wet samples an initial drop in mass occurs during the equilibration time as the water begins to evaporate immediately under the gas flow of the TGA. After this, as the temperature rises, the remaining water is evaporated and the mass loss stops at just below 100 °C. In the other 3 curves, very little mass loss is observed across the temperature range, indicating little water is present in these samples.

The initial series of polymers were selected based on their low cost and being composed of highly hydrophobic starting materials, benzene, triptycene, biphenyl, binaphthalene, TPB, and toluene (Figure 4.2). HCPs can be synthesised from more polar aromatic compounds, such as nitrogen containing heterocycles[18] or from chloroarenes,[19] although these were avoided so as not to introduce groups which may reduce hydrophobicity. The HCPs were also compared against activated charcoal powder as another example of a low cost amorphous microporous material.

Overall, it was found that all of the HCPs studied contained very little water after desolvation and even at 'wet' ambient conditions (Figure 4.4). All of the HCPs demonstrated the trend shown in Figure 4.3. The only samples with significant
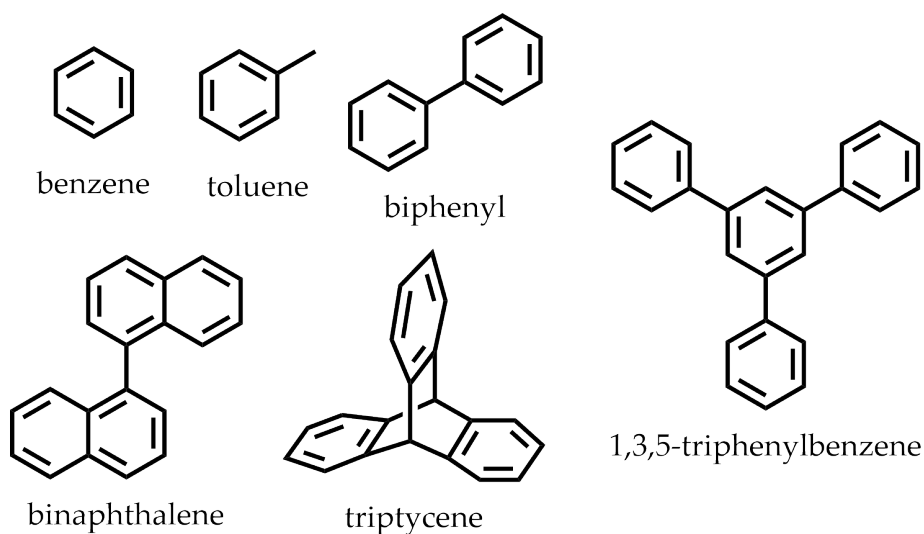
Figure 4.2: The molecular structures of the aromatic monomers used to synthesise the HCPs used during initial testing.

water content were the samples whose content was measured immediately after removing from water. For the sampels left for 30 minutes after being exposed to water, in the HCPs almost all of the water had been lost after being left under air for a short period, showing that the hydrophobicity of the polymers rapidly drives out the moisture, followed by its evaporation under ambient conditions. All of the HCPs performed better than activated charcoal, with even the 30 minute measurement after removing from water still showing the material contained a significant amount (19.2%).

Another useful method for determining relative hydrophobicity of materials is carrying out drop shape analysis of water at the surface of the HCP samples. While contact angle measurements of a sessile drop is a useful technique for measuring surface interaction energetics as it is directly related to the surface tension and
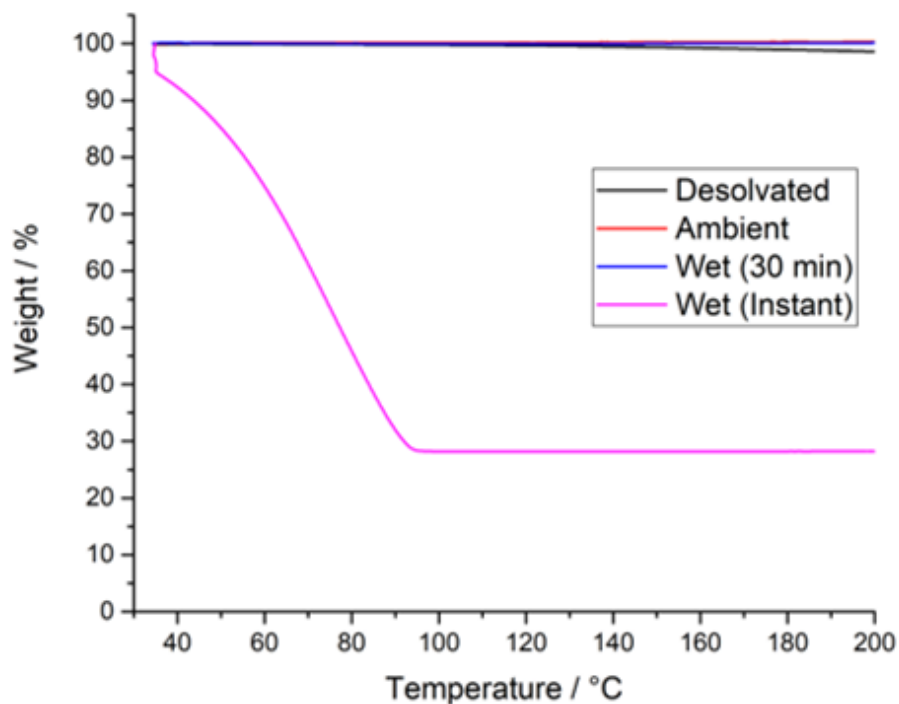
Figure 4.3: TGA of the 'knitted' benzene HCP after attempting to wet the powder. The desolvated (black) and ambient (red) samples showed effectively zero mass lost upon heating through the temperature range (0-300 °C), whereas the two wetted samples (blue and pink) both showed mass loss over the range.

Figure 4.4: The percentage mass loss of water form each of the HCPs used in this initial study, showing the quantity of water in the materials when desolvated, stored at ambient conditions and mixed with water.

Table 4.1: Measured contact angle for the investigated HCPs using the Krüss DSA100E.

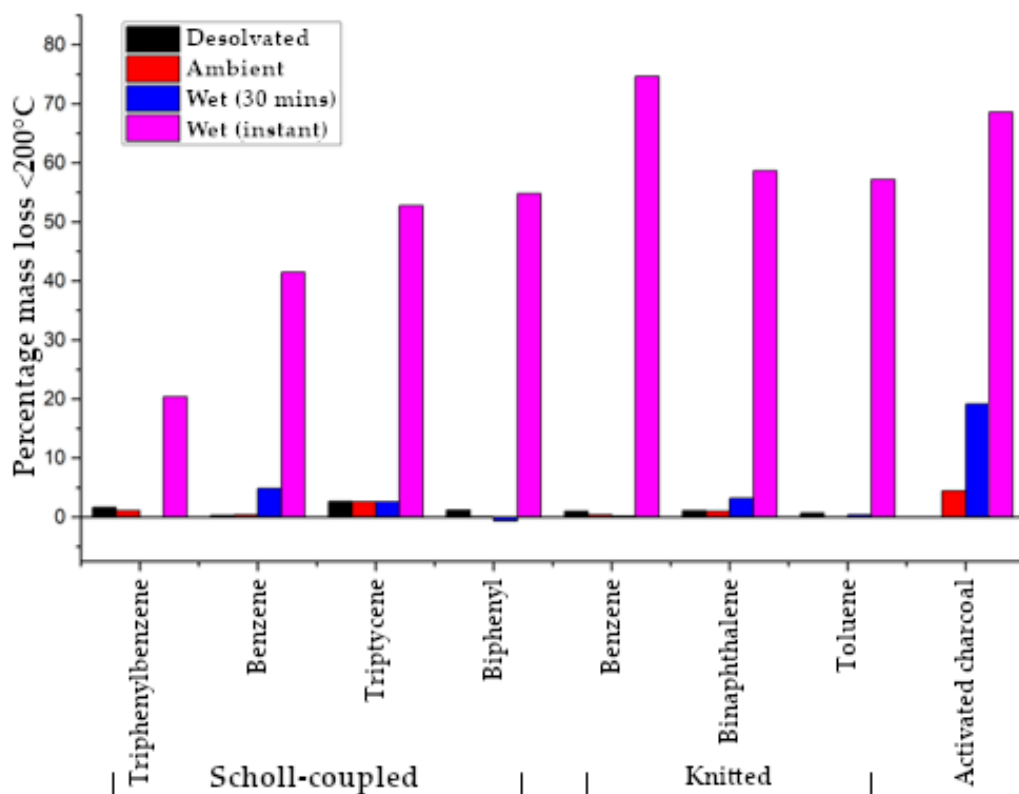| Material	Measured contact angle
Scholl coupled TPB	$149 \pm 5°$
Scholl coupled benzene	$122 \pm 12°$
Scholl coupled triptycene	$142 \pm 2°$
Scholl coupled biphenyl	$155 \pm 7°$
'Knitted' benzene	-
'Knitted' binaphthalene	-
'Knitted' toluene	-

surface adhesion between a solid and liquid, the sessile drop experiment is very sensitive to any surface roughness or heterogeneity.[20] In order to minimise this, the HCP powders were formulated into pellets using a hydraulic press to prepare as smooth a surface as possible.

The Scholl coupled HCPs gave very high contact angles (Table 4.1), confirming their very high hydrophobicity as expected, while with the 'knitted' HCPs it was not possible to measure contact angles due to the formed pellets absorbing the water droplet when placed at the surface (Figure 4.13). While contact angle measurement can be a useful technique for determining the relative hydrophobicity of materials, in this case other factors, such as the particles size and roughness as well as the quality of the pellet formed have a significant impact on the droplet at the surface. From this information it's not possible to compare between the two different classes of HCP, though may be useful in indicating

which polymers within each group are more hydrophobic. In this case, the Scholl coupled TPB and biphenyl HCPs exhibited the highest contact angles ($149\pm5°$ and $155\pm7°$), indicating increased hydrophobicity in these materials compared to the benzene and triptycene HCPs.

Within the group, the Scholl-coupled TPB HCP has been identified as a candidate HCP for CO_2 uptake under wet conditions and therefore was selected for this further investigation. This polymer exhibited the lowest water content by the TGA experiments and contact angle measurements showed that the polymer was among the most hydrophobic. Msayib *et al.* also found this polymer to be particcluarly high performing, with their examples exhibiting very high CO_2 uptake (5.9 mmol/g) as well as large pore volumes (1.6 cm^3/g).[13]

4.3   Reducing particle size for dispersing in water

As in Chapter 3 with the type 3 porous liquids, it is important to consider the particle size of the prepared materials in order to improve the dispersibility of the HCP, especially as the as prepared HCP forms as large solid pieces of polymer from the Scholl coupling reaction. Since control of particle size at the synthesis of the HCPs is not possible, instead post-synthetic processing in a ball mill was carried out. Processing the Scholl coupled TPB HCP with the ball mill allowed average particle sizes as low as 3-5 μm to be achieved (Figure 4.5).

This allowed for mixing of up to 12.5 wt.% of Scholl coupled TPB HCP with water after treatment of the polymer in this way, whereas larger particles, or higher particle loadings quickly cream or float on the surface of the water rapidly. While a
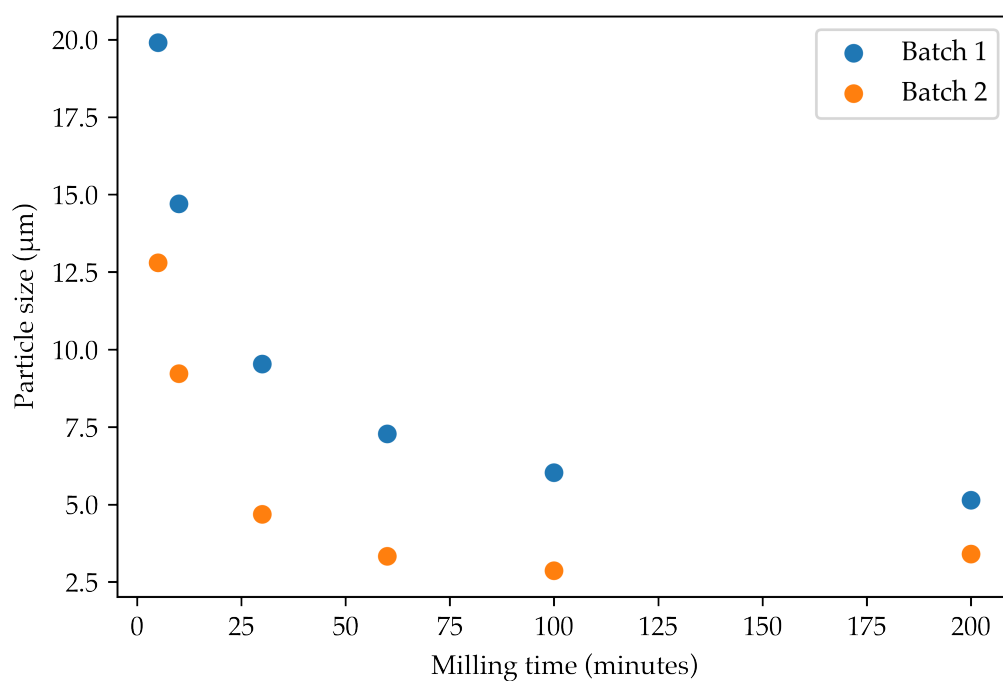
Figure 4.5: Reduction of the particle size in the Scholl coupled TPB HCP by a ball milling technique while varying the milling time.

single phase can be prepared at this loading, once agitation ceases the HCP slowly separates over time. Since the ball mill jars on this instrument could only accept *ca.* 1 g of polymer per batch, processing was transferred to an orbital mill for a time period of 24 hours to yield 3.1 μm particles on a 10 g per batch scale.

4.4   Investigating CO_2 uptake in HCP dispersions

Since it isn't possible to measure conventional gas sorption on the prepared dispersion in water, other techniques were investigated. Adaptation of the methods used previously to measure gas uptake by volumetric evolution in type 2 porous liquids was carried out, using gas evolution experiments to measure the gas uptake in the dispersion.[21]

In order to investigate the uptake capability of this dispersion, volumetric gas evolution was attempted from these materials in order to observe improvement in CO_2 uptake compared to water. The samples (3 mL) were saturated with CO_2 for 10 minutes in a GC vial before capping to seal the vial. Gas evolution was carried out by addition of DCM to the sample (600 μL, based on pore volume of 1.6 cm^3/g),[13] either as a single dose or in 50 μL increments, to attempt to displace or expel any absorbed CO_2 (Figure 4.6). When added in a single dose, the SC-TPB dispersion evolves less CO_2 than water, due to the rapid disruption of the dispersion and improper mixing of DCM with the polymer, but when the volume of DCM is added in 50 µL increments, a larger volume is evolved from the sample than from water. This indicates that the presence of the hydrophobic porous HCP is improving the CO_2 uptake, albeit marginally. Only a small amount
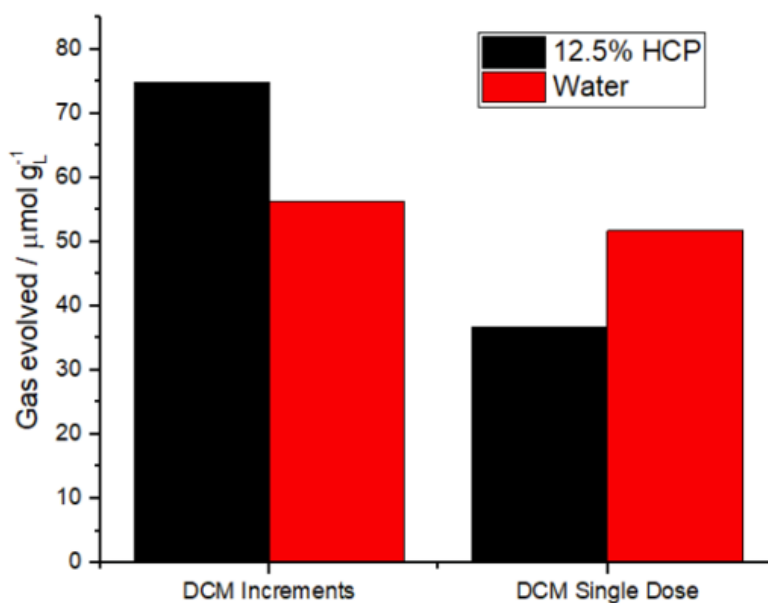
Figure 4.6: CO_2 evolution from the dispersion carried out by addition of DCM to accupy the HCP's pores.

(163 μmol/g_{HCP}) compared to the measured CO_2 uptake in the porous solid (2.98 mmol/g, Figure 4.11). This very small value relative to that of the dry polymer could be explained by the fact that only a very small proportion of the micropore volume is accesible to CO_2.

Using a temperature swing is an alternative method to determine whether CO_2 uptake is enhanced in the HCP dispersion (Figure 4.7). Temperature swing absorption and release is used for CO_2 capture when using and regenerating amine scrubbers.[22] The swing was carried out from 25 °C to 60 °C and 80 °C to determine the extent to which this could be used in this system to recover CO_2. In both cases the volume of CO_2 is increased with the presence of the HCP, showing a similar scaling to that of the evolution due to addition of DCM incrementally.

Since these HCPs usually have the best CO_2 uptake performance at pressures
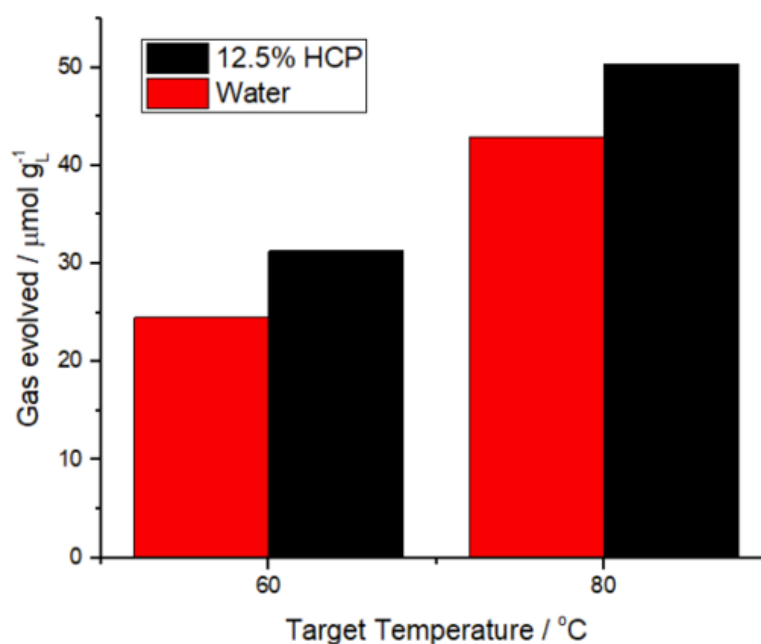
Figure 4.7: CO_2 evolution carried out by heating of the dispersion.

measured up to *ca.* 40 bar,[14] high pressure CO_2 release measurements were carried out by loading the HCP dispersion samples and water into a 75 mL Parr vessel fitted with a pressure gauge, CO_2 inlet, and outlet connected to an inverted 1 L measuring cylinder. CO_2 was added to the filled Parr vessel at pressures up to 50 bar to determine whether the CO_2 absorption would occur in the HCP in a dispersion in water (Figure 4.8).

No significant improvement in the gas uptake across this pressure range was observed using this method when compared to measurements carried out with water, indicating that this system is not effective for improving CO_2 gas uptake. While the HCP is highly hydrophobic, it is not sufficient to the extent that gas absorption can occur when mixed with water. In fact, at high pressures the phenomenon of forced intrusion can occur in hydrophobic microporous materials,
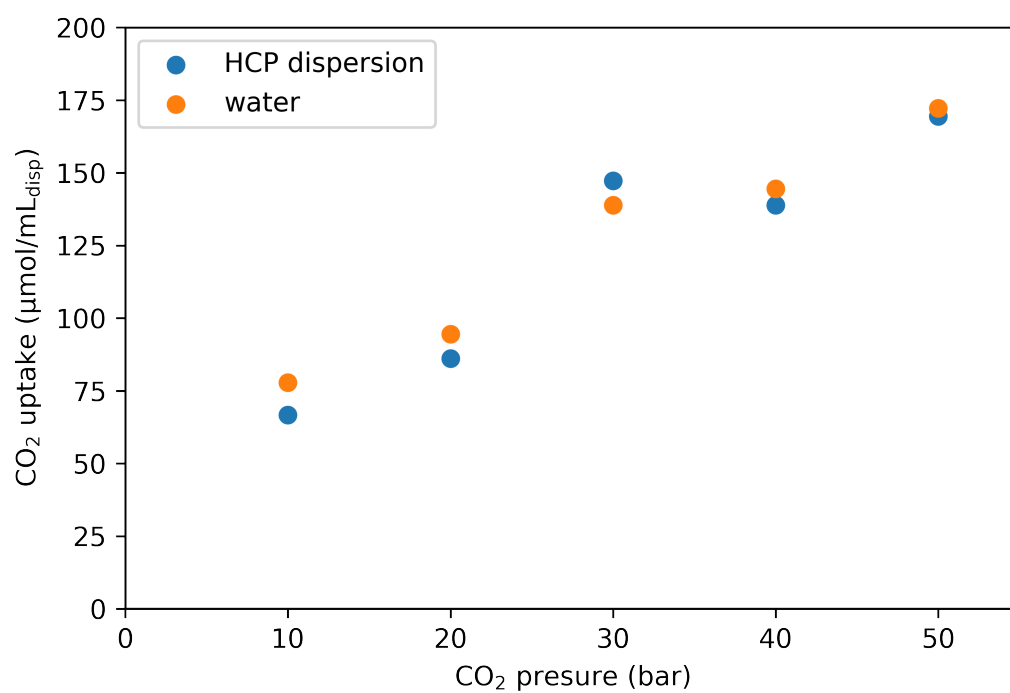
Figure 4.8: High pressure CO_2 uptake measured by gas evolution by release of pressure in the Scholl coupled TPB HCP.

where water can occupy the pores of materials that can effectively exclude moisture at ambient conditions, which may be occuring in the HCP.[23]

4.5 Absorption of small organic compounds

In order to verify other possible applications of these dispersions, absorption of organic compounds was also investigated. Toluene was selected as it is an important volatile organic compound (VOC) for absorption from the environment as it is produced in industrial settings and is a good simulant for benzenes and xylenes, which cause harm to humans by entering the body, passing through the lungs or skin and damaging organs.[24] DCM was also selected as it has been identified as a chemical warfare agents (CWA) simulant for phosgene, a choking agent.[25,26] We imagine that these dispersions could be used absorb VOCs or CWAs in their bulk form owing to the high hydrophobicity of the HCPs but dispersed in water to enable application of the material.

The Scholl coupled TPB HCP was dispersed in D_2O, to which either toluene or DCM were added in increments. The dispersions remained in a single homogenous phase upon addition of up to 20% v/v of toluene and 12% v/v of DCM. The fluid phase was filtered off from the dispersions and the remaining solid was washed with $CDCl_3$. Both the D_2O phases and the $CDCl_3$ washings were dissolved in acetonitrile-d_3 and analysed by ^1H NMR spectroscopy.

The NMR spectra show that the toluene (Figure 4.9) and DCM (Figure 4.10) is retained in the hydrophobic pores of the SC-TPB, as corresponding signals are not observed in the filtrates of the dispersion. This indicates that the dispersed

particles absorb and retain these organic liquids in their hydrophobic pore volume without disrupting the dispersion. This shows that these dispersions could be effective for cleaning up spills of harmful compounds, such as VOCs and CWAs, with the dispersibility either used as method for delivery or for removing the compounds from water.
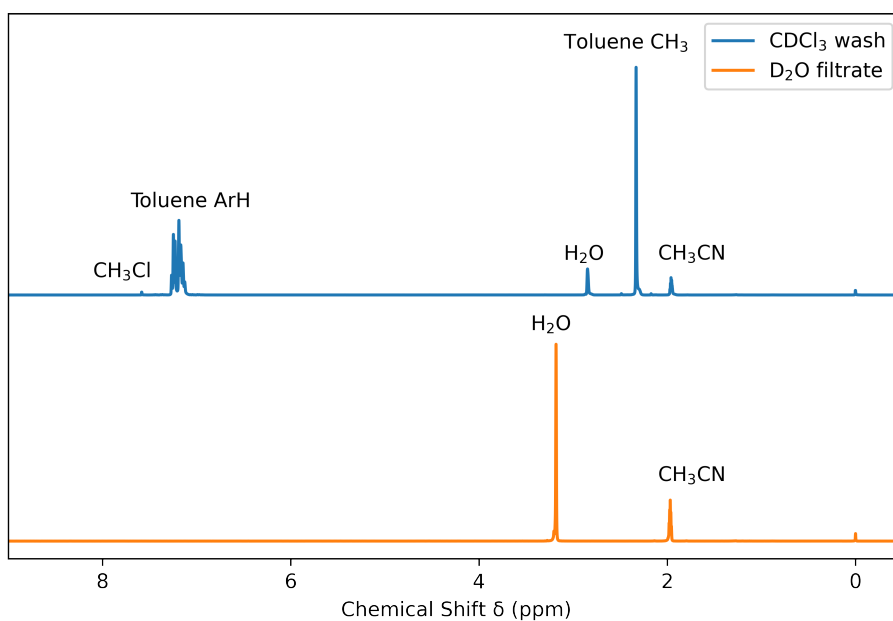

Figure 4.9: ^{1}H NMR spectra of the D_2O phase and $CHCl_3$ wash from the toluene-loaded Scholl coupled TPB HCP dispersion in water.
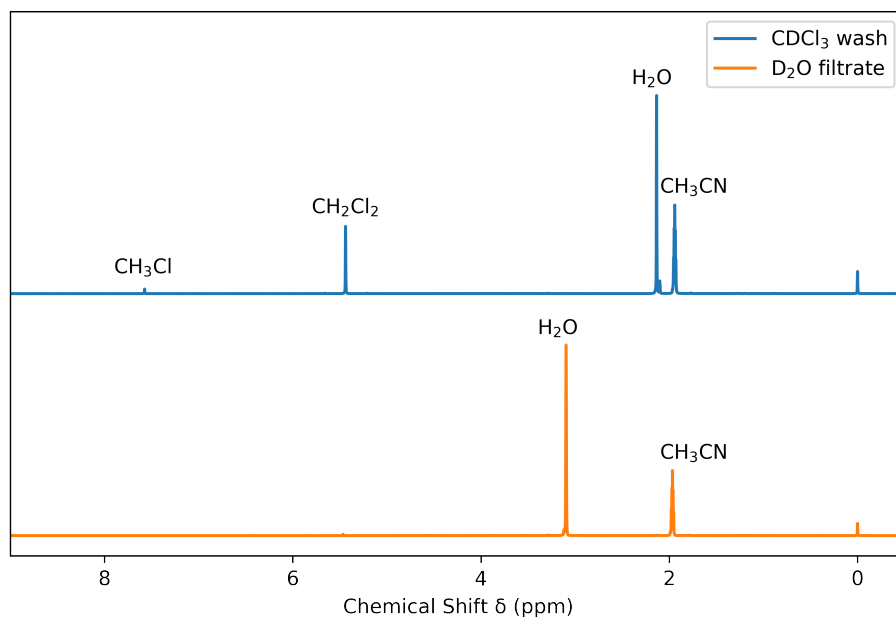
Figure 4.10: ^{1}H NMR spectra of the D$_2$O phase and CHCl$_3$ wash from the DCM-loaded Scholl coupled TPB HCP dispersion in water.

4.6   Conclusions

While exploiting a significant amount of the porosity in the Scholl coupled TPB HCP for CO$_2$ absorption when dispersed in water was not possible, a mild effect was observed at ambient pressures, but could not be replicated at the very high pressures at which significant gas uptake usually occurs in these materials.   The highly hydrophobic nature of these arene based HCPs was verified by measuring water absorption in the bulk solids and through acquiring water contact angle values, allowing the benchmarking of different HCPs to be carried out.   Furthermore, this hydrophobicity was shown to be sufficient to

absorb immiscible organic liquids into the dispersed solid while removing almost completely from the water in which the polymer is dispersed. The low cost and easy scalability of these HCPs allowed preparation of much larger scale samples compared to the other materials developed in chapters 2 and 3. Next steps should investigate further how effectively these suspensions could remove organic liquids from the environment, especially at lower concentrations.

Significant gas uptake enhancement hasn't been achieved, the results indicate that porosity does not arise in these materials due to their hydrophobicity, but rather competitive effects can allow the HCP to absorb hydrophobic liquids. The current materials do not form stable dispersions, with creaming/floating occurring when the mixtures are not stirred, a better approach could be to synthesise HCP nanoparticles[27] modified with a hydrophilic surface to enable surface cohesion between the polymer and water.

4.7 Experimental details

4.7.1 Materials

Materials: All chemicals were purchased from Sigma-Aldrich or TCI UK. Solvents were reagent or HPLC grade and purchased from Fisher Scientific. All materials were used as received unless stated otherwise.

4.7.2 General analytical techniques

Elemental analysis: A Thermo FlashEA 1112 Elemental Analyser was used to conduct CHN elemental analysis.

NMR: ^{1}H NMR spectra were acquired using an internal deuterium lock for the residual protons in $CDCl_3$ (δ = 7.26 ppm) or CD_2Cl_2 (δ = 5.32ppm) at ambient probe temperature on the following instruments: Bruker Avance400 (400 MHz) or Bruker DRX500 (500 MHz) spectrometers.

Gas sorption: Nitrogen isotherms of the HCP analogues were investigated by nitrogen adsorption and desorption at 77.3 K using an ASAP2420 volumetric adsorption analyser (Micrometrics Instrument Corporation) in order to calculate Brunauer-Emmett-Teller (BET) surface area was obtained in the relative pressure (P/P0)range of 0.05–0.20. Carbon Dioxide adsorption isotherms were aqcuired using Quantachrome Nova 4200e.

4.7.3 Synthesis of HCPs

The initial HCPs used in TGA and contact angle experiments were provided by Ammar Alahmed[28] (Scholl coupled HCPs) or Craig Wilson[29] ('knitted' HCPs).

Synthesis of Scholl coupled TPB

Under a nitrogen atmosphere, anhydrous $AlCl_3$ (4.9 g, 36 mmol) was added to a refluxing solution of 1,3,5-triphenylbenzene (1.5 g, 5 mmol) in anhydrous DCM (40 mL) and the mixture was heated under reflux overnight. The solid product was collected by filtration and washed thoroughly with ethanol and water until the filtrate was clear, then stirred under reflux for 6 hours in a) chloroform, b) methanol, c) ethanol, d) tetrahydrofuran, and e) acetone. The powder was then collected by filtration and dried for 24 hours at 60 °C under vacuum to produce Scholl coupled TPB (yield = 1.8 g). Surface area (BET) = 2535 m^2/g.

Synthesis of Scholl coupled benzene

Under a nitrogen atmosphere, anhydrous $AlCl_3$ (4.0 g, 30 mmol) was added to a refluxing solution of benzene (0.45 mL, 5 mmol) in anhydrous DCM (30 mL) and the mixture was heated under reflux overnight. The solid product was collected by filtration and washed thoroughly with ethanol and water until the filtrate was clear, then stirred under reflux for 6 hours in a) chloroform, b) methanol, c) ethanol, d) tetrahydrofuran, and e) acetone. The powder was then collected by filtration and dried for 24 hours at 60 °C under vacuum to produce Scholl coupled benzene (yield = 0.47 g).

Synthesis of Scholl coupled triptycene

Under a nitrogen atmosphere, anhydrous $AlCl_3$ (5.7 g, 43 mmol) was added to a refluxing solution of triptycene (1.1 g, 4 mmol) in anhydrous DCM (40 mL) and the mixture was heated under reflux overnight. The solid product was collected by filtration and washed thoroughly with ethanol and water until the filtrate was clear, then stirred under reflux for 6 hours in a) chloroform, b) methanol, c) ethanol,

d) tetrahydrofuran, and e) acetone. The powder was then collected by filtration and dried for 24 hours at 60 °C under vacuum to produce Scholl coupled triptycene (yield = 1.4 g). Surface area (BET) = 1760 m^2/g.

Synthesis of Scholl coupled biphenyl

Under a nitrogen atmosphere, anhydrous AlCl$_3$ (4.8 g, 36 mmol) was added to a refluxing solution of biphenyl (1.2 g, 8 mmol) in anhydrous DCM (30 mL) and the mixture was heated under reflux overnight. The solid product was collected by filtration and washed thoroughly with ethanol and water until the filtrate was clear, then stirred under reflux for 6 hours in a) chloroform, b) methanol, c) ethanol, d) tetrahydrofuran, and e) acetone. The powder was then collected by filtration and dried for 24 hours at 60 °C under vacuum to produce Scholl coupled biphenyl (yield = 1.8 g). Surface area (BET) = 1842 m^2/g.

Synthesis of 'knitted' HCPs

The monomer (benzene, toluene, or binaphthalene) (10 mmol) was added to anhydrous 1,2-dichloroethane (10 mL) under a flow of nitrogen, followed by formaldehyde dimethyl acetal (30 mmol, 3 eq.). An equimolar amount of iron(III) chloride (30 mmol, 3 eq.) was added and the reaction mixture heated at 80 °C for 18 hours. After cooling, the solid product was removed by filtration and washed with methanol several times. The product was then further purified by Soxhlet extraction with methanol for 18 hours, followed by drying *in vacuo* at 60 °C for 18 hours. CHN calc: benzene C, 92.26, H, 7.74; binaphthalene C, 94.45, H, 5.55; toluene C, 91.25, H, 8.75; Found: benzene C, 86.20, H, 5.06; binaphthalene C, 88.07, 4.89; toluene C, 87.86, H, 5.11.

Surface area (BET): benzene 1144 m^2/g, binaphthalene 1080 m^2/g, toluene 856

m^2/g.

Scaled up synthesis of Scholl coupled TPB HCP

Under an N_2 atmosphere, anhydrous $AlCl_3$ (10 equiv, 147 mmol) was added to a solution of 1,3,5-triphenylbenzene (TPB) (4.5 g, 1 equiv., 14.6 mmol) in DCM (180 mL). The reaction mixture was heated to reflux for 18-24 hours. The resulting brown precipitate was collected by filtration and washed with water then ethanol. The polymer was then purified by soxhlet extraction with methanol. The brown product is collected, ground into fine powder and dried at 90 °C in a vacuum oven to yield pure product. Yield 5.31 g, 118%. CHN Calc.: C, 94.08; H, 5.92; Found: C, 85.86, H, 5.00.
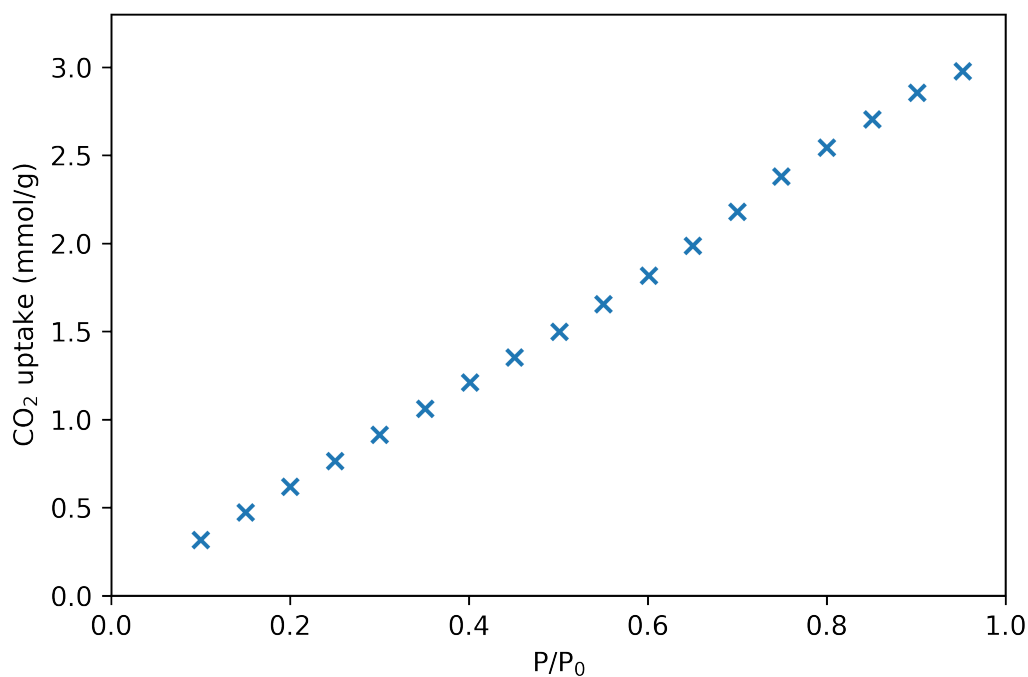

Figure 4.11: CO_2 adsorption isotherm of the scaled up Scholl coupled TPB HCP.

4.7.4   Thermogravimetric analysis (TGA)

For each of the synthesised polymers, HCP (3 x 100 mg) was placed into glass vials. For the desolvated samples, the samples were activated in a vacuum overnight at 90 °C. Another of the samples had water (1 mL) added and the vial was fitted with a stirrer bar, the vial was capped and stirred overnight. Before TGA acquisition, the polymer was transferred to a filter paper to absorb excess water. Finally the third sample was left open to the ambient conditions of the lab for several days before acquiring TGA. From each sample a small amount was transferred to a TGA pan and run immediately, except for the water stirred sample from which a second portion was taken and run 30 minutes after removing from water.

TGA was carried out using a Perkin Elmer TGA8000 thermogravimetric analyser according to the following program: hold at 35 °C for 1 minute followed by temperature ramp from 35 °C to 300 °C at 10 °C/minute then held at 300 °C for 5 minutes. The experiments were carried out under constant N_2 flow at 30 mL/minute.

4.7.5   Drop shape analysis

Drop shape analysis was carried out using a Krüss DSA100E automated drop shape analyser. Powders were ground in a mortar and pestle before using a hydraulic press to produce pellets with a smooth surface from the powders. The pellets were carefully transferred to the drop shape analyser. Water was dropped on the surface and measured using the Krüss software. The average is calculated from multiple measurements in-software, at least five for each sample.

Table 4.2: Results of the TGA experiments, demonstrating the percentage mass loss as samples were heated over the temperature range to determine the water content.

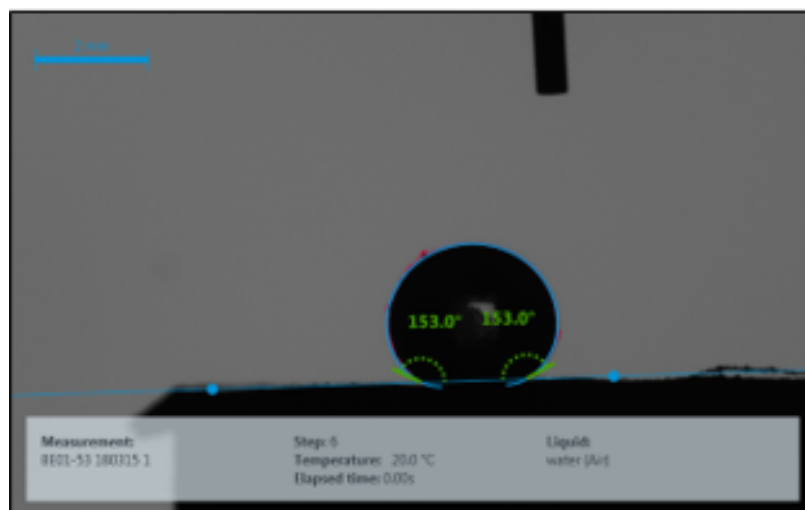| HCP	Desolvated	Ambient	Wet (30 mins)	Wet (instant)
Scholl coupled TPB	1.7%	1.1%	0.2%	20.4%
Scholl coupled benzene	0.3%	0.4%	4.9%	41.5%
Scholl coupled triptycene	2.7%	2.6%	0.7%	52.8%
Scholl coupled biphenyl	1.2%	0.4%	-0.6%	54.8%
'Knitted' Benzene	1%	0.4%	0.2%	74.7%
'Knitted' binaphthalene	1.1%	1%	3.2%	58.7%
'Knitted' toluene	0.7%	0%	0.4%	57.2
Activated charcoal	-	4.5%	19.2%	68.9%

Figure 4.12: Representative contact angle measurement using the Krüss DSA100E automated drop shape analyser. This sample was the Scholl coupled TPB HCP. Here, the droplet is automatically recognised by the software and contact angle is saved in the software.

Figure 4.13: Frames from video recording of dropping water onto the 'knitted' benzene HCP, where the water is fully absorbed by the droplet, in the third frame a small amount of swelling of the pellet can be observed.

4.7.6 Ball-milling of HCP

Initial ball milling experiments were carried out using a Retsch Mixer Mill MM 400 using stainless steel milling jars and 5 mm stainless steel ball-bearings. The
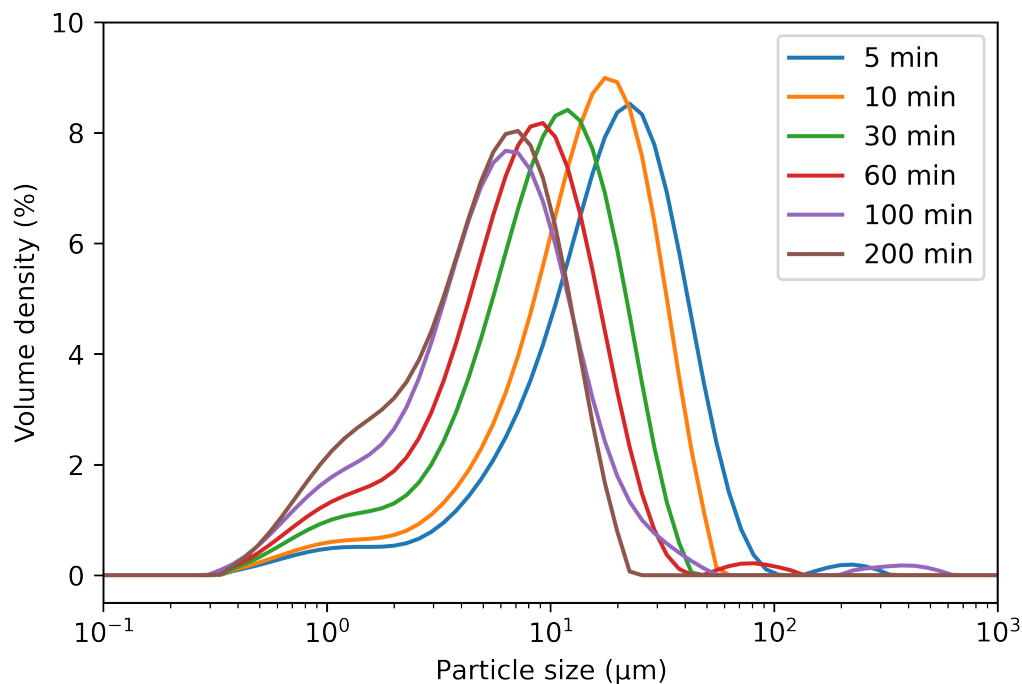
Figure 4.14: SLS measurements of the Scholl coupled TPB HCP at the time intervals of the ball-milling carried out to reduce particle size.

milling was carried out on 1 g samples of the Scholl coupled TPB for varying time intervals. The particle size was measured using a Mastersizer 3000 SLS instrument. Samples were dispersed in ethanol before dropping into sample chamber with constant stirring to ensure scattering intensity was within range.

In order to process a larger quantity of HCP at once, an orbital mill was employed. The HCP was loaded into a polyproplyene bottle fitted with ceramic beads and milled for 24 hours. SLS measurements determine the resulting powder had a particle size of 3.1 μm.

Table 4.3: Particle size of Scholl coupled TPB HCPs after ball milling at various time intervals in order to reduce particle size.

Time (minutes)	SC-TPB Batch 1 (μm)	SC-TPB Batch 2 (μm)
5	19.9	12.8
10	14.7	9.22
30	9.53	4.69
60	7.28	3.33
100	6.03	2.87
200	5.14	3.40
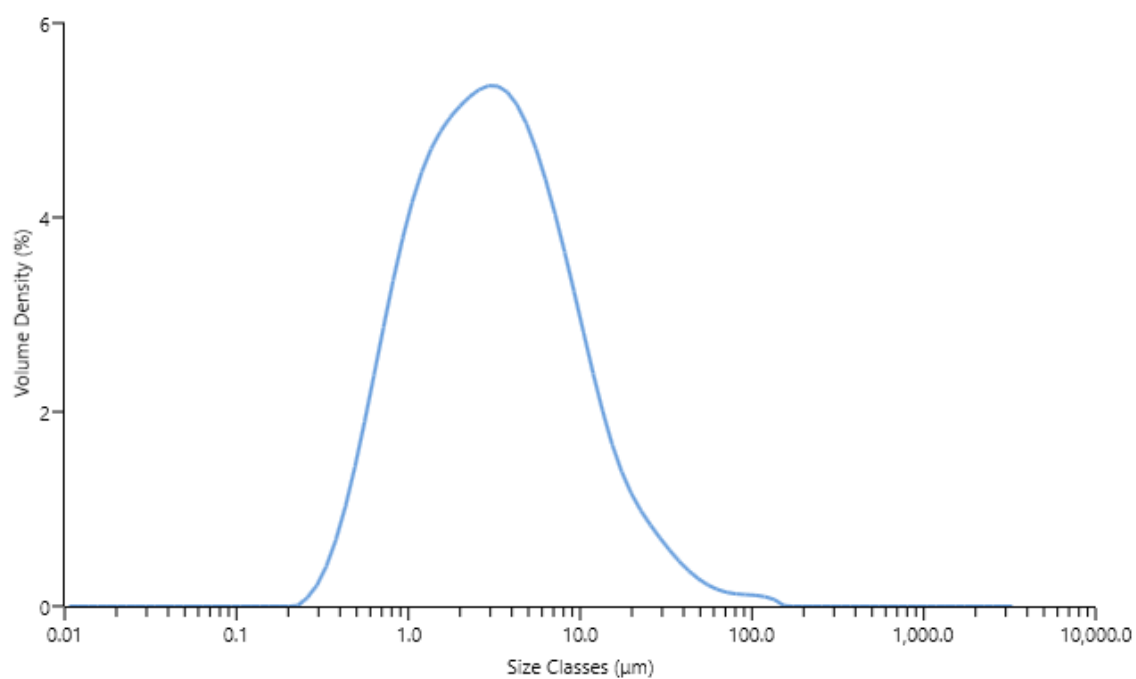
Figure 4.15: SLS measurement of the Scholl coupled TPB HCP after milling for 24 hours using the orbital mill. Average particle size = 3.1 μm.

4.7.7 CO_2 uptake at atmospheric pressure

The Scholl coupled TPB HCP was added to water to prepare a 3 mL sample at 12.5 wt.% in water in a capped GC vial. CO_2 gas was bubbled through the sample at 50-60 mL/min using a calibrated flowmeter for 10 minutes and the GC vial was capped and sealed. Gas release was carried out either with addition of DCM or by heating the sample up from room temperature to 60 °C or 80 °C and the evolved gas was captured in an inverted burette *via.* a PTFE tubing cannula. DCM was either added in 40 μL increments up to 240 μL or a single 240 μL dose.

Table 4.4: Results of gas evolution experiments carried out using various methods to evolve CO_2 gas from the Scholl coupled TPB HCP dispersions compared to water.

Evolution method	Gas evolved from dispersion (mL)	Gas evolved from water (mL)	CO_2 uptake in dispersion (μmol/mL)	CO_2 uptake in water (μmol/mL)	CO_2 uptake enhancement (μmol/mL)
60°C	2.1	1.5			
	2.3	1.5	31.9 ± 2.7	22.7 ± 3.2	9.3
	2.5	2.0			
80°C	3.4	3.0			
	3.9	2.9	50.4 ± 3.5	42.1 ± 2.1	8.3
	3.6	3.2			
DCM single dose	2.9	3.5			
	2.3	3.7	36.6 ± 4.2	50.9 ± 2.1	-14.4
	2.7	3.8			
DCM increments	5.1	4.2			
	5.6	3.9	75.0 ± 3.7	54.6 ± 3.5	20.4
	5.5	3.7			

4.7.8 CO_2 uptake at increased pressure

A Parr vessel with pressure guage was connected using swagelok fittings and piping to allow loading of CO_2 up to 50 bar in the Parr vessel, and with a gas outlet to allow capture of the CO_2 in an inverted 1 L measuring cylinder when released (Figure 4.16). Equilibration experiments were carried out with water at 50 bar CO_2 pressure, for 10, 30, 60 and 90 mins. Experiments were carried out with the 10 minute equilibration time rather than longer to determine whether there is any difference between the uptakes in the HCP dispersion compared to water. Ball milled Scholl coupled TPB HCP (12.5 g) was dispersed in water (100 mL) to produce a dispersion to load into the Parr vessel (75 mL). CO_2 was loaded into the vessel containing the dispersion at high pressure (10, 20, 30, 40 , 50 bar) and allowed to equilibrate for 10 mins. As pressure drops due to absorption of CO_2, the pressure was equalized with addition of more CO_2. Once the equilibration time has passed, gas is released via outlet and captured in the inverted measuring cylinder filled with water and immersed in a water bath. Leak tests were carried out at 10 bar and 50 bar to ensure the empty vessel retains pressure over the duration of the experiment.

Figure 4.16: Experimental set-up used to carry out high pressure CO_2 measurements. Consists of a 75 mL Parr vessel with pressure guage and connected to an inlet for 50 bar CO_2 and an outlet to capture the gas in an inverted measuring cylinder.
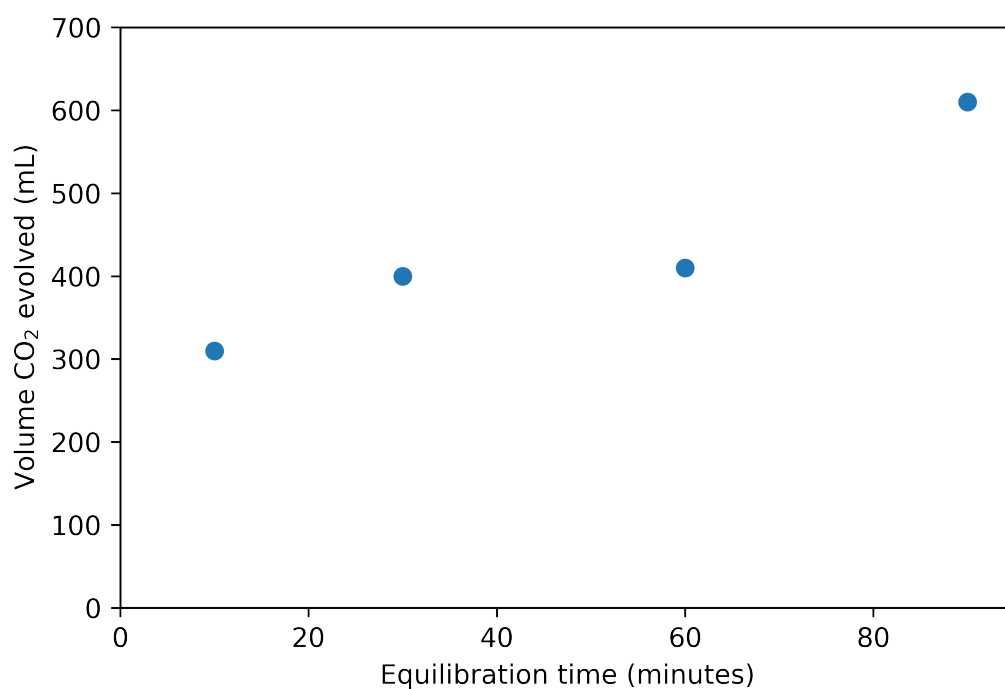
Figure 4.17:   Volumes of CO_2 released from water after exposure to 50 bar CO_2 with varied equilibration times at this pressure. Longer equilibration significantly increases the amount of gas that is evolved.

Table 4.5: Results of the high pressure CO_2 gas evolution experiments in the Scholl coupled TPB HCP dispersion and water.

CO_2 pressure (bar)	Gas evolved from dispersion (mL)	Gas evolved from water (mL)	CO_2 uptake in dispersion (μmol/mL)	CO_2 uptake in water (μmol/mL)
10	120	140	66.6	77.7
20	155	170	86.1	94.4
30	265	250	147.2	138.9
40	250	260	138.8	144.4
50	305	310	169.4	172.2

4.7.9   Absorption of small organic molecules

The Scholl coupled TPB HCP was added to water to prepare a 1 mL sample at 12.5 wt.% in water. To the samples, either toluene or DCM was added in 20 μL aliquots until a separate layer formed of the added liquid due to becoming immiscible, indicating the HCP dispersion had become saturated. The same TPB HCP samples were then prepared in D_2O at the maximum loading of toluene and DCM, before passing the dispersion through a small vacuum filter to separate and collect the fluid phase from the polymer dispersion. The remaining solid was then washed with $CDCl_3$ (1 mL) and the washings were collected. CD_3CN (0.5 mL) was added to both the D_2O and $CDCl_3$ phases collected and analysed by ^{1}H NMR spectroscopy.

Table 4.6: Maximum volumes of Toluene and DCM that can be added to 1 mL of of the Scholl coupled TPB HCP dispersion in water.

Liquid	Maximum loading (μL)
Toluene	200
DCM	120

References

(1) N. O'Reilly, N. Giri and S. L. James, *Chemistry - A European Journal*, 2007, **13**, 3020–3025.

(2) M. Z. Ahmad and A. Fuoco, *Current Research in Green and Sustainable Chemistry*, 2021, **4**, 100070.

(3) J. W. Barnett, M. R. Sullivan, J. A. Long, D. Tang, T. Nguyen, D. Ben-Amotz, B. C. Gibb and H. S. Ashbaugh, *Nature Chemistry*, 2020, DOI: `10.1038/s41557-020-0458-8`.

(4) F. Biedermann, W. M. Nau and H.-J. Schneider, *Angew. Chem. Int. Ed.*, 2014, **53**, 11158–11171.

(5) F.-T. Huang and S.-W. Cheong, *Nature Reviews Materials*, 2017, **2**, 17004.

(6) V. A. Davankov and M. P. Tsyurupa, *React. Polym.*, 1990, **13**, 27–42.

(7) B. Li, R. Gong, W. Wang, X. Huang, W. Zhang, H. Li, C. Hu and B. Tan, *Macromolecules*, 2011, **44**, 2410–2414.

(8) J. Germain, J. M. J. Fréchet and F. Svec, *Small*, 2009, **5**, 1098–1111.

(9) C. D. Wood, T. Bien, A. Trewin, N. Hongjun, D. Bradshaw, M. J. Rosseinsky, Y. Z. Khimyak, N. L. Campbell, R. Kirk, E. Stöckel and A. I. Cooper, *Chemistry of Materials*, 2007, **19**, 2034–2048.

(10) S. Yao, X. Yang, M. Yu, Y. Zhang and J.-X. Jiang, *J. Mater. Chem. A*, 2014, **2**, 8054–8059.

(11) B. Li, Z. Guan, X. Yang, W. D. Wang, W. Wang, I. Hussain, K. Song, B. Tan and T. Li, *J. Mater. Chem. A*, 2014, **2**, 11930–11939.

(12)   S. Hou, S. Wang, X. Long and B. Tan, *RSC Adv.*, 2018, **8**, 10347–10354.

(13)   K. J. Msayib and N. B. McKeown, *J. Mater. Chem. A*, 2016, **4**, 10110–10113.

(14)   R. T. Woodward, L. A. Stevens, R. Dawson, M. Vijayaraghavan, T. Hasell, I. P. Silverwood, A. V. Ewing, T. Ratvijitvech, J. D. Exley, S. Y. Chong, F. Blanc, D. J. Adams, S. G. Kazarian, C. E. Snape, T. C. Drage and A. I. Cooper, *Journal of the American Chemical Society*, 2014, **136**, 9028–9035.

(15)   A. W. Coats and J. P. Redfern, *Analyst*, 1963, **88**, 906–924.

(16)   G. R. Heal, in *Principles of Thermal Analysis and Calorimetry*, The Royal Society of Chemistry, 2002, pp. 10–54.

(17)   R. B. Prime, H. E. Bair, S. Vyazovkin, P. K. Gallagher and A. Riga, *Wiley Online Library*, 2008, 241–317.

(18)   C. Wilson, N. J. Cooper, M. E. Briggs, A. I. Cooper and D. J. Adams, *Org. Biomol. Chem.*, 2018, **16**, 9285–9291.

(19)   A. H. Alahmed, M. E. Briggs, A. I. Cooper and D. J. Adams, *Journal of Polymer Science, Part A: Polymer Chemistry*, 2018, **56**, 2513–2521.

(20)   O. I. del Rı'o, D. Y. Kwok, R. Wu, J. M. Alvarez and A. W. Neumann, *Colloids Surf., A*, 1998, **143**, 197–210.

(21)   R. L. Greenaway, D. Holden, E. G. B. Eden, A. Stephenson, C. W. Yong, M. J. Bennison, T. Hasell, M. E. Briggs, S. L. James and A. I. Cooper, *Chem. Sci.*, 2017, **8**, 2640–2651.

(22)   G. T. Rochelle, *Science*, 2009, **325**, 1652–1654.

(23) G. Fraux, F.-X. Coudert, A. Boutin and A. H. Fuchs, *Chem. Soc. Rev.*, 2017, **46**, 7421–7437.

(24) Y. Li, H. Chang, H. Yan, S. Tian and P. G. Jessop, *ACS Omega*, 2021, **6**, 253–264.

(25) D. Matatagui, J. Fontecha, M. J. Fernández, M. Aleixandre, I. Gràcia, C. Cané and M. C. Horrillo, *Talanta*, 2011, **85**, 1442–1447.

(26) D. Matatagui, M. J. Fernández, J. Fontecha, J. P. Santos, I. Gràcia, C. Cané and M. C. Horrillo, *Sens. Actuators, B*, 2012, **175**, 173–178.

(27) T. Mitra, R. S. Bhavsar, D. J. Adams, P. M. Budd and A. I. Cooper, *Chem. Commun.*, 2016, **52**, 5581–5584.

(28) A. Alahmed, Ph.D. Thesis, University of, Liverpool, England, UK, 2019.

(29) C. Wilson, Ph.D. Thesis, University of, Liverpool, England, UK, 2019.

5   Outlook and concluding remarks

After their conception in 2007,[1] many examples of porous liquids have been demonstrated in the literature, including examples of materials that are not labelled as such in their reports. The 'first' porous liquids were described in 2015[2,3] and, in the few years since, the three different categories have all been prepared. Type 1 porous neat liquids have proven to be the most difficult to synthesise, owing to the combination of properties required for a single molecular material. POCs have been proven as ideal candidates for making porous liquids, due to their small pore size and molecular nature, both in the literature and in this thesis.

In this thesis, investigation of ways to control and introduce permanent microporosity in the liquid state has been investigated. In Chapter 2, POCs were used for tuning pore size in porous liquids, transferring concepts previously investigated in solid POCs. This is the first demonstration of this effect and how it can be used to control gas uptake capacity in these materials. The almost complete shut-off of Xe uptake enhancement is drastic, showing how the singular pore cavities in the liquid state can differ greatly from solid-state pore networks. While the gas evolution method has been invaluable in early development of our understanding of type 2 porous liquids,[4] we are beginning to move past the limits of its utility, as the technique becomes less useful for studying uptake of larger gases.

Synthetic control of pore size was also used in POC based type 3 porous liquids which was outlined in Chapter 3, where the solids POCs were dispersed in silicone oil to transfer more directly the properties of solid microporous materials to a fluid.

Use of pore-modified porous liquids in chapters 2 and 3 have shown that we can design porous liquids to be selective towards certain gases by controlling the pore structure.

In Chapter 4, HCP suspensions were investigated as an alternative possibility for carrying out CO_2 absorption in a liquid by attempting to exploit their hydrophobicity to exclude water. While this ultimately proved to only be very mildly effective, we found they could possibly be used for absorbing organic pollutants, though this should be investigated further for a wider variety of liquids as well as at lower concentrations that may be found in the environment for real world use. These materials are particularly attractive due to their very low cost and scalability, owing to being based on simple organic polymers and water.

Porous liquids are a relatively young class of material, which have great promise for combining the properties of highly selective microporous solids with the flowing nature of liquid sorbents. The high selectivity of permanent micropores could allow for lower working pressures in industrial separations. More high pressure measurements need to be acquired to further this field, as industrial gas sorbents such as Genosorb 1753 used in the Selexol process usually operate best at *ca.* 30 bar.[5] The utility of molecular porous liquids at these pressures may be diminished as even at atmospheric pressures, the pores are approaching saturation with gas. The promise of zeolite and MOF based type 3 porous liquids will be important in this sense, as the microporous solids are some of the highest performing with respect to uptake and selectivity.

The future of the field also lies beyond the realm of conventional gas sorbents, potentially as more imaginative novel materials: Kearsey *et al.* have already shown

that the formation of gel-like materials from porous liquids can be achieved.[6] With careful design, porous gels could be developed, potentially using gel formation and destruction as a gas capture and release mechanism.

Little attention has been paid to designing the solvents or dispersing phases in porous liquids. Careful molecular design of solvents for type 2 porous liquids, for example, could enable improved porosity or selectivity, as the opposite was observed by Kearsey *et al.* where gas uptake was reduced at the same pore concentration with new solvents discovered *via.* high-throughput experimentation.[6] There are a variety of tools available for solvent selection, which could be combined with further computation to discover better performing systems.[7]

Permanent porosity in the liquid state could also be described as a new driving force for carrying out chemistry, through the process of minimising the internal energy of a system thermodynamically, in this case occupation of the empty cavities in a porous liquid is energetically favourable. This force has been shown to drive encapsulation of liquid guests by Ma *et al.* for small guests based on how effectively the guest occupies the entire pore volume[8] in the porous liquid and it could be envisaged that this process will be further exploited for molecular separation or binding or as a new tool in supramolecular assembly.

References

(1)   N. O'Reilly, N. Giri and S. L. James, *Chemistry - A European Journal*, 2007, **13**, 3020–3025.

(2)   N. Giri, M. G. Del Pópolo, G. Melaugh, R. L. Greenaway, K. Rätzke, T. Koschine, L. Pison, M. F. C. Gomes, A. I. Cooper and S. L. James, *Nature*, 2015, **527**, 216–220.

(3)   J. Zhang, S. H. Chai, Z. A. Qiao, S. M. Mahurin, J. Chen, Y. Fang, S. Wan, K. Nelson, P. Zhang and S. Dai, *Angewandte Chemie - International Edition*, 2015, **54**, 932–936.

(4)   R. L. Greenaway, D. Holden, E. G. B. Eden, A. Stephenson, C. W. Yong, M. J. Bennison, T. Hasell, M. E. Briggs, S. L. James and A. I. Cooper, *Chem. Sci.*, 2017, **8**, 2640–2651.

(5)   A. V. Rayer, A. Henni and P. Tontiwachwuthikul, *J. Chem. Eng. Data*, 2012, **57**, 764–775.

(6)   R. J. Kearsey, B. M. Alston, M. E. Briggs, R. L. Greenaway and A. I. Cooper, *Chem. Sci.*, 2019, **10**, 9454–9465.

(7)   P. M. Piccione, J. Baumeister, T. Salvesen, C. Grosjean, Y. Flores, E. Groelly, V. Murudi, A. Shyadligeri, O. Lobanova and C. Lothschütz, *Org. Process Res. Dev.*, 2019, **23**, 998–1016.

(8)   L. Ma, C. J. E. Haynes, A. B. Grommet, A. Walczak, C. C. Parkins, C. M. Doherty, L. Longley, A. Tron, A. R. Stefankiewicz, T. D. Bennett and J. R. Nitschke, *Nature Chemistry*, 2020, **12**, 270–275.